THESIS REPORT
Master's Degree

SYSTEMS
RESEARCH
CENTER

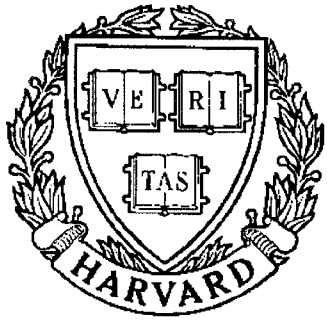

Supported by the National Science Foundation Engineering Research Center Program (NSFD CD 8803012), the University of Maryland, Harvard University, and Industry

An Investigation of Control Strategies for Friction Compensation

by N.E. Ehrich
Advisor: P.S. Krishnaprasad

M.S. 91-4

ABSTRACT

Title of Thesis: AN INVESTIGATION OF CONTROL STRATEGIES FOR FRICTION COMPENSATION

Name of degree candidate: Naomi Elizabeth Ehrich

Degree and Year: Master of Science in Electrical Engineering, 1991

Thesis directed by: P. S. Krishnaprasad
Professor
Electrical Engineering

Control strategies are investigated for friction compensation in servomechanisms. As part of the investigation, several different models of friction are reviewed and analyzed for their relevancy to the control problem. Models of friction at zero and near-zero velocities are of particular concern since in this regime friction can introduce oscillations. These different models are considered in friction-compensating adaptive control design. Three friction-compensating adaptive controllers are designed based on strategies proposed in the literature. Adaptive controllers are well-suited to the friction compensation problem since

they are nonlinear and have the additional advantage of providing system identification and tracking of slowly-varying parameters such as friction parameters. Stability analyses are performed for the controllers and yield asymptotic stability results for the system error. An original stability proof employing passivity theory is provided for one of the controllers. To test the effectiveness of the adaptive controllers, an experimental program is designed and implemented on a direct drive dc motor. Comparative position trajectory tracking experiments are performed with the three adaptive controllers, a controller with dither (a commonly-used heuristic friction-compensating controller), and a traditional linear controller used as a benchmark. The results show that the adaptive controllers outperform the more traditional heuristic and linear controllers. Additionally, the experiments yield insight into the appropriateness of the different friction models under the tested operating conditions. In particular, the less popular Dahl model is observed to provide a reliable representation of friction behavior near zero velocity.

AN INVESTIGATION OF CONTROL STRATEGIES FOR FRICTION COMPENSATION

by

Naomi Elizabeth Ehrich

Thesis submitted to the Faculty of the Graduate School
of The University of Maryland in partial fulfillment
of the requirements for the degree of
Master of Science
1991

Advisory Committee:

Professor P. S. Krishnaprasad, Chairman/Advisor
Assistant Research Scientist Josip Lončarić
Assistant Professor W. P. Dayawansa

ACKNOWLEDGEMENTS

I would like to express my sincere appreciation to my advisor Dr. P. S. Krishnaprasad for his guidance and encouragement on my graduate research. His unfailing enthusiasm for the study of friction compensation and related nonlinear control topics has made my work all the more stimulating. I would also like to thank Dr. Josip Lončarić who served as a co-advisor and provided many useful suggestions regarding friction models and experimental implementation issues. I owe additional thanks to Dr. Krishnaprasad, Dr. W. P. Dayawansa, and Dr. Lončarić for serving on my thesis advisory committee.

I am grateful to my colleagues in the Intelligent Servosystems Laboratory for all their help and for making the lab a great place for research. Additionally, I'd like to thank Reza Ghanadan in particular for his discussions on adaptive control.

Finally, I would like to thank both the System Research Center and the

Graduate School of the University of Maryland for my graduate fellowship support.

This research was supported in part by the National Science Foundation's Engineering Research Centers Program: NSFD CDR 8803012 and by the AFOSR University Research Initiative Program under grant AFOSR-90-0105.

Contents

List of Tables

List of Figures

Chapter 1

Introduction

Recent growth in the number and variety of robotics applications has led to a demand for increased precision in robotic manipulation. For example, robots that perform exacting industrial assembly tasks or manipulators employed in delicate surgical procedures must be capable of precisely controlled maneuvering. However, robotic manipulators are mechanical systems and must necessarily contend with physical realities. In particular, physical reality in the form of *friction* poses a serious challenge to precise manipulator control.

This thesis describes both theoretical and experimental results that provide insight into the friction-compensating control problem for servomechanisms. The first major effort involves a comprehensive review with analysis of a variety of different friction models with the goal of understanding which features of friction are most important to the control problem. Friction models developed throughout history including the most recent research results are examined.

The second major effort of this thesis deals directly with a variety of friction-compensating control strategies. Three adaptive control strategies in particular are explored in detail [Gilbart and Winston, 1974,Craig, 1988,Walrath, 1984]. These controllers use simple friction models as the basis for friction compensation. However, in this thesis design modifications to these controllers are proposed that introduce more detailed and complete friction models into the compensation schemes. Additionally, in the work of [Walrath, 1984], the author provided no control system stability analysis. A major theoretical contribution of this thesis is an original stability proof based on the passivity formalism of the friction-compensating control technique of [Walrath, 1984].

A comparative test program involving servomechanism tracking experiments performed with several different friction-compensating controllers provides the significant experimental contribution of this thesis. This effort addresses the lack of comparative experimental results on friction compensation and includes an assessment of the relative effectiveness of the different control strategies. Because there are still uncertainties as to how friction affects dynamic behavior, it is necessary that the true test of control strategies be experimental. Additionally, this thesis describes an important friction parameter relationship, empirically derived using the technique of [Walrath, 1984], that provides increased support for the less popular Dahl friction model.

The motivation for the research of this thesis derives from the fact that friction is typically undesirable, unavoidable, and difficult to model for servomechanism control problems. Friction is a force that opposes the motion of two surfaces rubbing or rolling against each other. It results from a complex of microscopic phenomena dependent on surface material, characteristics of lubrication between the surfaces, forces normal to the direction of motion, and the dynamics of the rubbing or rolling motion. On the macroscopic level, friction has been observed to hinder smooth motion. It is discontinuous at zero velocity and can generate oscillatory behavior at low speeds.

All mechanical systems with moving parts experience friction. In a typical robotic manipulator, the joints are driven by electric motors, and friction is present in the bearings of the motors and in the gears of the transmissions. Much can be done to reduce the level of friction by improving mechanical design. However, friction will always be present to some degree.

In the control of a mechanical system, failing to compensate for friction can lead to tracking errors when velocity reversals are demanded and oscillations when very small motions are required. For precise manipulator control, these performance deviations can be costly. To compensate for friction it is best to have some knowledge of the structure of friction. However, microscopic friction phenomena do not easily translate into a structural model of friction that accurately predicts the observed macroscopic behavior

of a dynamic mechanical system. Indeed, several different models of friction have been proposed by researchers in tribology, e.g. [Bowden and Tabor, 1982, Rabinowicz, 1965,Hess and Soom, 1990], and recently by researchers in control engineering [Dahl, 1976,Armstrong, 1988,Canudas de Wit, 1989], yet with little overall consensus in the literature. As a result, an engineer, attempting to compensate for friction in order to accurately control the movement of a mechanical system, is faced with an unclear choice of a friction model. The engineer cannot be sure which friction model incorporates the features necessary for friction prediction that will enable satisfactory control of the desired task.

In addition to the disruptive nature of friction and the lack of a universal model of friction, friction compensation is further complicated by the fact that friction parameters vary with temperature and age. This implies that a friction compensation scheme that works one day may not work the next day if the operating conditions have changed. Consequently, a good compensating scheme must take into account this potential for variation.

Traditionally, control engineers have used "heuristic" open-loop techniques, such as dither and pulse-width modulation, to compensate for friction in mechanical systems. These techniques perform signal averaging to smooth out the discontinuities introduced by friction. However, these techniques confound rigorous investigation of system performance measures such as stability and robustness. Pulse-width modulation is not easily handled mathematically since

it yields a control signal that is discontinuous. Dither can cause mechanical problems such as fatigue by exciting vibrations in manipulators.

As an alternative to these techniques, researchers in control engineering have recently considered adaptive control techniques for compensation of friction in mechanical systems [Gilbart and Winston, 1974,Walrath, 1984,Craig, 1988, Canudas et al., 1986]. These methods are suitable for control of nonlinear systems and have the additional advantage of providing system identification and tracking of slowly-varying system parameters such as friction parameters. However, adaptive compensation of friction assumes some knowledge of friction structure and so does not eliminate the problem of selecting an appropriate friction model.

Among the adaptive friction compensators proposed in the literature, a variety of friction models are assumed. Most of the researchers show experimental evidence that their friction model together with their compensation technique improves system performance. However, since each research team performed different experiments, there is no easy way to compare the relative effectiveness of the different control-technique/friction-model combinations. That is, the engineer still does not have a clear basis for judging which control technique and friction model best can handle a given problem.

Chapter 2 of this thesis describes the different models of friction

found in the literature. These models range from the classical friction model (originally developed by such distinguished figures in the history of science as Leonardo da Vinci and Charles de Coulomb) to the modern dynamic state-variable friction models proposed by geophysicists studying unstable sliding between rock surfaces to explain fault motions in the earth's crust [Horowitz, 1988,Nussbaum and Ruina, 1987, Rice and Ruina, 1983,Rice and Tse, 1986,Ruina, 1983]. To address the problem of understanding which friction features are most important for precision control, our descriptions of each friction model include not only an explanation of the model based on microscopic phenomena but also a discussion of the macroscopic dynamic behavior predicted by the model.

Chapter 3 offers a comprehensive review of control strategies for friction compensation and describes for each strategy the advantages and disadvantages with regard to control implementation, flexibility and performance. As mentioned above, the adaptive control techniques seem most well suited to the friction compensation problem since they are inherently nonlinear and they provide system identification and tracking of slowly-varying system parameters. As a result, they are explored most rigorously in this thesis. Section 3.4 describes in detail the control strategies tested in the experimental program, including modifications and improvements made to the friction models or controllers. Stability analyses accompany discussion of the controllers.

Chapter 4 provides the details of the experimental program and the experimental results. The subject of the experimental program was an electric motor, i.e., a single-degree-of-freedom servomechanism intended to represent one joint of a robotic manipulator. The experiments involved position trajectory tracking with velocity reversals which exercised the problems associated with friction at near-zero velocities and the discontinuous nature of friction at zero velocity. This focused testing of velocity reversals is appropriate since it is not practical in general to expect a unidirectional motion application. The digital implementation of the controllers is described as is an analysis of the effect of various hardware limitations on the experiments.

Conclusions are discussed in Chapter 5. Chapter 5 also includes some suggestions for future work. Since friction figures so prominently not only in control of mechanical systems with movable parts but also in other areas of research such as robotic grasping and walking, advances in our understanding of friction and our ability to control friction can yield significant and diverse rewards.

Chapter 2

Friction Structure and Dynamics

Researchers in a number of different fields have considered the problem of identifying and modelling the structure and dynamics of friction. Many of these investigators work in the area of tribology. Formally defined as the "science and technology of interacting surfaces in relative motion" [Bowden and Tabor, 1982], tribology encompasses the study of lubrication, rubbing, and wear. While some of the work in tribology concerns friction dynamics, for the most part tribologists have been interested in the consequences of steady-state rubbing in order to develop means to reduce machine wear and aging.

On the other hand, control engineers, who seek to drive mechanical systems with precision in the presence of friction, are typically interested in the effect that friction has on dynamic behavior. As a result, there has been a recent

effort by control engineers to study and model friction dynamics [Dahl, 1976, Walrath, 1984,Armstrong, 1988]. This new work by control engineers has proved enlightening, but as emphasized in [Armstrong-Hélouvry, 1991], control engineers concerned with friction compensation need to be aware of the important discoveries made in the field of tribology.

Other recent contributions to the investigation of friction dynamics have come from the field of geophysics. Researchers in this field test, model, and simulate friction dynamics between sliding rock surfaces to explain fault motions in the earth's crustal plates [Ruina, 1983,Rice and Ruina, 1983, Rice and Tse, 1986,Nussbaum and Ruina, 1987,Horowitz, 1988]. Their models and studies of a time lag in friction response to dynamic changes in motion appear to be relevant to the control engineer's problem.

This chapter presents friction structure and dynamics in terms of seven different elements and effects including:

1. Kinetic friction
2. Viscous friction
3. Static friction
4. Pre-sliding displacement referred to as "the Dahl effect"
5. Static friction dependence on dwell time

6. Friction variations with velocity referred to as "the Stribeck effect"

7. Frictional lag

Each friction component and effect is discussed in terms of predicted or measured microscopic phenomena, modelling, and macroscopic behavior prediction.

Although rolling friction is a physically different phenomenon from rubbing or sliding friction, the models reviewed in this chapter attempt to describe the dynamics of a system with rolling *or* sliding friction. Pure rolling friction conditions occur when the contact between two surfaces is a point. However, according to [Rabinowicz, 1965], the contact region between two surfaces is typically of larger area than a point because of elastic (and possibly plastic) deformation on one or both of the surfaces. The resulting "rolling" friction in this case involves a combination of sliding and pure rolling friction. In fact, although the sliding velocity is usually small compared to the rolling velocity, sliding friction often provides the major component of the total friction. Consequently, it is appropriate to consider the same models for sliding friction and "rolling" friction.

2.1 Kinetic Friction

Kinetic friction is the earliest type of friction recognized. As recorded in his notebooks of the late fifteenth and early sixteenth centuries, Leonardo da Vinci

identified friction, later referred to as kinetic friction, as a resistance to the motion of one body sliding over another. He and his successors, Guillaume Amonton of the late seventeenth century and Charles de Coulomb of the late eighteenth century, understood that kinetic friction is proportional to the force normal to the direction of sliding motion and independent of the area between the two surfaces [Bowden and Tabor, 1982]. Coulomb further indicated that kinetic friction is independent of the relative velocity of the sliding surfaces. For this contribution, kinetic friction is also often referred to as dynamic friction or Coulomb friction.

To understand what accounts for the characteristic behavior of kinetic friction, the contact of the rubbing solid surfaces must be examined on a microscopic level. According to the original tribologists, on a microscopic scale all surfaces are rough, looking more or less like mountain ranges [Bowden and Tabor, 1982]. The "mountains" are referred to as surface asperities. Figure 2.1 illustrates two surfaces in contact on this minute scale. As is shown in the figure, all of the load is borne by the "mountain peak" interfaces, better known as the asperity junctions.

The *true* area of contact, as indicated in Figure 2.1, is the sum of the asperity junction areas. The asperities will plastically deform as necessary when the normal load increases. In fact, the true area of contact will be proportional to

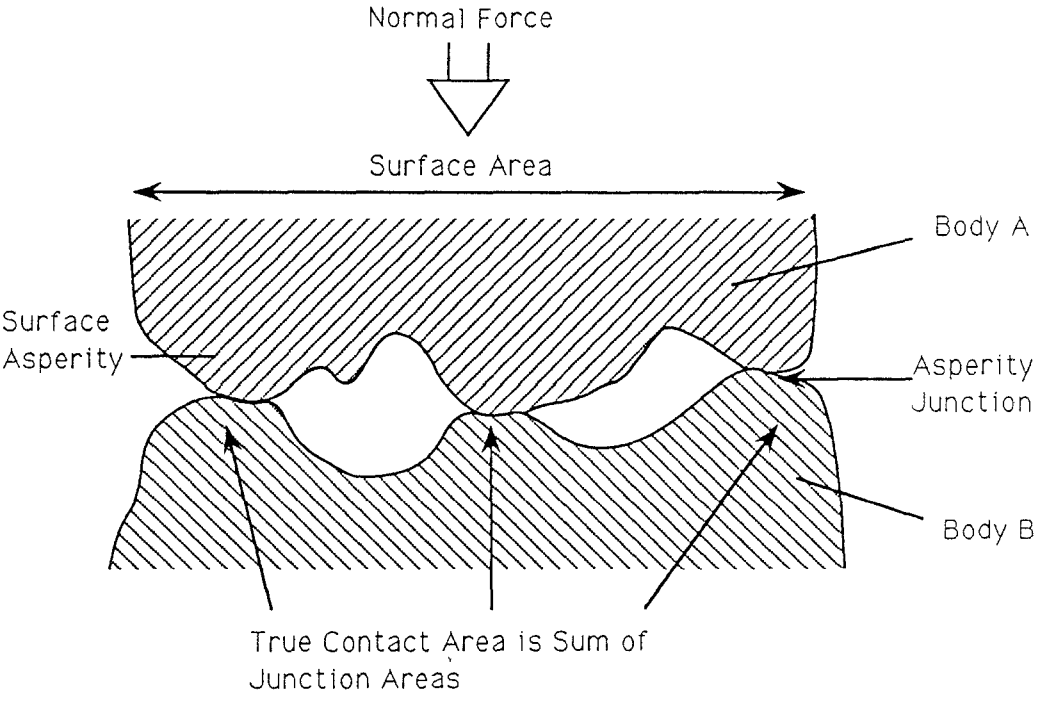

Figure 2.1: Microscopic View of Two Contacting Surfaces

the load as

$$\text{True Area of Contact} = \frac{\text{Load}}{\text{Yield Pressure}}, \tag{2.1}$$

where the yield pressure is a material property. If the surface area of the bodies is increased with the load held constant, the individual asperity junction areas may be dispersed, but the total true area of contact will remain the same. Figure 2.2 illustrates that true contact area is independent of surface area.

According to [Bowden and Tabor, 1982], friction is the shear strength of the asperity junction areas. Due to interatomic forces at these junctions, the two surfaces adhere. Friction is the force necessary to break the adhesion. Therefore,

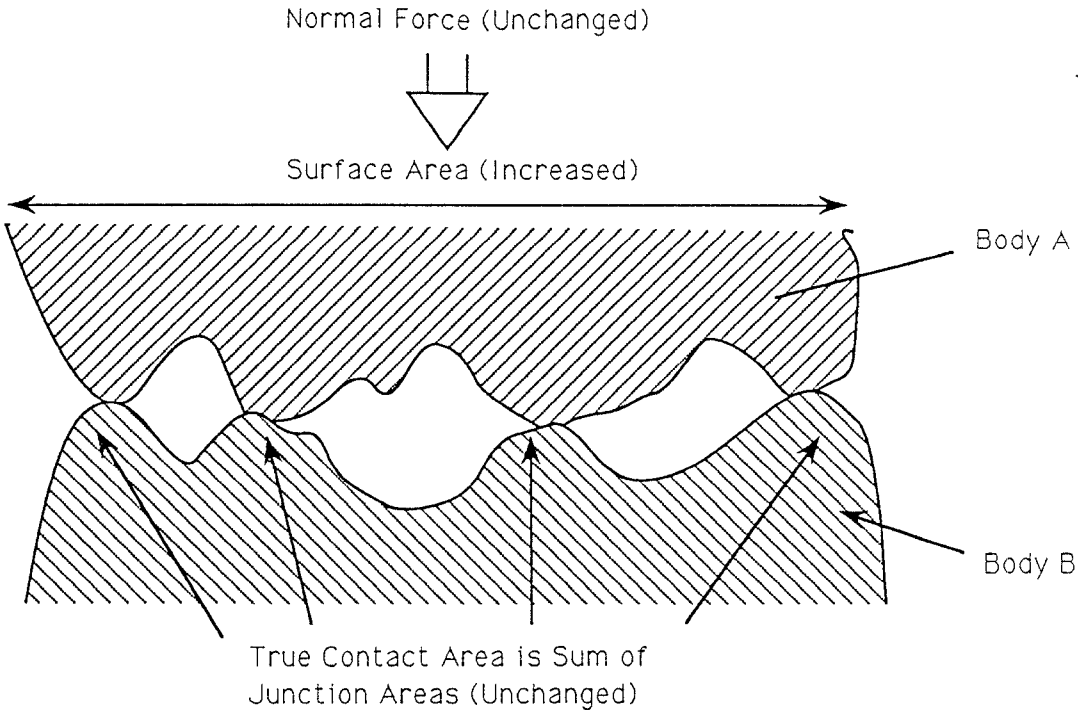

Figure 2.2: True Contact Area Independent of Surface Area

friction is proportional to the true contact area as

$$\text{Friction force} = (\text{True Area of Contact})\ (\text{Shear Force per Unit Area}), \quad (2.2)$$

where the required shear force per unit area is a material property. As a result, friction follows the same relationships as true area of contact, i.e., friction is proportional to the normal load and independent of the surface area as claimed above. Additionally, in this setting, the magnitude of the sliding velocity has no effect on kinetic friction. According to [Rabinowicz, 1965], the approximate independence of friction from sliding velocity magnitude is due to the approximate independence of material strength from stress application rate. The sliding

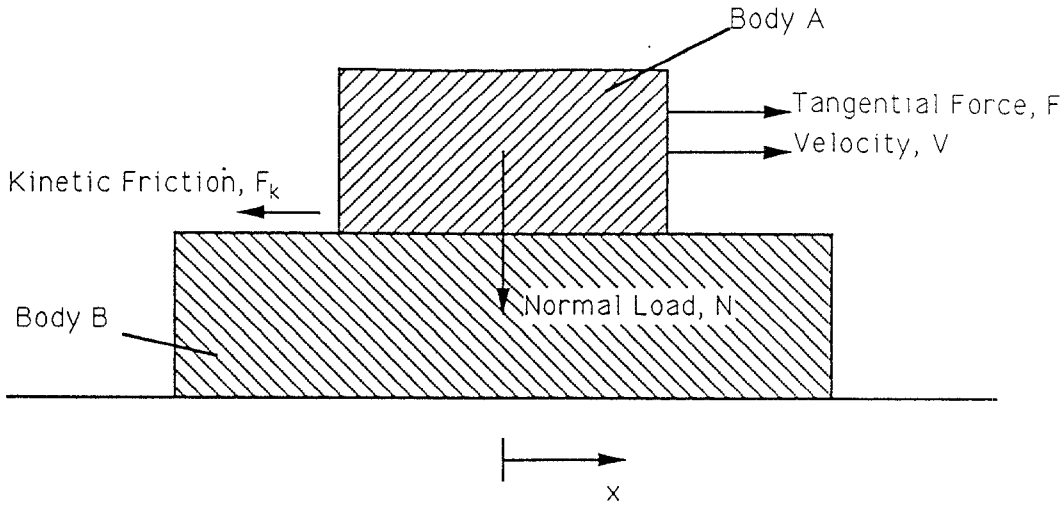

Figure 2.3: Kinetic Friction due to Relative Sliding Between Two Bodies

velocity direction is important, however, in that friction acts in the opposite direction of motion.

Based on these properties, the kinetic friction force F_k that results when one body slides over another, as shown in Figure 2.3, can be simply modelled as the product of the normal force N and a constant of proportionality f_k referred to as the coefficient of kinetic friction. The direction of F_k depends on the direction of the sliding velocity V as follows:

$$F_k = f_k N sgn(V) \,, \tag{2.3}$$

where

$$sgn(V) = \begin{cases} +1 & \text{if } V > 0 \\ -1 & \text{if } V < 0 \end{cases} . \tag{2.4}$$

A plot of this kinetic friction model is shown in Figure 2.4.

Some experimentalists have noted that in machines with rubbing parts more

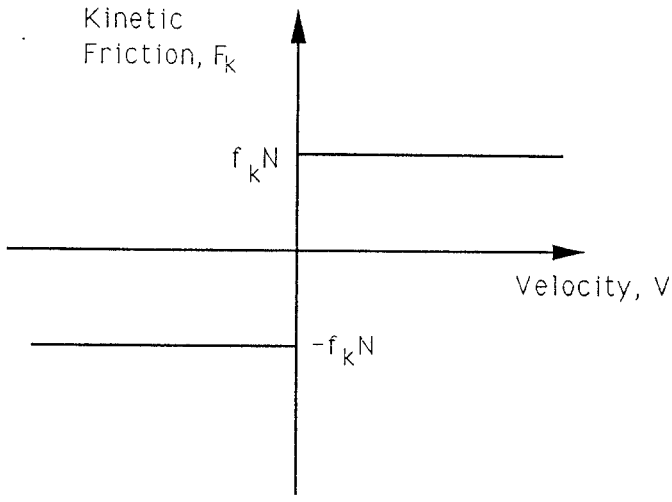

Figure 2.4: Kinetic Friction Model

complicated and numerous than a single body sliding over a second body, the magnitude of kinetic friction is not the same in the positive and negative directions [Canudas et al., 1986,Armstrong-Hélouvry, 1991,Wang, 1987]. A more general model of kinetic friction that accounts for this asymmetry is as follows:

$$F_k = \begin{cases} f_{k_p} N & \text{if } V > 0 \\ -f_{k_n} N & \text{if } V < 0 \end{cases} \tag{2.5}$$

where f_{k_p} and f_{k_n} are the kinetic friction coefficients in the positive and negative directions respectively. Figure 2.5 illustrates this asymmetrical kinetic friction model.

The model (2.3) or (2.5) indicates that kinetic friction simply acts as a constant retarding force for positive or negative velocities but that at zero velocity, friction is discontinuous. This behavior can be classified as a "hard nonlinearity". The relationship of Figure 2.4 is sometimes referred to as a relay type of

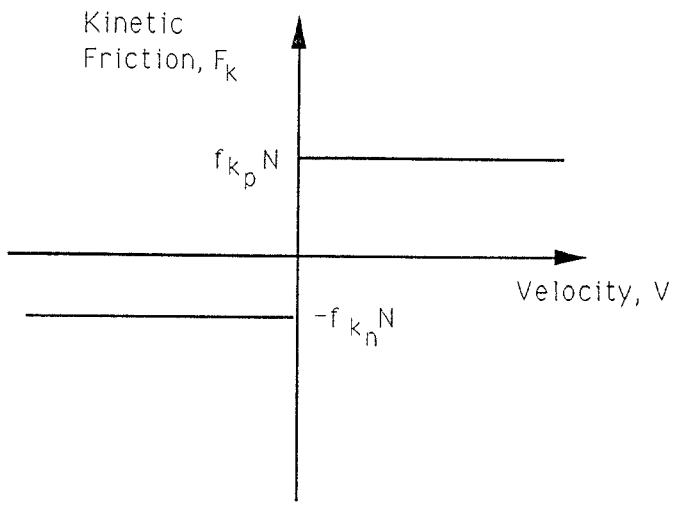

Figure 2.5: Asymmetrical Kinetic Friction Model

hard nonlinearity [Tsypkin, 1984].

According to nonlinear system theory, a closed loop system with a hard nonlinearity can produce a limit cycle. Limit cycles are manifest as self-sustained system oscillations. System oscillations, as a type of instability, can cause poor control accuracy. Therefore, it is important to determine whether or not friction can generate limit cycles. In [Slotine and Li, 1991] the authors use describing function analysis to show limit cycle existence and stability prediction for closed-loop systems with a hard nonlinearity of the form shown in Figure 2.6. The linear portion of the plant, $G(j\omega)$ is represented as a function of frequency ω, and j denotes $\sqrt{-1}$. The hard nonlinearity is approximated by a describing function $N(A,\omega)$ which is a function of the amplitude A and frequency ω of the time t dependent sinusoidal error signal $e(t)$. For single-valued hard nonlinearities

$$N(A,\omega) = N(A) \tag{2.6}$$

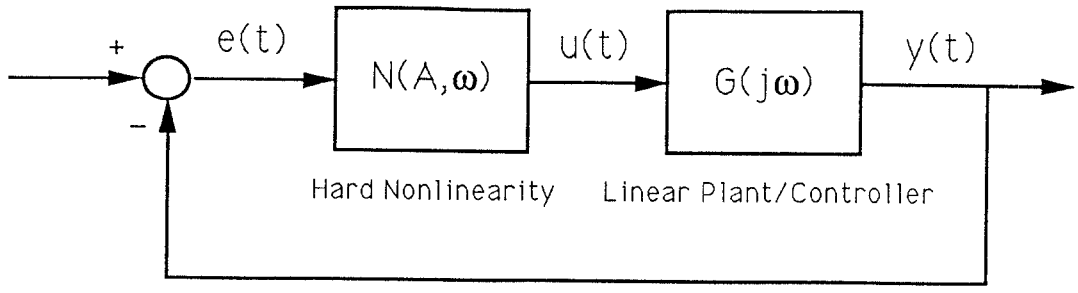

Figure 2.6: Standard Form for Describing Function Analysis of Closed Loop System with Hard Nonlinearity

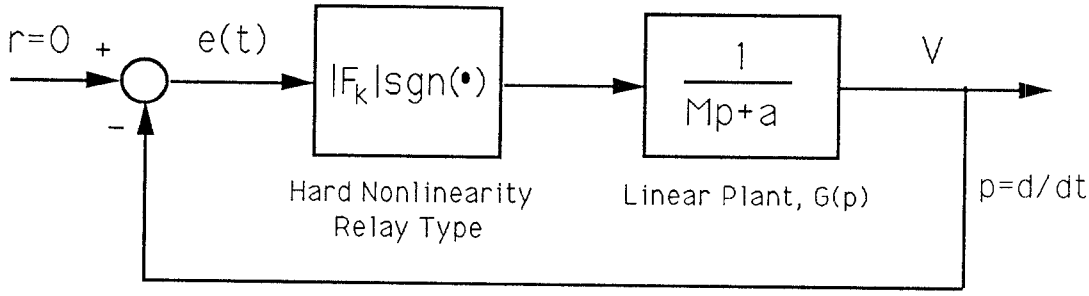

Figure 2.7: Dynamic System with Kinetic Friction and Damping

and is, therefore, always real-valued.

To check for the possibility of a limit cycle due to kinetic friction, first consider the equation of motion for Body A of Figure 2.3 with mass, $M > 0$, acceleration $\dot{V}$ and damping $a > 0$, that experiences kinetic friction:

$$M\dot{V} + aV = -|F_k|sgn(V)\,. \tag{2.7}$$

These dynamics can be represented by the block diagram of Figure 2.7. Note that if the hard nonlinearity is replaced by its describing function and $G(p)$ by its frequency domain representation $G(j\omega)$ then the system of Figure 2.7 conforms

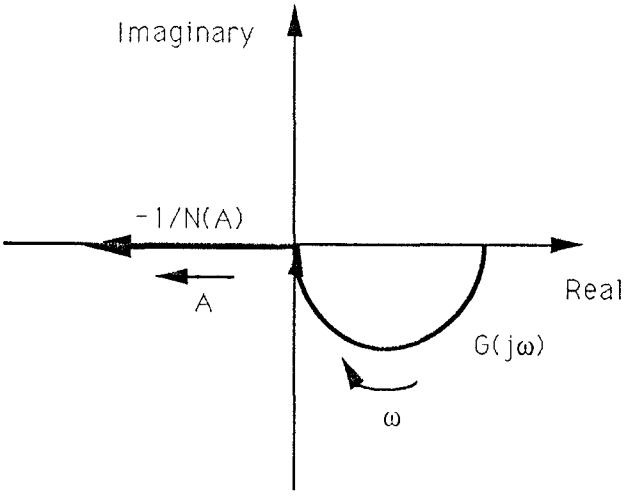

Figure 2.8: Describing Function Analysis Plot for Limit Cycle Detection in System of Figure 2.7

to the standard of Figure 2.6. Describing function analysis then predicts a limit cycle of amplitude A and frequency ω if

$$1 + G(j\omega)N(A,\omega) = 0\ , \tag{2.8}$$

i.e.,

$$G(j\omega) = -1/N(A,\omega)\ . \tag{2.9}$$

From [Slotine and Li, 1991], the describing function for the relay-type hard nonlinearity of Figure 2.4 is

$$N(A) = \frac{4|F_k|}{\pi A}\ . \tag{2.10}$$

Therefore, if $A > 0$ then $N(A) > 0$. Both $G(j\omega)$and $-1/N(A)$ for the dynamic system of Body A are plotted on the complex plane in Figure 2.8. As can be seen

from this figure, $G(j\omega)$and $-1/N(A)$ do not intersect for any $A > 0$; therefore, no limit cycle is predicted for the nonlinear system of (2.7).

Consider next a feedback control system that regulates the position of Body A of Figure 2.3 by applying a tangential force F that is proportionally controlled:

$$F = K_p(x_d - x) = K_p e \tag{2.11}$$

where

K_p is a constant proportional gain,

x_d is the demanded position,

x is the position,

e is the position error.

Since $|F|$ must exceed $|F_k|$ in order to provide an accelerating force on Body A, the force F_L applied to the linear part of the system is calculated as follows:

$$M\ddot{x} + a\dot{x} + bx = F_L \; = \begin{cases} F - |F_k| sgn(V) & \text{if } |F| > |F_k| \\ 0 & \text{if } |F| \leq |F_k| \end{cases} \tag{2.12}$$

where system stiffness $b > 0$ is assumed. This corresponds to a dead-zone for small forces. Figure 2.9 shows the closed loop system with proportional control and a dead-zone type of hard nonlinearity. From [Slotine and Li, 1991], for the dead-zone type nonlinearity of Figure 2.9

$$N(A) = \frac{2}{\pi}\left(\frac{\pi}{2} - sin^{-1}(\tfrac{|F_k|}{A}) - \tfrac{|F_k|}{A}\sqrt{1 - (\tfrac{|F_k|}{A})^2}\right) . \tag{2.13}$$

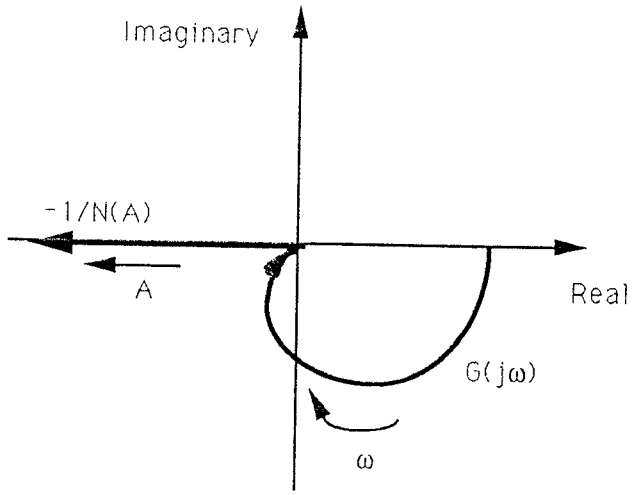

Figure 2.10: Describing Function Analysis Plot for Limit Cycle Detection in System with Proportional Control

respectively and

$$G(p) = \frac{K_i}{Mp^3 + ap^2 + bp} \,. \tag{2.16}$$

Since $G(p)$ is now a third order system, an intersection between $G(j\omega)$ and $-1/N(A)$ is possible as shown in Figure 2.11. This implies that integral position control of the mechanical system of Figure 2.3 which experiences kinetic friction may lead to a limit cycle. Assuming that $G(p)$ has no unstable poles, Figure 2.11 shows that the predicted limit cycle is stable, since with increasing A the $-1/N(A)$ curve increases away from the interior of the $G(j\omega)$ encirclement.

The above analysis yields predictions regarding the existence and stability of limit cycles in a simple mechanical system with kinetic friction for the various cases with and without proportional and integral control. However, because describing function analysis is an approximate technique, the predictions may

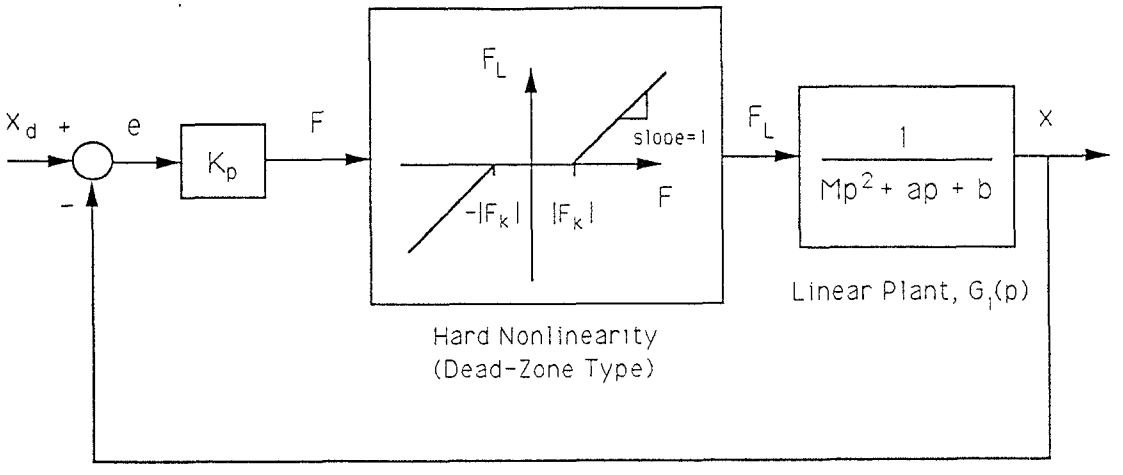

Figure 2.9: Dynamic System with Kinetic Friction, Damping and Proportional Control

To make Figure 2.9 fit the form of Figure 2.6 let

$$G(j\omega) = K_p G_1(j\omega) \, . \tag{2.14}$$

Figure 2.10 shows the corresponding plots of $G(j\omega)$ and $-1/N(A)$ on the complex plane. Again since it is not possible for the two lines to intersect, a limit cycle is not predicted.

However, it becomes clear that if integral control is used to regulate the position of Body A instead of (or in addition to) proportional control then

$$F = K_i(\int x_d - \int x) = K_i \int e \tag{2.15}$$

where K_i is a constant integral gain. The resulting closed loop system looks the same as in Figure 2.9 except that x_d and x are replaced with $\int x_d$ and $\int x$

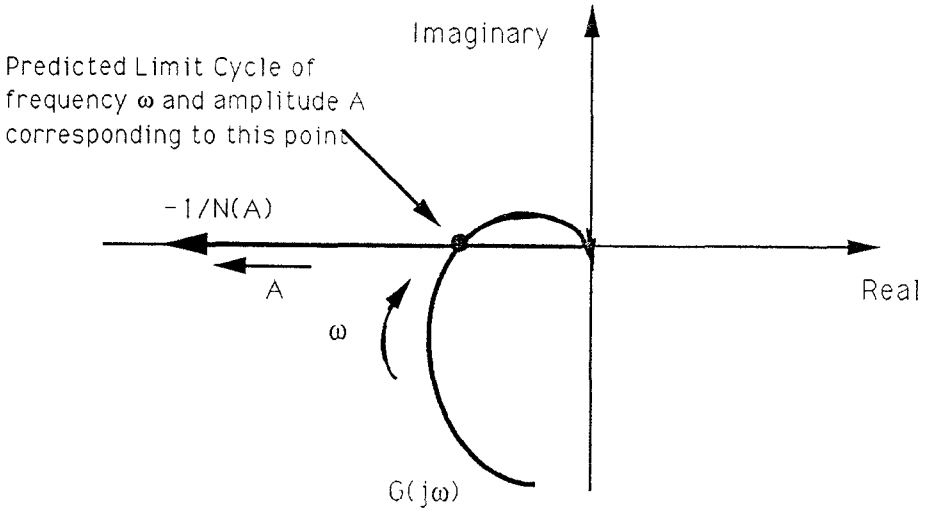

Figure 2.11: Describing Function Analysis Plot for Limit Cycle Detection in System with Integral Control

not be accurate especially if they are to be extended to more complex mechanical systems. In particular, for the describing function to be accurate, the assumption that high-frequency harmonics are negligible must hold [Slotine and Li, 1991], i.e.,

$$|G(j\omega)| \gg |G(jn\omega)| \text{ for } n = 2, 3, ... \tag{2.17}$$

If this assumption is not justified then there is the possibility that limit cycles have been erroneously predicted or omitted. The best way to confirm a limit cycle prediction or omission is by computer simulation. However, see [Bass, 1960,Mees, 1981] for mathematical support for the describing function technique.

Other researchers who have studied the possibility of kinetic friction generated limit cycles have found a variety of different results for a variety of different

systems. For example, in [Tou and Schultheiss, 1953] the authors performed a describing function analysis of a rotating member with kinetic friction and no damping. In addition to proportional and derivative control, they applied a two-stage lag network to regulate the angular position of the rotating member. A lag network is an approximation to integration that is practical for analog implementation. Based on the describing function analysis, they predicted a stable oscillation of 2 radian/second frequency. This prediction was confirmed using an analog computer implementation of the system and controller which calculated an oscillation of 1.6 radian/second. For the case with only a one-stage lag network, no limit cycle was predicted or calculated.

In their studies of force control in [Townsend and Salisbury, 1987], the authors found that kinetic friction produced only a simple response time delay when the transmission was modelled as nearly massless. However, when kinetic friction was included in a massive transmission, an actuator limit cycle was produced even though steady state force error went to zero.

In [Kubo et al., 1986] the authors considered a typical robotic manipulator with kinetic friction and proportional plus derivative (PD) position control. Using phase plane analysis, they determined that the position error would enter a limit cycle if the linear portion of the system had a pair of unstable poles and the input to the system was a ramp.

In [Radcliffe and Southward, 1990] the authors performed numerical simulation on a simple sliding block with kinetic friction like the one in Figure 2.3. Proportional, integral, and derivative (PID) control was used to regulate position and velocity to zero. Their system generated no limit cycles.

2.2 Viscous Friction

Viscous friction results from the viscous behavior of a fluid lubricant layer between two rubbing surfaces. The behavior of lubrication at a friction contact was first theoretically analyzed by Osborne Reynolds in the late nineteenth century [Bowden and Tabor, 1982]. Reynolds, who was studying locomotive wagon axles and bearings, described the mechanism for hydrodynamic lubrication of a shaft rotating in a bearing in the presence of a viscous fluid such as oil.

Specifically, when the shaft rotates it is drawn toward one side of the bearing. However, as the shaft moves, it drags with it some oil which flows between the shaft and the bearing at the side of close contact. Because it is close to the bearing, the oil velocity at the close contact side increases. The increased flow velocity results in increased pressure since the oil is viscous. As long as the speed of rotation of the shaft is high enough, the pressure will be large enough to maintain separation between bearing and shaft. The same argument holds for lubrication of two flat rubbing surfaces if one of the surfaces is slightly inclined

[Bowden and Tabor, 1982].

Hydrodynamic lubrication, which is a common form of lubrication in mechanical systems [Armstrong-Hélouvry, 1991], governs friction at nonzero velocities of sufficiently high magnitude. In particular, the viscosity of the lubricant determines the resulting friction/velocity relationship. According to [White, 1979], viscosity relates local stresses to strain rate in a moving fluid. Typically, for a fluid such as oil, the shear stress applied to the fluid element is proportional to the resulting strain rate which is equal to the velocity gradient. The constant of proportionality is referred to as the viscosity coefficient. Consequently, viscous friction F_v of a lubricated contact is represented as a linear function of velocity V as follows:

$$F_v = \mu V \tag{2.18}$$

where μ is the viscous friction coefficient. This model is represented in Figure 2.12.

As in the case of kinetic friction, experimentalists [Canudas et al., 1986, Armstrong-Hélouvry, 1991,Wang, 1987] have found different viscous friction coefficient values in the positive and negative velocity directions. A more general model of viscous friction which addresses these findings is as follows:

$$F_v = \begin{cases} \mu_p V & \text{if } V > 0 \\ \mu_n V & \text{if } V < 0 \end{cases} \tag{2.19}$$

where μ_p and μ_n are viscous friction coefficients in the positive and negative

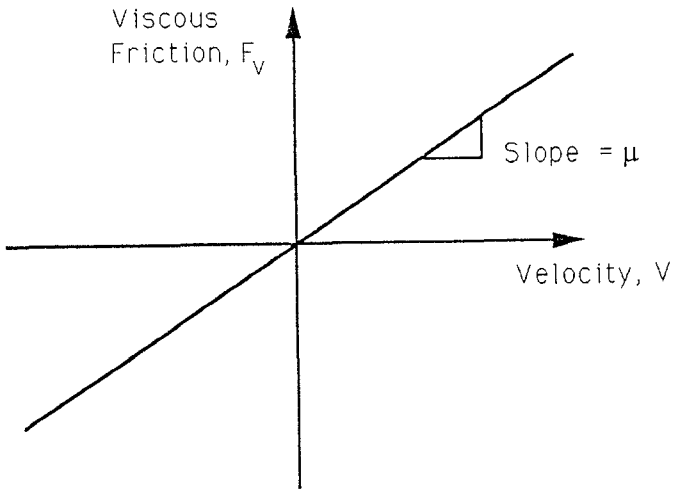

Figure 2.12: Viscous Friction Model

directions respectively. Figure 2.13 shows the general kinetic plus viscous friction model incorporating this asymmetric feature.

Tribologists have generally been concerned with the design of lubricants to minimize friction and wear in machinery. Indeed lubricants with high viscosity such as oil greatly reduce friction levels by decreasing the amount of solid-to-solid rubbing. As one might expect, however, different lubricants have different qualities. For example, viscosity decreases with temperature. Therefore, since high fluid velocities generate high temperatures, lubricants that have minimal viscosity dependence on temperature are preferable for friction reduction at high velocities.

From a dynamic point of view, viscous friction adds damping to a mechanical system. In fact, the damping assumed in the system of Figure 2.9 for the

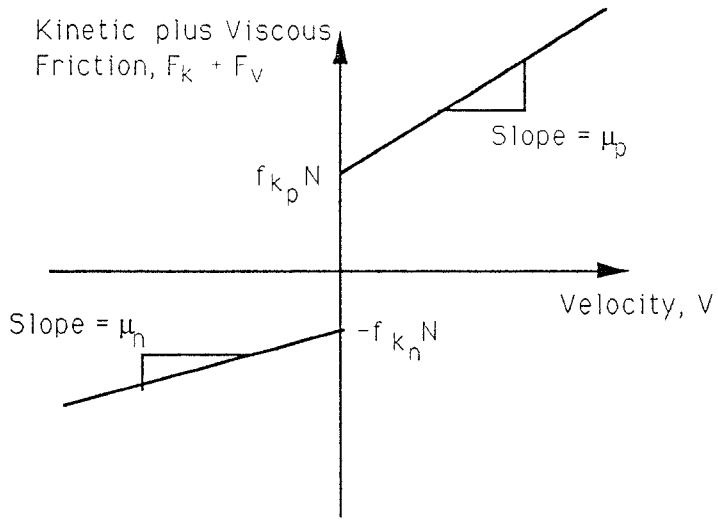

Figure 2.13: General Kinetic Plus Viscous Friction Model

describing function analyses of the previous section comes from viscous friction. To meet performance requirements, it may at times be desirable to adjust this level of damping. This can be achieved by changing the type of lubricant. However, an easier alternative for the control engineer would be to adjust damping artificially using velocity feedback control.

2.3 Static Friction and Stick-Slip

Initiating motion between two surfaces in contact typically requires more force than does sustaining that motion. Since friction provides the force that resists motion, the above observation implies that friction of a body at rest is greater than friction of a body in motion. As was discussed in Section 2.1, friction of body in motion corresponds to kinetic friction. To distinguish it from kinetic

friction, friction of a body at rest is commonly referred to as static friction or stiction.

In [Bowden and Tabor, 1982] the authors proposed three mechanisms that likely contribute to the greater magnitude of static friction relative to kinetic friction. First is the possibility that the true area of contact between surfaces at rest increases due to creep. This implies that friction, which is proportional to true area of contact, will be higher for surfaces at rest than for surfaces in motion. Second is the suggestion that interatomic forces at the asperity junctions grow with time of contact as atoms diffuse across the interface. This implies that higher forces are necessary to shear asperity junctions for surfaces at rest. Bowden and Tabor's third proposal pertains to surfaces covered with a contaminant or a lubricant film. They suggested that an increase in friction due to breakdown and penetration of the film may occur when a tangential force is applied to stationary surfaces. On the other hand, moving surfaces may simply slide over the film with no penetration and no increase in friction. The net effect is higher static friction than kinetic friction.

Static friction, like kinetic friction, is typically modelled as a function of normal force N, velocity V, and the static friction coefficient f_s. A static friction coefficient distinct from the kinetic friction coefficient was first proposed by A. Morin in the 1830's [Rabinowicz, 1956]. As a result, the classical lumped friction model F_f of static friction F_s, kinetic friction F_k, and viscous friction F_v, which

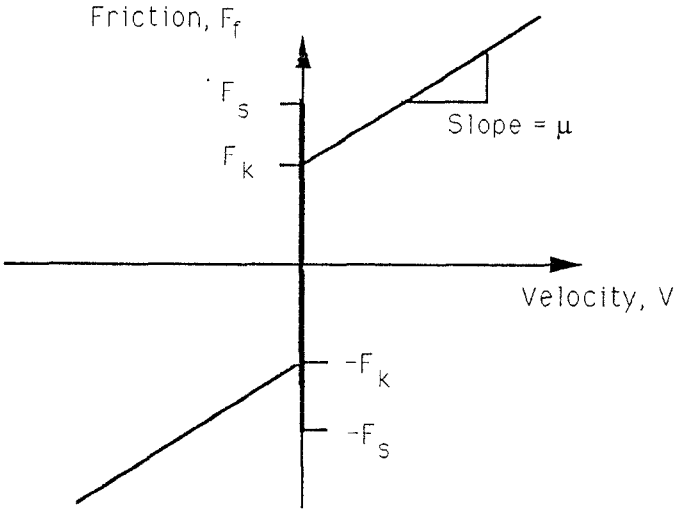

Figure 2.14: Classical Model of Static, Kinetic and Viscous Friction

depends on the applied tangential force F, is as follows:

$$F_f = \begin{cases} F_k sgn(V) + F_v & \text{if } V \neq 0 \\ F_s sgn(F) & \text{if } V = 0 \end{cases} \tag{2.20}$$

where

$$F_s = f_s N \tag{2.21}$$

$$F_k = f_k N \tag{2.22}$$

$$F_v = \mu V \, . \tag{2.23}$$

This basic model is illustrated in Figure 2.14. The model can be adjusted as necessary to account for asymmetrical friction coefficients in the positive and negative velocity directions.

When static friction in a mechanism is indeed greater than kinetic friction, intermittent motion known as "stick-slip" may result. Stick-slip manifests itself as repeated sequences of sticking between two surfaces with static friction

followed by sliding or slipping of the two surfaces with kinetic friction.

A simple system as shown in Figure 2.15 can be used to illustrate the stick-slip phenomenon [Bowden and Tabor, 1982]. A mass M resting on a surface is pulled at constant velocity V. The system stiffness K is represented by a spring located between the mass and the point moving at velocity V. Initially, the spring is not extended and so no force is applied to the mass (Figure 2.15(a)). With time t the force in the spring F_{spring} grows as

$$F_{spring} = KVt \; . \tag{2.24}$$

When static friction F_s is present, the mass will not accelerate until time t_1 when

$$F_{spring} = KVt_1 = F_s \; . \tag{2.25}$$

At this time t_1 the mass will begin to move, i.e., to slip (Figure 2.15(b)). Once motion is initiated friction drops to the kinetic friction level and

$$F_{spring} = F_s > F_k \; . \tag{2.26}$$

Therefore, an accelerating force is applied to the mass, and the mass accelerates in the direction of V. It is possible that the mass will achieve a velocity greater than V (Figure 2.15(c)). If this happens, the spring will begin to be compressed. When the spring is compressed back to its unextended length, the accelerating force applied to the mass will go to zero. Damping between the mass and the surface, generated by viscous friction, will drive the velocity of the mass to zero.

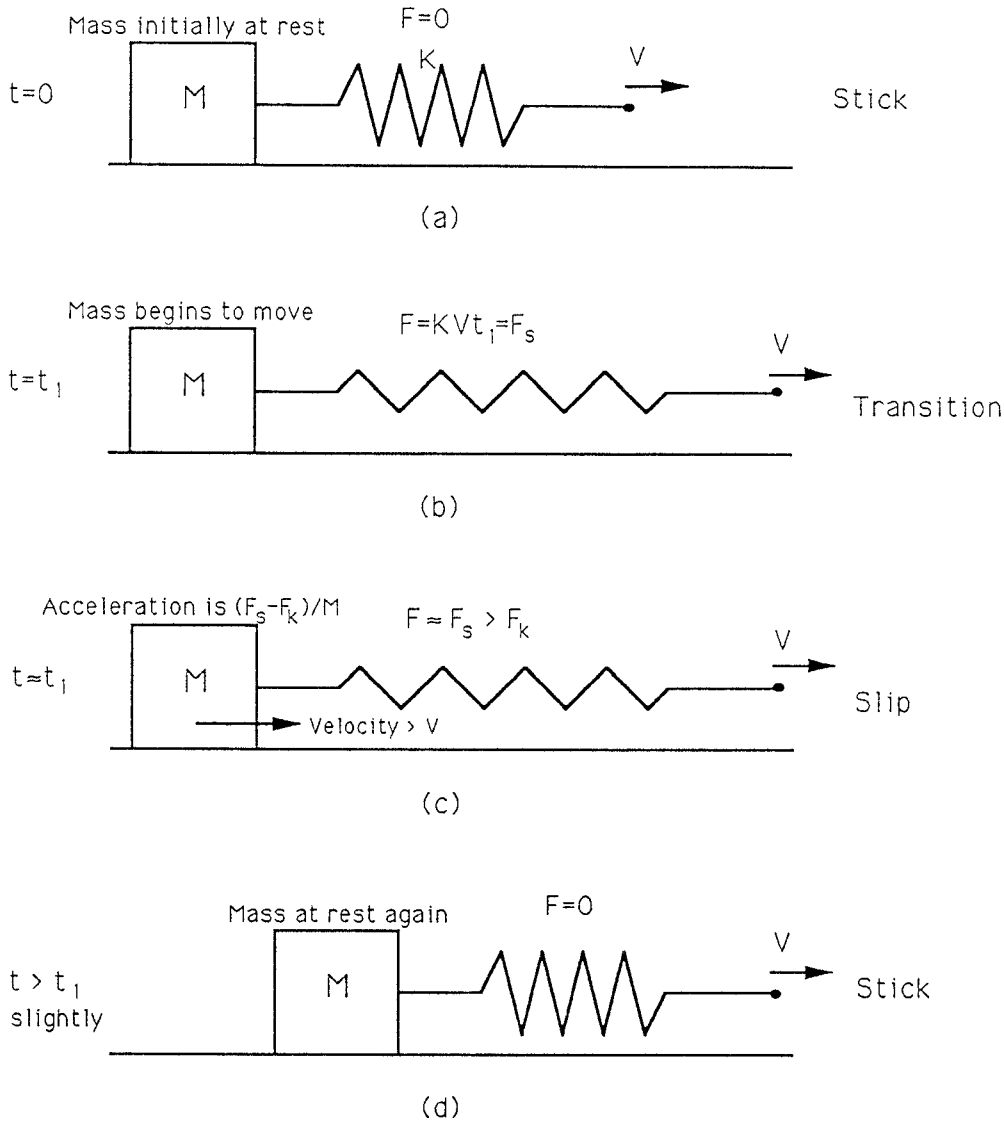

Figure 2.15: Stick-Slip in a Sliding Mass System

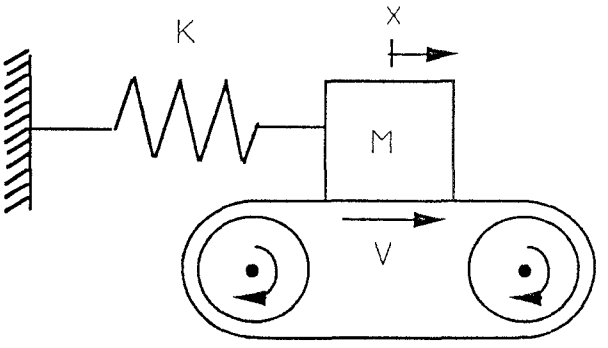

Figure 2.16: Sliding Mass System Used for Phase Plane Analysis of Stick-Slip

At this time the system will be back in its initial state, and the cycle will repeat (Figure 2.15(d)).

Stick-slip is evident in many everyday activities. The classic example of stick-slip occurs when a piece of chalk is dragged slowly across a chalkboard. Stick-slip causes the chalk to skip and skid leaving behind a dashed line instead of a solid line. Other examples of stick-slip include the creaking of doors, the squealing of automobile tires, and the music of a violin [Rabinowicz, 1956].

Phase plane analysis techniques can be used to further illustrate the stick-slip phenomenon and to estimate conditions that may lead to stick-slip. Consider, for example, Figure 2.16 which models a system with friction and compliance [Gogoussis and Donath, 1987]. In this system, a mass M rests on a belt that moves at constant velocity V. The mass is fixed to a wall by means of a spring with stiffness K. At the contact between the mass and the belt, static friction F_s is greater than kinetic friction F_k. From [Gogoussis and Donath, 1987],

this model can be interpreted as a representation of a simple motor where the observer is located on the rotating shaft. In this frame of reference the belt corresponds to the bearing housing and the mass-spring component corresponds to the rotating shaft.

Assuming first that the system has no static friction or viscous damping, the equation of motion of the (slipping) mass is

$$M\ddot{x} + Kx = F_k \, . \tag{2.27}$$

Thus, there is an equilibrium point at

$$x = F_k/K \, . \tag{2.28}$$

where the mass will remain in position as the belt slides by under it. If the position of the mass is perturbed, the system will behave like a simple harmonic oscillator, the mass oscillating about the equilibrium point. The phase plane plot of this system is shown in Figure 2.17.

When static friction is introduced, the mass will stick and travel with the belt if

$$\dot{x} = V \, . \tag{2.29}$$

The mass will then remain in the stuck position until the force in the spring equals the static friction force, i.e.,

$$x = F_s/K \, . \tag{2.30}$$

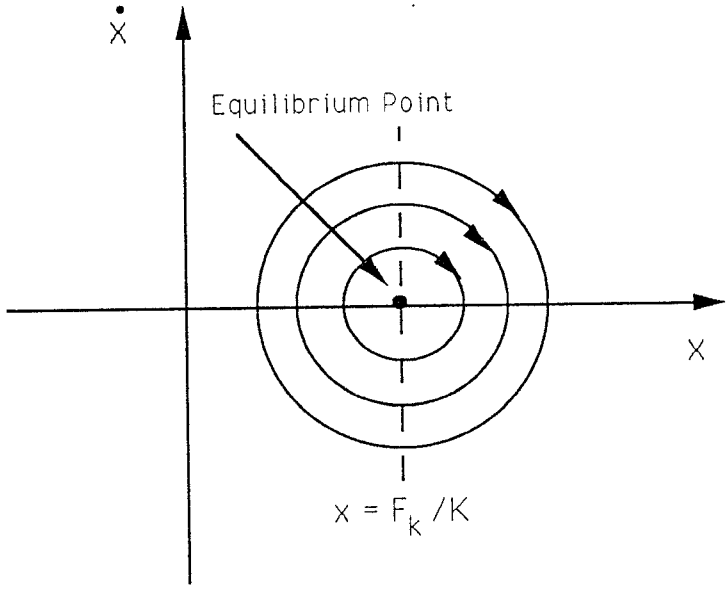

Figure 2.17: Phase Plane Diagram of Sliding Mass System with Kinetic Friction Only

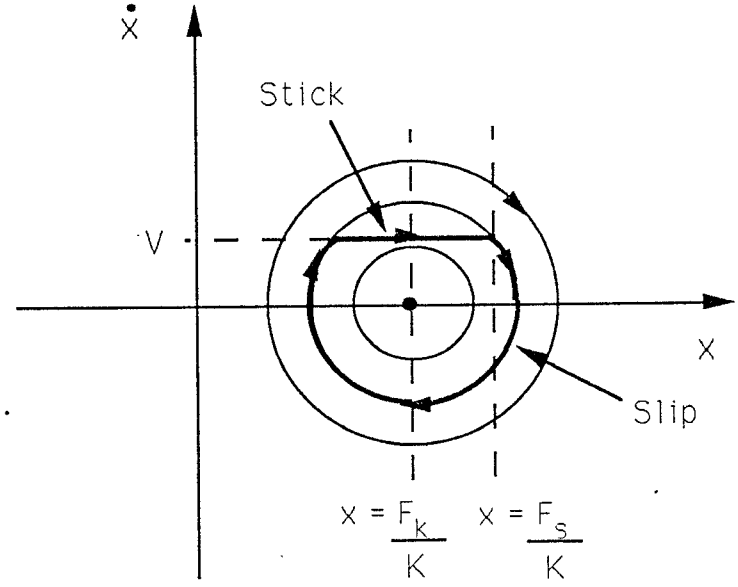

Figure 2.18: Phase Plane Diagram of Sliding Mass System with Static and Kinetic Friction

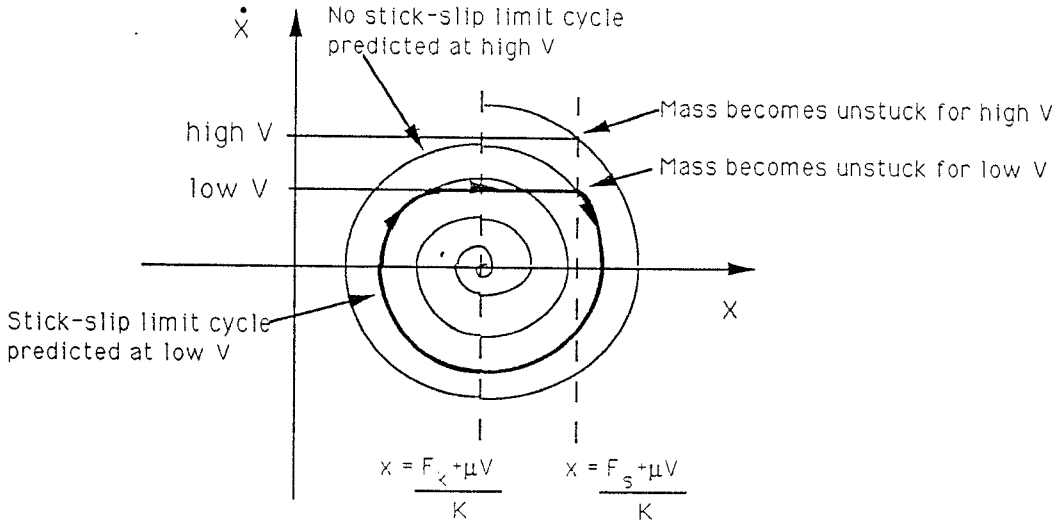

Figure 2.19: Phase Plane Diagram of Sliding Mass System with Static, Kinetic and Viscous Friction

This sticking behavior is shown in Figure 2.18.

Now suppose viscous damping is introduced into the system. Damping will be proportional to the relative velocity between the mass and the belt. The system equation for slipping becomes

$$M\ddot{x} + \mu(\dot{x} - V) + Kx = F_k \tag{2.31}$$

where μ is the viscous friction coefficient. The new equilibrium will occur at

$$x = \frac{F_k + \mu V}{K} . \tag{2.32}$$

Figure 2.19 shows the phase plane diagram for the system (2.31). For a given level of damping, it can be seen that under certain initial conditions if the belt velocity is relatively low, a stick-slip limit cycle is predicted, while if

the belt velocity is relatively high stick-slip is not predicted. Similarly, for a given belt velocity, it can be seen that stick-slip can be avoided if the damping or the stiffness is high enough. An example calculation of conditions that yield the possibility of such a stick-slip limit cycle is described in Section 4.2 for the motor under investigation in this thesis.

Because simplifying assumptions are typically made in modelling a system for phase plane analysis, it is always best to confirm behavior predictions with numerical or experimental data. However, the model of static, kinetic, and viscous friction (2.20) is difficult to implement numerically since neither $F(V)$ nor $V(F)$ is a single-valued function.

In [Karnopp, 1985] the author presented a model for sticking and slipping that assumes static friction persists for a range of very low velocities and kinetic friction applies for velocities outside this range. Using this model, Karnopp was able to numerically predict stick-slip for complicated sliding mass systems. In [Radcliffe and Southward, 1990] the authors applied Karnopp's model to a simple sliding mass control system and predicted a stick-slip limit cycle with PID control but not with PD control.

In [Haessig and Friedland, 1990] the authors presented an alternative numerical model of stick-slip friction based on a "bristle model". This model represents the contact surface asperities as bristles and predicts how the bristle bonds will be created, strained and broken. The bristle behavior determines the friction

dynamics. Simulations with the bristle model showed effective stick-slip prediction for a simple sliding spring-mass system. The bristle model, when applied to a position-controlled rotary gimbal, predicted no limit cycle. As confirmation, no limit cycle was observed in the experimental data.

Some of the researchers who considered only kinetic friction conditions, as described in Section 2.1, also considered the case with static friction present. For example, in [Townsend and Salisbury, 1987] the force control studies predicted that the static plus kinetic friction model leads to a stable limit cycle when integral control is used. Analyzing a rotating member with static and kinetic friction, the authors of [Tou and Schultheiss, 1953] predicted the possibility of a limit cycle when a one stage lag network is applied in series with PD control. In particular, they found that the likelihood of the limit cycle depends on the ratio of static to kinetic friction.

2.4 Pre-Sliding Displacement

Contrary to the predictions derived from the classical friction model of the previous sections, small relative displacements between two bodies in contact do occur when the applied relative tangential force F_{appl} is *less* than the static friction F_s. The magnitude of these pre-sliding displacements is typically smaller than the diameter of an asperity junction [Courtney-Pratt and Eisner, 1957].

However, with sufficient gain, as in a robot with a fairly long link, small displacements at the rubbing surface can translate into significant displacements elsewhere in the mechanism [Armstrong-Hélouvry, 1991]. Most importantly, the nature of pre-sliding displacements provides insight into the transition between sticking and sliding.

In [Courtney-Pratt and Eisner, 1957] the authors investigated the pre-sliding displacement phenomenon in their experiments on rubbing metal surfaces. While applying a monotonically increasing tangential force to one of the surfaces under constant normal load N, they measured the microscopic displacements using a multiple-beam interferometer. From these measurements, they plotted the relationship between the displacement x and the coefficient of friction f where

$$f = F_{appl}/N \ . \tag{2.33}$$

They found both elastic (reversible) and plastic (irreversible) components in the relationship as shown in Figure 2.20. The shape of the friction-displacement curve was the same for all metals and all loads tested. Even application of a lubricant at the rubbing surfaces did not affect the nature of the relationship. In each case with increasing displacement, the friction coefficient increased smoothly from zero asymptotically approaching the static friction coefficient level. The displacements measured were on the order of a few microns.

Courtney-Pratt and Eisner interpreted the pre-sliding phenomenon within the framework of the theory of asperity junction adhesion, described in Section

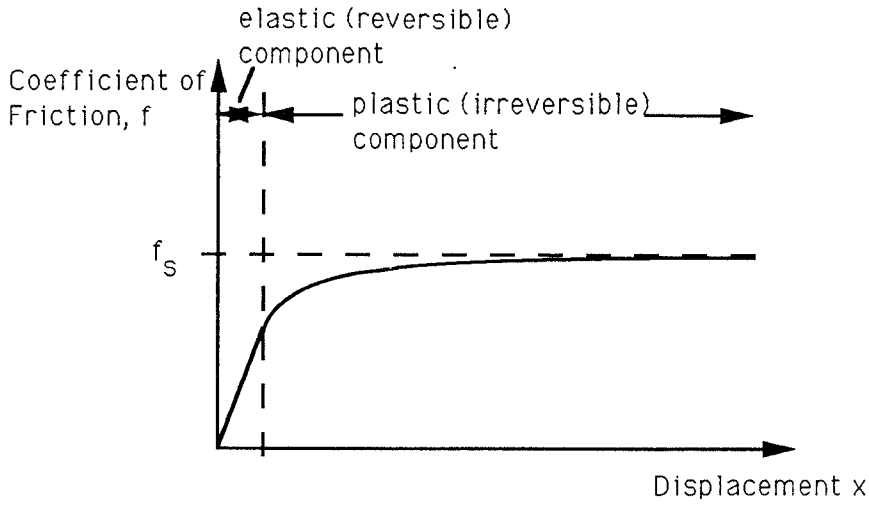

Figure 2.20: Friction-Displacement Relationship

2.1. Basically, as the shear force at the contact surface increases, the asperity junctions deform elastically and then plastically. When the applied force finally reaches the static friction level, the asperity junctions break and sliding begins.

Because the asperity junctions experience plastic deformation as the applied tangential force is increased, a subsequent monotonic decrease in applied tangential force yields a different friction-displacement relationship. When the force begins to decrease, the relationship is first elastic and then plastic. As a result, alternate increases and decreases in applied tangential force manifest themselves as hysteresis loops as shown in Figure 2.21 [Courtney-Pratt and Eisner, 1957].

Further evidence of the pre-sliding displacement phenomenon has come from several other researchers who have performed tests on a variety of experimental setups. For example, [Burdekin et al., 1978] investigated tangential deflections

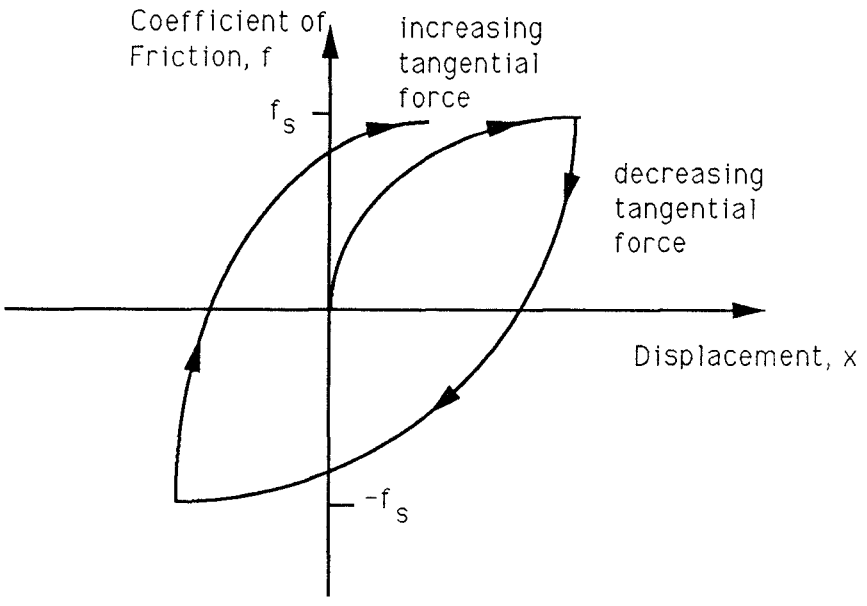

Figure 2.21: Friction-Displacement Hysteresis Loops

at the interface of preloaded machined surfaces in contact. In their experiments they applied normal and tangential forces to a stack of grey cast-iron rings and measured normal and tangential displacements. The tangential forces applied were less than the static friction. Their results confirm the results of Courtney-Pratt and Eisner since the relationship between the applied tangential force and the measured tangential displacement, at several different constant normal loads, takes the form of Figures 2.20 and 2.21. In [Gassenfeit and Soom, 1988] the authors observed elastic and plastic pre-sliding displacement in their experiments on an aluminum block sliding between two steel beams.

In [Rabinowicz, 1951] the author also performed experiments to measure pre-sliding displacements of surfaces in contact. In his experiments, Rabinowicz

rolled a small spherical ball against a large block on an inclined plane, measured the distance travelled by the large block, and thus was able to predict the critical displacement at which sliding would occur. The critical displacements predicted were on the order of a few microns and, therefore, agree with the other results cited above.

Rabinowicz's experimental findings supported using the asperity junction adhesion theory as a theoretical basis for the observed pre-sliding displacements. In particular, since the theory predicts that sliding occurs when the asperity junctions break, it is expected that the critical displacement should be about equal to the asperity junction diameter. His calculations showed that the diameter of the asperity junctions for one of his experiments was 17 microns compared to the calculated critical displacement of 7 microns. These distances are in fairly close agreement.

In [Dahl, 1976,Dahl, 1977] the author provided a good model of the pre-sliding displacement phenomenon that generates the observed hysteresis loops. This model assumes that friction F_f is a function of displacement x and time t. Therefore,

$$\frac{dF_f(x,t)}{dt} = \frac{\partial F_f(x,t)}{\partial x} \cdot \dot{x} + \frac{\partial F_f(x,t)}{\partial t} , \tag{2.34}$$

it is assumed that $\partial F_f/\partial t = 0$, and as an approximation to observations

$$\frac{\partial F_f(x,t)}{\partial x} = \sigma |1 - \frac{F_f}{F_{f_c}} sgn(\dot{x})|^i \cdot S , \tag{2.35}$$

where

$\dot{x}$ is velocity,

σ is the slope of the F_f versus x curve at $F_f = 0$,

F_{f_c} is the magnitude of friction that is approached asymptotically,

i is an exponent parameter,

S is a factor that Dahl includes to ensure computer simulation stability.

In his work on a ball bearing friction experiment, Dahl [Dahl, 1977] measured the hysteresis loop and then determined the various unknown parameters of his model. Of most interest is his calculation of $i \approx 1.5$ as the best fit exponential parameter. For these contributions, the pre-sliding displacement phenomenon is often referred to as the "Dahl effect".

Armstrong observed the Dahl effect in his low velocity friction measurements [Armstrong, 1988,Armstrong-Hélouvry, 1991]. In his experiments, performed on a PUMA 560 arm, Armstrong found that the rise in friction corresponding to a change from zero velocity to a low positive velocity was constant with position change. That is, the PUMA joint was displaced roughly the same amount each time the conditions changed from sticking to sliding. The magnitude of this pre-sliding displacement was approximately 2 microns, computed from an observed 0.0003 radian transition distance on a bullgear. This is of the same order as previously described displacements.

Other researchers investigating pre-sliding displacements have developed alternative models to Dahl's model. In [Villanueva-Leal and Hinduja, 1984] the authors represented the hysteresis loops of Figure 2.21 using third-degree polynomials. They performed finite element analyses using this model and confirmed their results with experimental data. In [Cheng and Kikuchi, 1985] the authors also performed finite element analyses of contact surfaces. They modelled friction with pre-sliding displacements according to rules that characterize the behavior of an "elastic work-hardening" material.

Many researchers are cited in [Dahl, 1977] as having successfully used Dahl's friction model in simulations of bearing friction. Most recently Dahl's model has been used for control applications. In particular, a friction-compensating adaptive controller based on Dahl's model was designed for the stabilization of an airborne pointing and tracking system [Walrath, 1984]. The resulting success at reducing position error by accounting for friction provides further evidence for the accuracy of Dahl's model.

Because of his particular application, Walrath was most concerned with accurately modelling transient friction behavior when the relative motion of the rubbing parts experiences velocity reversals, i.e., from positive to negative to positive velocity, etc. He found from experimentation that friction responds smoothly to velocity reversals as shown in Figure 2.22. Using the classical discontinuous static-kinetic friction model, Walrath could not re-create this smooth

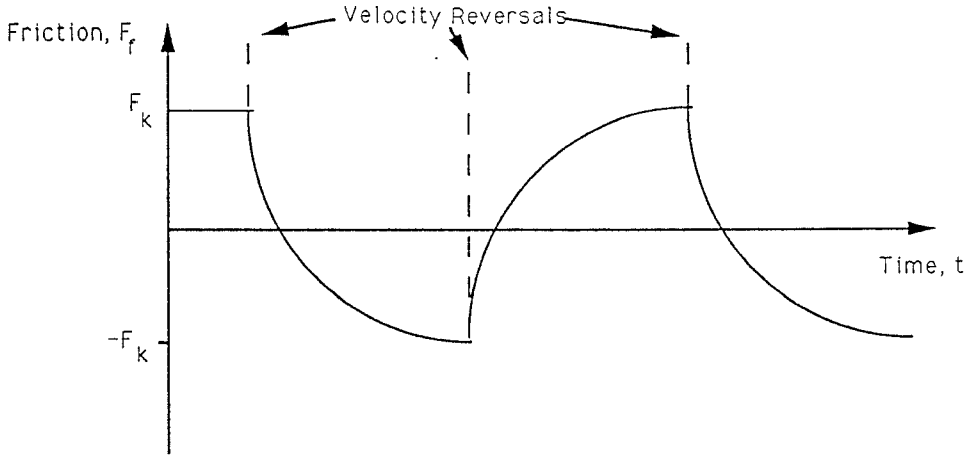

Figure 2.22: Friction Response to Velocity Reversals

behavior. Instead the classical model predicted the jerky behavior shown in Figure 2.23. Dahl's model, on the other hand, predicted the smooth behavior of Figure 2.22. This result illustrates that during velocity reversals there is a smooth friction transition through zero velocity effectively characterized by the pre-sliding displacement phenomenon. The classical friction model predicts behavior more characteristic of a system that spends longer periods of time at zero velocity. The effect of time on static friction is described in the next section.

Walrath's control strategy is described in further detail in Chapter 3. A control strategy very much like it has been implemented for the investigation that is central to this thesis. Its implementation and results are discussed in Chapters 4.

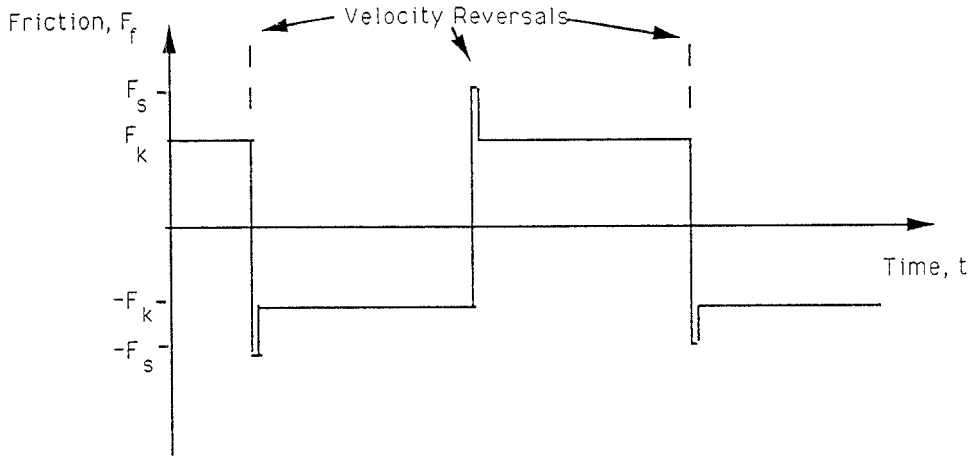

Figure 2.23: Classical Friction Model Prediction of Response to Velocity Reversals

2.5 Static Friction Dependence on Dwell Time

The physical mechanisms responsible for the positive difference between static friction and kinetic friction rely on the fact that static friction occurs when the time of contact between surfaces is nonzero. As described in Section 2.3, static friction is high because when the surfaces are at rest, asperity junction area will grow due to creep, or interatomic forces will increase as atoms diffuse across the interface. These physical mechanisms suggest that the magnitude of static friction is dependent on the length of time the surfaces are at rest, i.e., the "dwell time". According to the data of Ishlinski, Kragelski, and Dokos [Rabinowicz, 1958] and [Sampson et al., 1943], static friction is roughly linear with the logarithm of dwell time t_d. When two surfaces come to rest, static friction initially increases quickly. As the dwell time increases, static friction

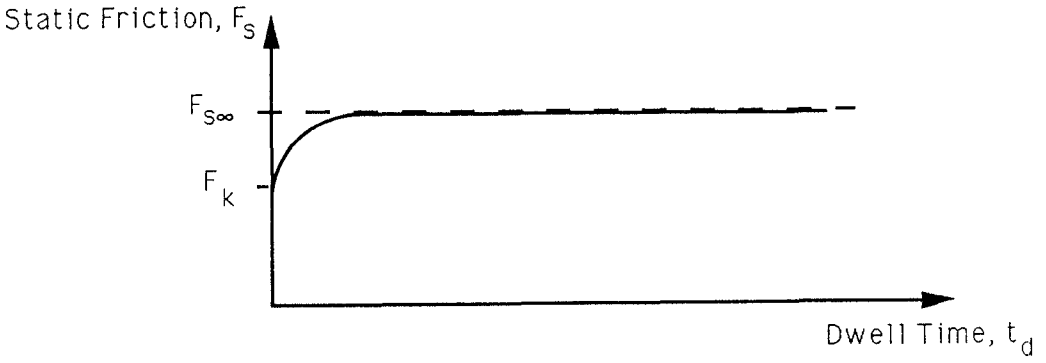

Figure 2.24: Static Friction Dependence on Dwell Time

grows more slowly, asymptotically approaching some infinite static friction level $F_{s\infty}$. Figure 2.24 depicts this relationship between static friction and dwell time. [Kato et al., 1972] confirmed this relationship with experiments in which static friction was measured as a function of dwell time.

Providing further support for this relationship, Rabinowicz used the time dependence of static friction to explain observed variations in stick-slip amplitude with changes in velocity [Rabinowicz, 1958] . Referring to a system similar to that of Figure 2.16, Rabinowicz claimed that according to the observations of Blok, under stick-slip conditions the amplitude of the stick-slip limit cycle decreases with increasing velocity. An increase in velocity implies a shorter dwell time and therefore lower static friction. As illustrated in Figures 2.18 and 2.19, the amplitude of the stick-slip limit cycle is proportional to the difference between static and kinetic friction. Thus, at increased velocity, the resulting lower static friction will yield a smaller stick-slip limit cycle amplitude. In fact, above some critical velocity the stick-slip oscillations disappear altogether.

This is because at velocities greater than or equal to the critical velocity, dwell time is too short to generate a level of static friction that will lead to stick-slip [Armstrong-Hélouvry, 1991].

In [Kato et al., 1972] the authors presented the following model of time-dependent static friction based on their empirical results:

$$F_s(t_d) = F_k + (F_{s\infty} - F_k)(1 - e^{-\gamma {t_d}^m}) , \tag{2.36}$$

where γ and m are empirical parameters. In [Derjaguin et al., 1957] the authors proposed a slightly different model of static friction as

$$F_s(t_d) = F_k + (F_{s\infty} - F_k)\frac{t_d}{t_d + \alpha} , \tag{2.37}$$

where α characterizes the time of static friction rise.

Armstrong verified these models in experiments on one joint of a PUMA 560 robot [Armstrong-Hélouvry, 1991]. He plotted measured values of $(F_s - F_k)$ versus t_d under stick-slip conditions for several different velocities and stiffnesses. After determining the best-fit parameters: γ, m, and α; Armstrong plotted the curves predicted by the two models above. He found that the curves predicted similar behavior and both closely approximated the empirical data.

Using the static friction model of (2.37), Armstrong analyzed the stick-slip behavior of a system as in Figure 2.16. By means of perturbation analysis, Armstrong isolated the effect of static friction as described by (2.37) on the existence of a stick-slip limit cycle. His analytic results confirmed Rabinowicz's

conclusion that due to static friction variation with dwell time, stick-slip will not occur above a critical velocity (dependent on many factors such as $F_{s\infty}$, α, and stiffness).

2.6 Friction Variations with Velocity

While the simple static plus kinetic friction model offers an intuitive explanation for the possibility of stick-slip oscillations, it inadequately justifies the existence of these limit cycles for all the conditions under which they have been observed [Dudley and Swift, 1949]. For example, several of the researchers cited at the end of Section 2.3 were unable to theoretically or numerically predict stick-slip limit cycles based on the static plus kinetic friction model unless integral control was used. However, stick-slip oscillations have been observed even when integral control was not used [Armstrong, 1988].

Using phase plane analysis, in [Dudley and Swift, 1949] the authors showed that a negatively-sloped kinetic friction versus velocity relationship near zero velocity was a sufficient condition for stick-slip oscillations at low velocities. In other words, Dudley and Swift expected that with increasing velocity, friction will drop gradually from the static friction level to the kinetic friction level rather than abruptly as predicted by the classical friction model of Figure 2.14. An example of this friction variation with velocity is depicted in Figure 2.25.

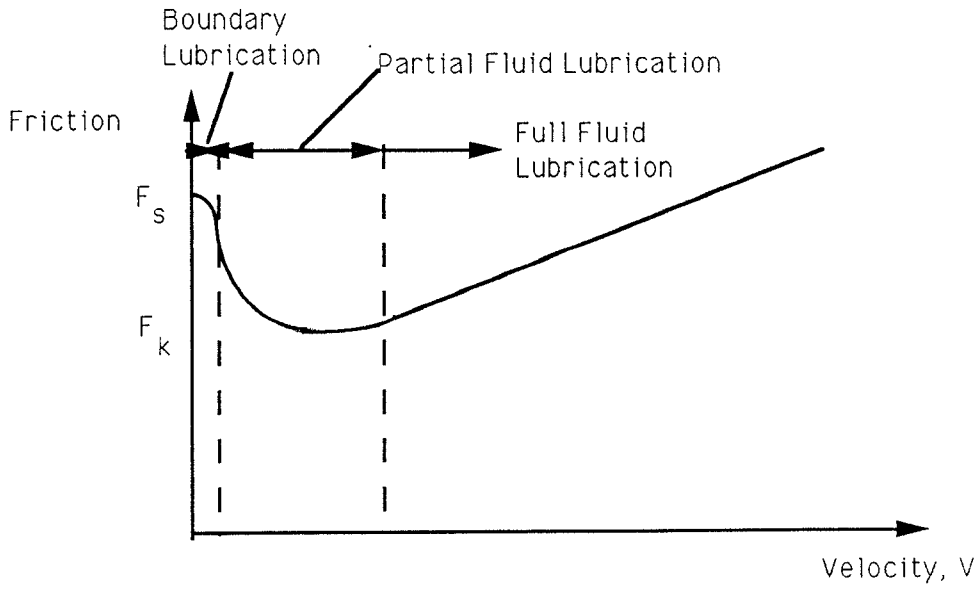

Figure 2.25: Friction Variation with Velocity

In [Gassenfeit and Soom, 1988] the authors, performing experiments on an aluminum block sliding between steel beams, observed this expected friction-velocity relationship. Plots of their measurements of friction versus velocity take the form of the velocity-dependent friction curve of Figure 2.25. Curves of this form were generated for an unlubricated interface as well as for most lubricated interfaces.

The velocity-dependent friction behavior can be explained from a physical perspective most easily for a lubricated interface. The following discussion (including the discussion of lubricant additives) is taken from [Armstrong-Hélouvry, 1991] which follows the argument of earlier tribology literature, e.g., [Bowden and Tabor, 1982,Rabinowicz, 1965]. At the lowest velocities, just as slip begins, the surfaces in contact experience boundary lubrication

as indicated in Figure 2.25. In this range the velocity is too low to produce a fluid layer between the surfaces. As a result, the outer boundary layer serves as lubricant and solid-to-solid rubbing prevails. However, the shear force required for sliding under these conditions is less than that required to break the initial asperity junction adhesion. Therefore, friction decreases slightly in the boundary lubrication range.

At higher velocities, the lubrication becomes partially fluid as shown in Figure 2.25. As velocity increases fluid lubrication predominates instead of boundary layer lubrication, and the shear force required for sliding drops. This is manifest as a decrease in friction with increasing velocity until viscous friction becomes significant and friction begins to rise with velocity. Above some critical velocity, lubrication is fully fluid and viscous friction predominates. In unlubricated interfaces, similar behavior may result when contaminants and oxide layers play the same role as a lubricant.

Lubricant additives make it possible to change the friction-velocity curve such that there is no negatively-sloped range. In effect these additives reduce static friction and friction in the boundary lubrication regime. For example, certain types of "way oils" can lower static friction *below* the level of kinetic friction so that friction always increases with velocity. However, these oils only work at relatively low temperatures so that if there is a lot of heat generated from friction they will become ineffective. Extreme pressure agents are another

alternative that reduce solid friction at relatively high temperatures; however, they have the disadvantage of being corrosive.

Several models have been proposed of the velocity-dependent friction component, often referred to as the "Stribeck effect". These models have been derived to approximate empirical data. They are generally of the form: kinetic friction (2.22) plus viscous friction plus a Stribeck friction term F_{str} that includes static friction, i.e.,

$$F_f(V) = F_k sgn(V) + \mu V + F_{str}(V) sgn(V) \; . \tag{2.38}$$

In [Hess and Soom, 1990] the authors proposed the following:

$$F_{str}(V) = F_{sk} \left(\frac{1}{1 + (V/V_{str})^2} \right) \tag{2.39}$$

where V_{str} is a critical velocity related to the Stribeck effect and $F_{sk} = F_s - F_k$. Others use a model of the form

$$F_{str}(V) = F_{sk} e^{-(V/V_{str})^a} \tag{2.40}$$

where a is a parameter. Variations on these include multiple terms [Armstrong-Hélouvry, 1991]:

$$F_{str}(V) = F_{sk_1} e^{-(V/V_{str_1})^a} + F_{sk_2} e^{-(V/V_{str_2})^a} \tag{2.41}$$

or

$$F_{str}(V) = F_{sk_1} \left(\frac{1}{1 + (V/V_{str_1})^2} \right) + F_{sk_2} \left(\frac{1}{1 + (V/V_{str_2})^2} \right) \; , \tag{2.42}$$

and offsets:

$$F_{str}(V) = F_{sk_1} e^{-((V - V_{o_1})/V_{str_1})^a} + F_{sk_2} e^{-((V - V_{o_2})/V_{str_2})^a} \tag{2.43}$$

[Armstrong, 1988] found that (2.41) with $a = 2$ best fit his data.

To best match his needs for an adaptive control implementation, i.e., to derive system equations linear in the parameters, Canudas de Wit proposed a linearized friction model that included Stribeck friction [Canudas de Wit, 1989]:

$$F_f(V) = \alpha_0 sgn(V) + \alpha_1 V + \alpha_2 |V|^{1/2} sgn(V) \,, \tag{2.44}$$

where α_0, α_1, and α_2 are the adaptive parameters.

Since each of these models preserves the negatively sloped friction-velocity curve at low velocities, each can be used to illustrate stick-slip behavior. Researchers, e.g. [Gogoussis and Donath, 1987], have used nonlinear analysis techniques such as phase plane analysis to predict limit cycles in sliding systems as a consequence of this negatively-sloped region of the friction curve. These limit cycles are predicted *without* integral control.

Using the model of (2.40) with $a = 2$, Armstrong investigated limitations posed by the Stribeck effect on mechanism performance [Armstrong, 1989, Armstrong-Hélouvry, 1990]. By means of dimensional analysis, he derived theoretical predictions for important stick-slip characteristics such as the minimum velocity that can be achieved without stick-slip and the distance slipped during stick-slip motion.

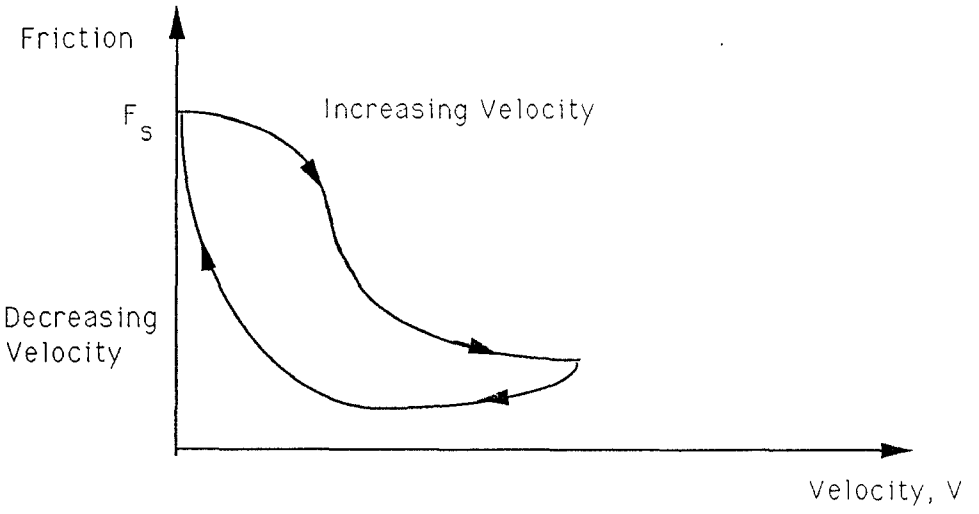

Figure 2.26: Hysteresis Friction Effect Due to Frictional Lag

2.7 Frictional Lag

Considerable empirical evidence has recently become available indicating that friction does not respond instantaneously to a change in velocity. One of the first to recognize this delayed behavior was [Rabinowicz, 1958]. Describing his previously obtained data, Rabinowicz noted that an abrupt change in sliding velocity results in a slow change in friction such that friction gradually approaches a steady state value. He attributed this frictional lag to a dependence on previous sliding history determined by a critical previous sliding distance. Pointing to data obtained by [Sampson et al., 1943] that showed different friction-velocity curves for accelerating and decelerating conditions, Rabinowicz provided frictional lag as the explanation. The observed hysteretic friction effect is illustrated in Figure 2.26.

In [Brace and Byerlee, 1966], the authors investigated the dynamic mechanisms of earthquakes and proposed that stick-slip is responsible for unstable fault slip at the edges of the earth's crustal plates. As a result, many researchers interested in predicting earthquake-related behavior have performed extensive theoretical and experimental work on friction and the existence of stick-slip. Of particular note, Rice and Ruina [Rice and Ruina, 1983] indicated that velocity-dependent friction as described by Figure 2.25 did not adequately explain observed sliding behavior. Specifically, they observed low-velocity steady sliding when the friction model of Figure 2.25 would have predicted unstable behavior. To resolve this contradiction, Ruina [Ruina, 1983] determined that friction is dependent not only on current sliding conditions but also on previous sliding history, that is,

$$F_f = F_f(V, \theta) \,, \tag{2.45}$$

where θ represents the state of the surface. This state does not change instantaneously with velocity, i.e.,

$$\frac{d\theta}{dt} = G(\theta, V) \,. \tag{2.46}$$

The notion of a delayed friction response is similar to Rabinowicz's claim, although the delay is not necessarily related to a critical slip distance.

In [Hess and Soom, 1990] the authors also found strong evidence of frictional lag in their experiments on a flat steel button rubbing against a rotating steel disk. At constant normal load, they applied velocity oscillations to the disk in

a triangular wave pattern, i.e., they ran repeated series of constant acceleration and deceleration. Measuring friction under these conditions, they found that the relationship between friction and velocity took the form of Figure 2.26, i.e., yielded hysteretic loops. These loops were measured for a variety of normal loads, velocity oscillation frequencies, and lubricants. This hysteretic behavior they attributed to a time delay in friction response to velocity changes. By simulating such a delay and fitting the simulation results to the experimental data, they found that the delay was better characterized by a constant time lag than by a characteristic slip distance as proposed by Rabinowicz.

Hess and Soom modelled frictional lag such that

$$F_f(t) = F_f(V(t-\tau)) \,, \tag{2.47}$$

where τ is the constant time lag [Armstrong-Hélouvry, 1991] so that from (2.39) Stribeck friction becomes

$$F_{str}(t) = F_s \left(\frac{1}{1 + (V(t-\tau)/V_{str})^2} \right) \,. \tag{2.48}$$

Ruina [Ruina, 1983] developed state-variable friction models according to (2.45) and (2.46). His models were developed to approximate his own experimental observations and those of Dieterich and Johnson [Ruina, 1983], and [Rabinowicz, 1958]. Ruina's experiments as well as those of Dieterich and Johnson were performed on sliding rocks while Rabinowicz's involved sliding metals. The observed characteristic friction behavior that Ruina attempted to model

included: a steady state friction level for a given velocity; a slow (delayed) decrease in friction for an increase in velocity (at low velocities, i.e., in the regime of the Stribeck effect); a characteristic slip distance independent of velocity that governs the delayed increase in friction; and an instantaneous increase in friction with an increase in velocity. This last characteristic was observed in the experiments on sliding rocks but was *not* observed in the metallic surface experiments of [Rabinowicz, 1958] or [Hess and Soom, 1990]. An example of one of the state-variable models of [Ruina, 1983] follows:

$$F_f = F_o + \theta + A \cdot ln(V/V_o) \,, \tag{2.49}$$

$$\dot{\theta} = -V/d_c(\theta + B \cdot ln(V/V_o)) \,. \tag{2.50}$$

where (F_o, V_o) corresponds to any point on the steady state friction-velocity curve [Dupont, 1991], d_c is the characteristic slip distance, and A and B are constants.

Many researchers have used the state-variable models to analyze stability criteria for sliding rocks [Ruina, 1983,Rice and Ruina, 1983,Rice and Tse, 1986, Nussbaum and Ruina, 1987,Horowitz, 1988]. For example, in [Ruina, 1983, Rice and Ruina, 1983] the authors found that stick-slip instability can be avoided if the system stiffness is greater than some critical stiffness K_c. Similarly, Dupont [Dupont, 1991] used a state-variable friction model in his representation of a single robot joint to analyze stability properties. By means of a linearized model, Dupont also found that if stiffness (equivalently position feedback gain)

is higher than some K_c then stick-slip will be avoided.

Armstrong [Armstrong-Hélouvry, 1991] analyzed stick-slip stability with a model of frictional lag as in (2.48). Using perturbation analysis, he derived criteria to predict stick-slip oscillations as a function of the time delay τ, velocity V, and stiffness K. From his results and those of the researchers cited above, he concluded that frictional lag makes stick-slip instabilities less likely. Because a decrease in friction occurs *slowly* when velocity is increased, stiff systems will not be unstable. In a control system, stiffness can be increased by increasing position feedback gain.

Chapter 3

Friction-Compensating Control Strategies

Friction introduces complexities in the servomechanism control problem that can lead to inaccurate and even oscillatory behavior. The greatest difficulties occur at zero and near-zero velocities where friction is discontinuous and possibly destabilizing. Even at relatively high velocities where friction is fairly accurately modelled as a linear function of velocity, ignoring friction in the control design can result in suboptimal servomechanism performance.

In order to limit performance error, the mechanism under control should be designed to minimize friction. For example, decreasing the number of sources of rubbing will reduce friction. Equally important, the type of lubrication should be carefully selected to minimize friction based on the expected operating conditions. Also, inclusion of a lubrication additive could reduce static and boundary

layer friction and contribute to preventing stick-slip as described in Section 2.6.

In many designs, however, friction is not a priority consideration and modification of the mechanism or lubricant to reduce friction is not a viable option. Even when friction has been considered in the mechanical design stage, it cannot be eliminated completely and may still have a significant effect on system dynamics. Therefore, to achieve precision, servomechanism control should provide some kind of friction compensation.

This chapter describes several different types of friction-compensating control strategies. In Section 3.1, traditional ways of modifying PID control to accommodate friction-related nonlinearities are discussed. Section 3.2 provides insight into the friction-compensating capabilities of heuristic smoothing techniques such as dither and presents recent work from [Cebuhar, 1988] on improved methods for linearizing and smoothing discontinuities. The disadvantages of PID control and smoothing techniques are discussed in these first two sections, and an argument for adaptive control as the preferred alternative is introduced in Section 3.3. Various adaptive control strategies for friction compensation provided in the literature are described in Section 3.3. Finally, Section 3.4 provides a rigorous presentation of the adaptive control techniques tested in the experimental program of this thesis. These techniques are based on the strategies of Section 3.3 but include original modifications and improvements. An original stability analysis is provided for the controller of [Walrath, 1984].

3.1 Modified PID Control

One of the most widely used controllers in industry is the standard PID controller. As indicated by its name, the PID controller provides three terms: one proportional (P) to the feedback error signal $e(t)$; a second proportional to the integral (I) of the error; and a third proportional to the derivative (D) of the error. The PID control signal $u(t)$ is

$$u(t) = K_p e(t) + K_i \int e(t) + K_d \frac{de(t)}{dt} \tag{3.1}$$

where K_p , K_i , and K_d are constant gains.

When the system to be controlled is linear, many techniques are available for selecting the values of K_p , K_i , and K_d to ensure a stable, well-behaved response. However, when nonlinearities such as friction significantly affect system dynamics, the standard PID design techniques often prove to be unreliable.

If the system with friction is linear and is to be operated only at relatively high velocities without changing directions, i.e., without crossing zero velocity, friction can be modelled as a linear function of velocity as in (2.18). Under these conditions, the standard PID design techniques can be applied to the dynamics of the linear system plus viscous friction with reliable results.

On the other hand, if the system is to be operated at low velocities or with direction reversals, then the standard PID design techniques may be unsuitable.

To understand what modification can be made to PID control under these conditions, consider a system with non-negligible friction. For reference, let the system be a simple rotating servo-system with friction and let the dynamics be described by

$$\ddot{\theta}_p(t) + c_1\dot{\theta}_p(t) = -c_2T_f + c_3u(t)\ , \tag{3.2}$$

where

θ_p, $\dot{\theta}_p$, $\ddot{\theta}_p$ are plant angular position, velocity, and acceleration,

T_f is the friction and may depend on θ_p, $\dot{\theta}_p$, etc.,

$u(t)$ is the control input,

c_1, c_2, c_3 are constants (c_1 includes viscous friction).

Let the PID type control input be defined by

$$u(t) = \frac{1}{c_3}\left(\ddot{\theta}_d + K_pe(t) + K_i\int e(t) + (K_d - c_1)\dot{e}(t)\right) \tag{3.3}$$

where θ_d, $\dot{\theta}_d$, and $\ddot{\theta}_d$ are the desired angular position, velocity, and acceleration, respectively, and

$$e(t) = \theta_d(t) - \theta_p(t)\ . \tag{3.4}$$

Then substituting (3.2) into (3.3) yields

$$\ddot{e}(t) + K_d\dot{e}(t) + K_pe(t) + K_i\int e(t) = c_2T_f + c_1\dot{\theta}_d(t) \tag{3.5}$$

Assuming that this is a regulator problem, i.e., $\dot{\theta}_d(t) = 0$, and no integral control is used, i.e., $K_i = 0$ then (3.5) becomes

$$\ddot{e}(t) + K_d\dot{e}(t) + K_pe(t) = c_2T_f \tag{3.6}$$

which is equivalent to (2.31) with e replacing x, except that the "damping" K_d and the "stiffness" K_p can be set as desired.

Let the friction T_f be static plus kinetic friction as illustrated in Figure 2.14. Then the phase plane analysis in Section 2.3 of the system described by (2.31) also applies to the system described by (3.6). According to this phase plane analysis, friction can yield a limit cycle under the appropriate conditions as shown in Figure 2.19. However, the limit cycle can be avoided if the damping is high enough. Therefore, using a large enough derivative gain K_d can prevent limit cycling generated by the static-kinetic friction discontinuity at zero velocity.

As indicated, the solution above assumes that integral control is not used. However, this is typically not the case, since integral control is important for its ability to eliminate steady state error. As discussed at the end of Section 2.3, several researchers have shown that under certain conditions in which PD control yields no oscillations, the addition of integral control leads to limit cycling. Since steady state error usually cannot be tolerated, elimination of integral control to avoid limit cycling is not a satisfactory solution. A preferable alternative is the addition of a dead-zone to the integral control such that the input to the integrator is as follows [Shen and Wang, 1964]:

$$\text{input to integrator} = \begin{cases} e(t) - \eta & \text{if } e(t) > \eta \\ 0 & \text{if } |e(t)| \leq \eta \\ e(t) + \eta & \text{if } e(t) < -\eta \end{cases} \tag{3.7}$$

where η is a (small) positive constant. In effect, the dead-zone eliminates integral control for low values of $e(t)$. Shen and Wang showed for a ramped position demand signal to the system described by (3.2) and (3.3) with static plus kinetic plus viscous friction, that above some critical dead-zone limit $\eta = \eta_{cr}$, integral control does not produce a limit cycle.

If the servomechanism is to be operated at very low velocities, the controller must also deal with the possibility of instabilities generated by the Stribeck effect. Armstrong [Armstrong-Hélouvry, 1990] analyzed stick-slip oscillations for a system with friction that included a model of the Stribeck curve. He found that for any pair of desired velocity and system stiffness, there is a minimum value of damping that will eliminate stick-slip. Similarly, when Dupont [Dupont, 1991] included frictional lag in his model of friction with the Stribeck effect, he found a minimum stiffness that would prevent stick-slip.

All of these results indicate that for PID control, high gains are generally necessary to avoid limit cycling. However, high gain control has its own practical disadvantages [Kubo et al., 1986]. For example, high gain control can cause instability if there is compliance in the drive train of the servomechanism. Also, actuator signals necessarily have physical maximum values which limit controller gains. Further, time delays associated with digital control implementation can limit gains. As a result, high gain PID control may not always be a practical solution to friction-compensating control.

3.2 Smoothing and Linearizing Techniques

Smoothing and linearizing techniques have been developed to deal with the inaccuracies and oscillations in system response generated by discontinuities such as the one associated with the basic kinetic friction model at zero velocity shown in Figure 2.4. The goal is to perform some operation on the system that will transform the dynamics into smooth and, if possible, linear dynamics that can be more easily controlled with standard techniques.

Dither is a commonly used smoothing technique which has the effect of "averaging" out a discontinuity. Characteristically a high frequency signal, dither is added to the error signal in a feedback loop before it is input to the system. If the frequency is chosen to be higher than the cut-off frequency of the system, the high-frequency behavior is filtered out leaving only the low-frequency "average" response [Cebuhar, 1988]. The effect of a triangular wave dither signal on a simple relay with unit feedback control is shown in Figure 3.1 [Åström and Wittenmark, 1989]. Ideally, for linear results the dither signal should be a triangular wave. However, a sinusoidal dither signal is more practical since, unlike the triangular wave, the sinusoid will be preserved even if the dither signal is integrated or differentiated before reaching the discontinuity. The sinusoidal dither signal will smooth out the discontinuity, but the result will not be linear as in the ideal case.

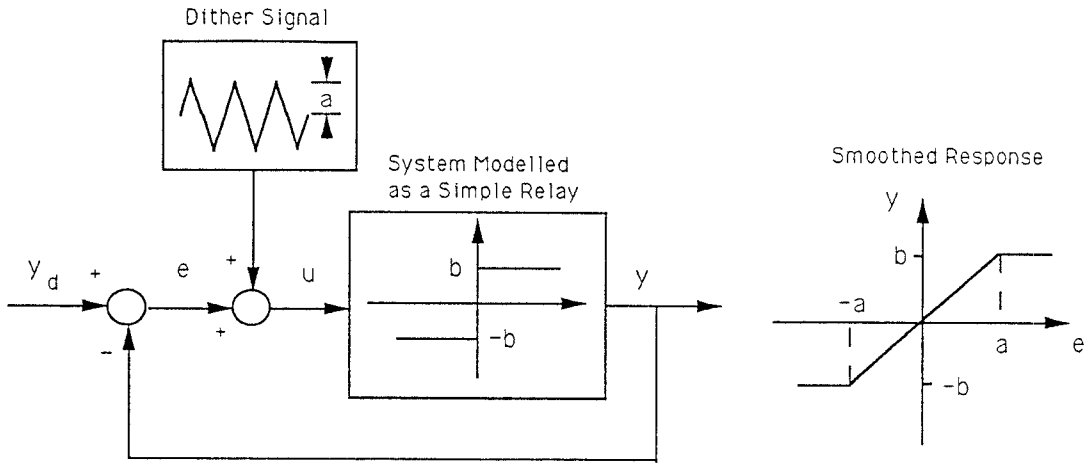

Figure 3.1: Smoothing Effect of Triangular Wave Dither on Relay-Type Discontinuity

Pulse-width modulation is another commonly used and effective smoothing technique that also works on the principle of averaging. The scheme operates by mapping a periodically sampled error signal e(t) into a signal of pulses u(t) which is then used as input to the system with the discontinuity. Each pulse has magnitude M or $-M$ and width τ as follows [Skoog and Blankenship, 1970]:

$$u(t) = \begin{cases} M sgn(e(kT)) & kT \leq t < kT + \tau[e(kT)] \\ 0 & elsewhere \end{cases}, \tag{3.8}$$

and

$$\tau[e(kT)] = \begin{cases} \beta|e(kT)| & |e(kT)| \leq T/\beta \\ T & |e(kT)| > T/\beta \end{cases} \tag{3.9}$$

where T is the sample time period and β is a constant. A typical pulse-width modulation signal is shown in Figure 3.2. When this signal is then input to the system with a discontinuity, the averaged output is relatively smooth [Brockett and Cebuhar, 1988].

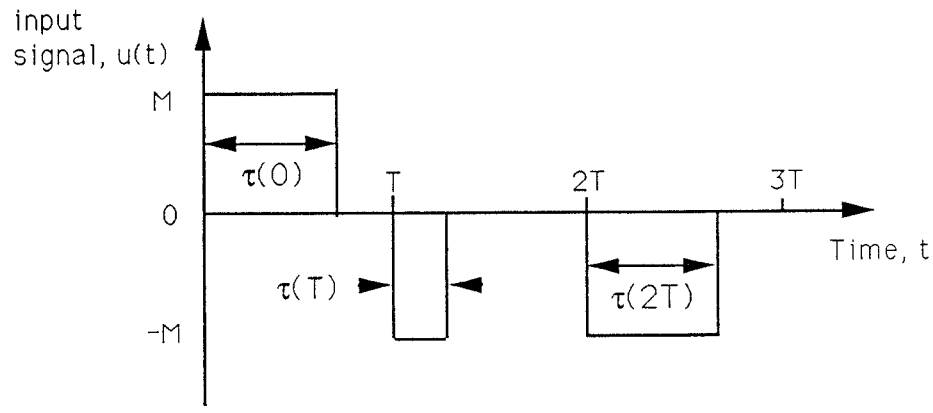

Figure 3.2: Typical Pulse-Width Modulation Signal

Experience has proven that dither and pulse-width modulation can reduce friction-related errors and instabilities. In fact, Chapter 4 documents the results of using dither to improve the tracking performance of the motor under investigation in this thesis. However, both dither and pulse-width modulation have serious inherent disadvantages. On the theoretical side, analysis and prediction of system characteristics such as stability and robustness are difficult to perform when dither or pulse-width modulation is applied. Pulse-width modulation in particular creates complexities since it produces an input signal that is not continuous. On the implementation side, the effectiveness of dither is often compromised due to digital implementation limitations of dither frequency. Additionally, dither can cause mechanical problems in a system such as a robot by exciting vibrations. Vibrations can not only foil precision control but also lead to fatigue and failure of parts.

[Cebuhar, 1988] has made significant advances in improving smoothing and

linearizing techniques. In his work, Cebuhar considered both feedforward and feedback methods in terms of a rigorous mathematical criteria that judges the degree to which smoothness and linearity is achieved. Within this framework, he determined optimal dither parameters and developed a filtered pulse-width modulation scheme that produces a smooth input signal and minimizes total energy. He also derived a feedforward continuous controller that is locally optimal in the least-squares sense.

With regard to feedback strategies, Cebuhar considered two different paths: one that uses an optimal differentiable feedback control to compensate the nonlinearity aided by a precompensation technique such as dithering; and another that optimally linearizes the averaged system that has been smoothed by precompensation. A smooth approximation to the discontinuous system is needed for analysis of these feedback techniques. Cebuhar considered optimal approximations of $sgn(x)$, singularly perturbed differential equations, and Volterra series approximations.

Cebuhar's work improves on the traditional heuristic techniques; however, it does not eliminate all of the disadvantages cited above. Additionally, smooth approximations to the discontinuous systems may be flawed for analytical purposes since they will not produce the various characteristic frictional effects such as stick-slip which may be the limiting factors for accurate control.

The impulsive force controller designed by Armstrong is another friction-compensating heuristic technique that has proved effective in experiments on a PUMA 560 robot [Armstrong, 1988]. To overcome friction this controller uses hard quick motions. The controller calculates force error and sends a sequence of torque impulses taken from a lookup table to the motor. The lookup table contains precomputed impulsive torque sequences each associated with a different force step. In Armstrong's experiments the magnitude of the force steps was lower than the magnitude of the static friction. Specifically, his experiments involved inserting wire wrap into a hole in a glass plate. This task required very small movements corresponding to points along the Stribeck friction curve. The success rate was about fifty percent. Although the technique requires a great deal of work up front and is very limited in its flexibility, it is noteworthy in its ability to provide high precision control in a very unstable regime.

3.3 Adaptive Control Strategies

Adaptive control strategies are naturally suited to the problem of friction compensation because they can control nonlinear systems; they generate a time-varying control law that tracks slowly-varying system parameters; and they provide system identification when an accurate system model is not available. Additionally, adaptive control techniques can be designed to take advantage of what is known about the structure of friction.

In [Gilbart and Winston, 1974] the authors proposed one of the earliest approaches to adaptive friction compensation in their work on control of a satellite-tracking telescope. Their problem consisted of accurately controlling each axis of a two-axis telescope to follow a demanded velocity input $\dot{\theta}_d$. Since friction was a significant limiting factor in achieving satisfactory performance, for their design they included the classical kinetic plus viscous friction model in the dynamic system equations (Figures 2.4 and 2.12). To drive the system as desired they used an adaptive control input in addition to unit velocity feedback control. The following equation represents the closed loop dynamics of one axis of the telescope,

$$\ddot{\theta}_p + c_1\dot{\theta}_p = c_3\dot{z} - c_2 sgn(\dot{\theta}_p) + c_3 u \ , \tag{3.10}$$

where the variables are as defined for (3.2) except that $u(t)$ is the adaptive control input, c_1, c_2, and c_3 may be slowly varying with time, and $\dot{z} = \dot{\theta}_d - \dot{\theta}_p$.

Gilbart and Winston based their design of u on a model reference adaptive control (MRAC) approach. According to [Åström and Wittenmark, 1989], MRAC yields a mechanism that dynamically adjusts the control law parameters according to changes in error between an ideal model response and the measured system response as shown in Figure 3.3. For Gilbart and Winston the ideal model dynamics took the form

$$\ddot{\theta}_m + c_{1_m}\dot{\theta}_m = c_{3_m}\dot{z} \tag{3.11}$$

where $\dot{\theta}_m$ and $\ddot{\theta}_m$ are model velocity and acceleration, respectively, and c_{1_m} and

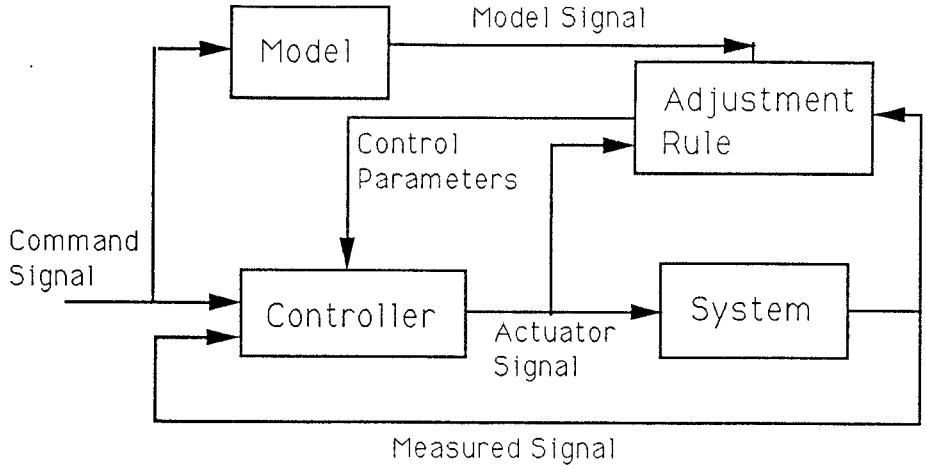

Figure 3.3: Model Reference Adaptive Control

c_{3_m} are constants. Subtracting (3.10) from (3.11) yields the error equation

$$\ddot{e} + c_{1_m}\dot{e} = (c_1 - c_{1_m})\dot{\theta}_p + (c_{3_m} - c_3)\dot{z} + c_2 sgn(\dot{\theta}_p) - c_3 u \ , \tag{3.12}$$

where $e = \theta_m - \theta_p$. The adaptive control u was defined as

$$u = K_1\dot{\theta}_p + K_2\dot{z} + K_3 sgn(\dot{\theta}_p) \tag{3.13}$$

where K_1, K_2, and K_3 are the time-dependent adaptive control parameters. Substituting (3.13) into (3.12) yields

$$\ddot{e} + c_{1_m}\dot{e} = \sum_{j=1}^{3} x_j g_j \tag{3.14}$$

where $x_1 = c_1 - c_{1_m} - c_3 K_1$, $x_2 = c_{3_m} - c_3 - c_3 K_2$, $x_3 = c_2 - c_3 K_3$, $g_1 = \dot{\theta}_p$, $g_2 = \dot{z}$, $g_3 = sgn(\dot{\theta}_p)$. Using Lyapunov's direct method, Gilbart and Winston then determined the adaptive control laws $K_j(t)$ such that $\dot{e} = 0$ was an asymptotically stable equilibrium point.

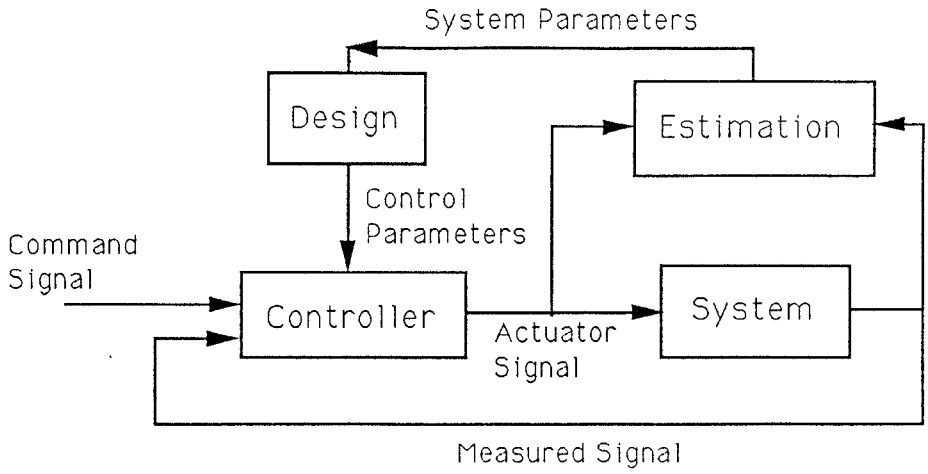

Figure 3.4: Self-Tuning Regulator

By performing several experiments on a 24-inch telescope, Gilbart and Winston demonstrated the improved control accuracy provided by their friction-compensating adaptive controller. They considered experiments with step changes in demanded velocity as well as various velocity trajectory tracking experiments. The adaptive controller improved accuracy by a factor of six in the velocity tracking experiments.

Instead of using MRAC, in [Canudas et al., 1986] the authors proposed an alternative friction-compensating adaptive controller based on a self-tuning regulator (STR) approach. As shown in Figure 3.4 an STR consists of an algorithm that estimates system parameters which are used to dynamically generate control parameters [Åström and Wittenmark, 1989]. In the scheme developed by Canudas et. al., the controller provided cancellation of friction plus linear

control to drive the remaining frictionless system. A recursive least squares algorithm was used to provide an estimation of the friction parameters. Friction was modelled according to the asymmetric kinetic plus viscous friction structure of Figure 2.13.

The friction-compensating STR was tested on a servomechanism consisting of a dc motor driving a load by means of a geared transmission. Sinusoidal and square wave velocity trajectory tracking was performed with adaptive friction compensation and with a linear fixed-gain control. Comparative plots of the test results showed that the adaptive controller provided improved tracking performance over the linear fixed-gain controller.

Craig [Craig, 1988] also considered friction-compensating adaptive control assuming the classical (symmetrical) model of kinetic plus viscous friction. Specifically, in his design of an adaptive robotic manipulator controller, Craig included terms to account for friction. While his design provided for a manipulator with multiple joints, for simplicity the following discussion assumes a single-joint device.

Craig described the dynamics of the manipulator as follows:

$$M(\theta_p)\ddot{\theta}_p + Q(\theta_p, \dot{\theta}_p) = u \tag{3.15}$$

where M is the inertia, Q includes terms like friction and gravity and u is the

control torque. The computed torque method sets

$$u = \hat{M}(\theta_p)(\ddot{\theta}_d + K_d\dot{e} + K_p e) + \hat{Q}(\theta_p, \dot{\theta}_p) \tag{3.16}$$

where $\hat{M}$ and $\hat{Q}$ are estimates of M and Q, respectively, and $e = \theta_d - \theta_p$. Substituting (3.16) into (3.15) yields the error equation:

$$\ddot{e} + K_d\dot{e} + K_p e = \hat{M}^{-1}(\theta_p)[\tilde{M}(\theta_p)\ddot{\theta}_p + \tilde{Q}(\theta_p, \dot{\theta}_p)] \tag{3.17}$$

where $\tilde{M} = M - \hat{M}$ and $\tilde{Q} = Q - \hat{Q}$. Assuming that there are r unknown parameters, the error equation can then be rewritten as:

$$\ddot{e} + K_d\dot{e} + K_p e = \hat{M}^{-1}W(\theta_p, \dot{\theta}_p, \ddot{\theta}_p)\Phi \tag{3.18}$$

where Φ is an rx1 vector containing all of the unknown parameter errors and W is a 1xr vector of functions. Let P be an rx1 vector containing the unknown parameters and $\hat{P}$ be the corresponding rx1 vector of parameter estimates. Then

$$\Phi = P - \hat{P}\ . \tag{3.19}$$

The adaptive law, describing how to update the parameter estimates $\hat{P}$ was based on a MRAC approach. Specifically, the adaptive law was designed using Lyapunov's direct method to ensure that $(e, \dot{e}) = (0, 0)$ was an asymptotically stable equilibrium point.

Craig implemented his adaptive controller on two links of an Adept One, which is a partially direct-drive "Scara"-style manipulator. He assumed the kinetic plus viscous friction model with two unknown parameters per joint: F_k

and μ. In addition there were three other unknown parameters related to inertias and masses. His results showed good position trajectory tracking accuracy with the adaptive controller. However, the benefit of the friction compensation component alone was not investigated.

Walrath [Walrath, 1984] developed a friction-compensating adaptive control strategy based on the Dahl friction model. As described in Section 2.4, Walrath was concerned with the stabilization of an airborne pointing and tracking system. To study the dynamics of this system, Walrath ran a series of experiments in which he angularly perturbed the base of the tracking and pointing system's gimbal sinusoidally over a large frequency and amplitude range. While the stabilization system attempted to regulate a desired position, motion of the system over time was measured. Based on the results of these experiments, Walrath postulated the following first-order model of the bearing friction T_f

$$\tau \frac{dT_f}{dt} + T_f = T_c sgn(\dot{\theta}_p) \tag{3.20}$$

where T_c is the rolling bearing friction (i.e. kinetic friction) and τ is a time constant. Equation (3.20) is based on the Dahl friction model of (2.34) and (2.35). In fact, substituting (2.35) into (2.34) with $i = 1$ and $S = 1$ and replacing F_f with T_f, F_{f_c} with T_c and x with θ_p yields

$$\frac{dT_f}{dt} = \sigma \dot{\theta}_p - \frac{T_f}{T_c} \sigma \dot{\theta}_p sgn(\dot{\theta}_p) \, . \tag{3.21}$$

Multiplying both sides of (3.21) by $T_c/(\sigma\dot{\theta}_p sgn(\dot{\theta}_p))$ gives

$$\left(\frac{T_c}{\sigma|\dot{\theta}_p|}\right)\frac{dT_f}{dt} + T_f = T_c sgn(\dot{\theta}_p) \tag{3.22}$$

which is identical to (3.20) if

$$\tau = \frac{T_c}{\sigma|\dot{\theta}_p|}\,. \tag{3.23}$$

Walrath incorporated the friction model (3.20) into his controller by using it to predict friction torque. The predicted friction torque was added to the standard fixed-gain feedback control signal and the sum was input to the system. Walrath empirically determined the value of τ for a given control experiment by repeating the experiment many times, each time varying only τ, until the optimum τ was found, i.e., the τ that yielded the minimum stabilization error. Based on optimum τ values (τ_{opt}) calculated for a range of operating conditions, Walrath empirically derived the following relationship which predicts τ_{opt} as a function of root-mean-square system acceleration $\ddot{\theta}_{rms}$:

$$1/\tau_{opt} = \omega_{opt} = 1 + 0.37\,\ddot{\theta}_{rms} \tag{3.24}$$

It should be noted that this relationship predicts that τ is inversely proportional to acceleration whereas the Dahl model predicts that τ is inversely proportional to velocity (3.23). This discrepancy is discussed further in Section 3.4.

Walrath incorporated the relationship (3.24) for τ into his controller. As a

result, friction was dynamically predicted based on the system operating conditions. Extensive testing was performed using the friction-compensating controller to evaluate its performance. Significant reductions in stabilization error were measured when the friction compensator was implemented. In the low and mid-frequency regions, error was typically reduced by a factor of three. At higher frequencies, the improvement was not so dramatic partly due to processing time delays inherent to the digital implementation.

Canudas de Wit [Canudas de Wit, 1989] recently proposed a friction-compensating adaptive control technique for a robotic manipulator based on a model of friction that included a term for the Stribeck effect. His model described by (2.44) is linear in the parameters. To determine the friction parameters dynamically, Canudas de Wit used an estimation algorithm that minimized an exponentially weighted least-squares cost function with a noise constraint. The control law was based on the computed torque method with integration and with the friction torque predicted by the estimated parameters. To avoid overcompensation, the controller included only between 80 and 90 percent of the predicted friction torque.

Using this controller, Canudas de Wit performed low velocity tracking experiments on a robotic manipulator. Tracking error was reduced when the friction-compensating controller component was implemented. However, friction prediction error was greater for low velocity tracking than for high velocity tracking.

This is to be expected since friction is more difficult to model at low velocities.

3.4 Design and Analysis of Adaptive Strategies Used in Experiment

As will be presented in Chapter 4, this thesis describes an experimental program on an electric motor in which several friction-compensating control strategies are tested. Of the control strategies implemented, three are adaptive control techniques. The techniques are based on the methods described in the previous section. However, several improvements have been made to these methods. For example, new terms have been added to the friction models to increase friction prediction accuracy.

The design of the improved techniques is described in this section. Additionally, a stability analysis is provided for each technique. The analysis of the first controller is modified and more complete than in the literature; the analysis of the second controller contains minor changes to the original; and the stability analysis of the third controller is new.

The experimental system is a direct-drive, dc motor which behaves according to the dynamical equation (3.2). All of the experiments involve position trajectory tracking where θ_d, $\dot{\theta}_d$, and $\ddot{\theta}_d$ are available. Later, in Chapter 4, Section

4.2 describes the derivation of the dynamical motor equation and Section 4.3 details the tests that comprise the experimental program.

3.4.1 Adaptive Controller I

Adaptive Controller I incorporates a friction-compensating strategy based on the method of [Gilbart and Winston, 1974] described in Section 3.3. However, while Gilbart and Winston considered velocity trajectory tracking in their design, this controller was required to handle position trajectory tracking. In effect, the Gilbart and Winston design which supported a first-order system was insufficient for control of the second-order system that describes position tracking of the electric motor. As a result, Adaptive Controller I is a modified version of the Gilbart and Winston design, incorporating filters to reduce the order of the system as suggested by [Gilbart et al., 1970].

Additionally, to accommodate the observed asymmetrical nature of friction in the motor [Wang, 1987], kinetic friction is modelled as follows:

$$T_f = \alpha_1 \left(\frac{sgn(\dot{\theta}_p) + 1}{2} \right) + \alpha_2 \left(\frac{sgn(\dot{\theta}_p) - 1}{2} \right) , \tag{3.25}$$

where α_1 and α_2 are slowly-varying parameters that represent the magnitude of kinetic friction in the positive and negative directions, respectively.

While Gilbart and Winston used only proportional feedback control in addition to the adaptive control, our controller uses a control input based on the

computed torque method with integration in addition to the adaptive control. The control signal is

$$u = \ddot{\theta}_d/c_3 + K_p z + K_i \int z + K_d \dot{z} + p_3 \dot{u}_a + p_4 u_a \ , \tag{3.26}$$

where $z = \theta_d - \theta_p$, p_3 and p_4 are constants, and u_a is the adaptive control input. The $\dot{u}_a$ term is included since the system is of second order. Substituting (3.26) into (3.2) yields

$$\ddot{\theta}_p = -c_1 \dot{\theta}_p - c_2 T_f + c_3(\ddot{\theta}_d/c_3 + K_p z + K_i \int z + K_d \dot{z} + p_3 \dot{u}_a + p_4 u_a) \ . \tag{3.27}$$

The ideal model is also of second order and takes the form

$$\ddot{\theta}_m + (p_1 + p_2)\dot{\theta}_m + (p_1 p_2)\theta_m = d_1 \dot{\theta}_d + d_2 \theta_d \tag{3.28}$$

where p_1, p_2, d_1, and d_2 are constants. Therefore, the transfer function of the ideal model has the form

$$\frac{\Theta_m}{\Theta_d} = \frac{d_1(s + d_2/d_1)}{(s + p_1)(s + p_2)} \tag{3.29}$$

The error equation is obtained by subtracting (3.27) from (3.28). Defining $d_2 = p_1 p_2$ yields

$$\begin{aligned} \ddot{e} + (p_1 + p_2)\dot{e} + (p_1 p_2)e \ &= \ (d_1 - c_3 K_d)\dot{z} + (d_2 - c_3 K_p) z \\ &\quad + (d_1 + c_1 - p_1 - p_2)\dot{\theta}_p + c_2 T_f \\ &\quad - c_3 K_i \int z - c_3 p_3 \dot{u}_a - c_3 p_4 u_a - \ddot{\theta}_d \ . \end{aligned} \tag{3.30}$$

To use the technique of [Gilbart et al., 1970], the order of the error equation should be reduced by one. To do so, take the Laplace Transform of (3.30) and

multiply both sides by $1/(s+p_1)$ such that

$$\begin{aligned}(s+p_2)e(s) &= (d_1 - c_3K_d)\tfrac{sz(s)}{s+p_1} + (d_2 - c_3K_p)\tfrac{z(s)}{s+p_1} + (d_1 + c_1 - p_1 - p_2)\tfrac{\dot{\theta}_p(s)}{s+p_1} \\ &\quad + c_2\tfrac{\mathcal{L}(T_f)}{s+p_1} - c_3K_i\tfrac{z(s)}{s(s+p_1)} - c_3p_3\tfrac{su_a(s)}{s+p_1} - c_3p_4\tfrac{u_a(s)}{s+p_1} - \tfrac{\ddot{\theta}_d(s)}{s+p_1}\,.\end{aligned} \tag{3.31}$$

Notice that the Laplace transform $\mathcal{L}(T_f)$ exists since T_f is piecewise continuous and bounded [Boyce and DiPrima, 1977]. Also note that

$$\frac{sz(s)}{s+p_1} = \frac{sz(s)}{s+p_1} + \frac{p_1z(s)}{s+p_1} - \frac{p_1z(s)}{s+p_1} = z(s) - \frac{p_1z(s)}{s+p_1}\,. \tag{3.32}$$

Similarly,

$$\frac{su_a(s)}{s+p_1} = u_a(s) - \frac{p_1u_a(s)}{s+p_1}\,. \tag{3.33}$$

Substituting (3.32), (3.33), and (3.25) into (3.31) yields

$$\begin{aligned}(s+p_2)e(s) &= \delta_1z(s) + \delta_2\tfrac{z(s)}{s+p_1} + \delta_3\tfrac{u_a(s)}{s+p_1} + \delta_4\tfrac{\dot{\theta}_p(s)}{s+p_1} + \delta_5\tfrac{z(s)}{s(s+p_1)} \\ &\quad + \tfrac{\delta_6}{s+p_1}\mathcal{L}(\tfrac{sgn(\dot{\theta}_p)+1}{2}) + \tfrac{\delta_7}{s+p_1}\mathcal{L}(\tfrac{sgn(\dot{\theta}_p)-1}{2}) + \delta_8\tfrac{\ddot{\theta}_d(s)}{s+p_1} - c_3p_3u_a(s)\end{aligned} \tag{3.34}$$

where

$$\begin{cases} \delta_1 = d_1 - c_3K_d \\ \delta_2 = d_2 - c_3K_p - p_1(d_1 - c_3K_d) \\ \delta_3 = p_1c_3p_3 - c_3p_4 \\ \delta_4 = d_1 + c_1 - p_1 - p_2 \\ \delta_5 = -c_3K_i \\ \delta_6 = c_2\alpha_1 \\ \delta_7 = c_2\alpha_2 \\ \delta_8 = -1\,. \end{cases} \tag{3.35}$$

Taking the inverse Laplace Transform of (3.34) gives

$$\dot{e} + p_2 e = \sum_{j=1}^{8} \delta_j g_j - c_3 p_3 u_a \tag{3.36}$$

where

$$\begin{cases} g_1 &= z(t) \\ g_2 &= \mathcal{L}^{-1}[z(s)/(s+p_1)] \\ g_3 &= \mathcal{L}^{-1}[u_a(s)/(s+p_1)] \\ g_4 &= \mathcal{L}^{-1}[\dot{\theta}_p(s)/(s+p_1)] \\ g_5 &= \mathcal{L}^{-1}[z(s)/(s(s+p_1))] \\ g_6 &= \mathcal{L}^{-1}[\mathcal{L}(\frac{sgn(\dot{\theta}_p)+1}{2})/(s+p_1)] \\ g_7 &= \mathcal{L}^{-1}[\mathcal{L}(\frac{sgn(\dot{\theta}_p)-1}{2})/(s+p_1)] \\ g_8 &= \mathcal{L}^{-1}[\ddot{\theta}_d(s)/(s+p_1)] \, . \end{cases} \tag{3.37}$$

The adaptive input can be defined by

$$u_a = \sum_{j=1}^{8} K_j g_j \tag{3.38}$$

where the K_j are the adaptive parameters. Then

$$\dot{e} + p_2 e = \sum_{j=1}^{8} (\delta_j - c_3 p_3 K_j) g_j = \sum_{j=1}^{8} x_j g_j \tag{3.39}$$

where $x_j = \delta_j - c_3 p_3 K_j$. Let $x = (x_1, ..., x_8)^T$. Now Lyapunov's direct method is used to derive an adaptation law for the parameters K_j such that $e = 0$ is an asymptotically stable equilibrium point. Let V be defined as follows [Gilbart and Winston, 1974]:

$$V(e, x) = e^2 + \sum_{j=1}^{8} \frac{1}{\alpha_j} (x_j + \beta_j e g_j)^2 \tag{3.40}$$

where α_j and β_j are arbitrary positive constants. Recall that from (3.37)

$$g_6(s) = \mathcal{L}(\tfrac{sgn(\dot{\theta}_p)+1}{2})/(s+p_1)\ . \tag{3.41}$$

Multiplying both sides by s yields

$$sg_6 = \mathcal{L}(\tfrac{sgn(\dot{\theta}_p)+1}{2}) - p_1\mathcal{L}(\tfrac{sgn(\dot{\theta}_p)+1}{2})/(s+p_1) = \mathcal{L}(\tfrac{sgn(\dot{\theta}_p)+1}{2}) - p_1 g_6(s)\ . \tag{3.42}$$

Since $\mathcal{L}(\frac{sgn(\dot{\theta}_p)+1}{2})$ exists, then $\mathcal{L}^{-1}(sg_6) = \dot{g}_6(t)$ exists and

$$\dot{g}_6(t) = \tfrac{sgn(\dot{\theta}_p)+1}{2} - p_1 g_6(t)\ . \tag{3.43}$$

Similarly $\dot{g}_7(t)$ exists and is piecewise continuous. Therefore, V is continuously differentiable. Also note that since $V(0,0) = 0$ and $V(e,x) > 0$ for $(e,x) \neq (0,0)$, then V is a positive definite function and therefore a Lyapunov function candidate [Vidyasagar, 1978]. Differentiating V with respect to time results in the following

$$\dot{V} = 2e\dot{e} + \sum_{j=1}^{8} \frac{2}{\alpha_j}(x_j + \beta_j e g_j)(\dot{x}_j + \beta_j \frac{d}{dt}(e g_j))\ . \tag{3.44}$$

Substituting (3.39) for $\dot{e}$ into (3.44) gives

$$\dot{V} = -2p_2e^2 + 2e\sum_{j=1}^{8} x_j g_j + \sum_{j=1}^{8} \frac{2}{\alpha_j}(x_j + \beta_j e g_j)(\dot{x}_j + \beta_j \frac{d}{dt}(e g_j))\ . \tag{3.45}$$

Let $\dot{x}_j$ be defined by

$$\dot{x}_j = -\alpha_j e g_j - \beta_j \frac{d}{dt}(e g_j)\ . \tag{3.46}$$

Then by substitution of (3.46) into (3.45)

$$\dot{V} = -2(p_2 + \sum_{j=1}^{8} \beta_j (g_j)^2)e^2\ . \tag{3.47}$$

So $\dot{V} < 0$ for all $e \neq 0$ and $\dot{V} = 0$ for $e = 0$. By Lyapunov's direct method, this implies that $e = 0$ is an asymptotically stable equilibrium point [Vidyasagar, 1978].

Assuming that δ_j, $\forall j$ is constant or slowly varying then from (3.39)

$$\dot{x}_j = -c_3 p_3 \dot{K}_j \qquad j = 1, ..., 8 \,. \tag{3.48}$$

Substituting (3.46) into (3.48) gives the adaptation law:

$$\dot{K}_j = \frac{1}{c_3 p_3}[\alpha_j e g_j + \beta_j \frac{d}{dt}(e g_j)] \qquad j = 1, ..., 8 \tag{3.49}$$

or equivalently

$$K_j = B_j \int e g_j + C_j e g_j \tag{3.50}$$

where $B_j = \alpha_j/(c_3 p_3)$ and $C_j = \beta_j/(c_3 p_3)$ are arbitrary positive constants. Figure 3.5 provides a comprehensive diagram of Adaptive Controller I.

3.4.2 Adaptive Controller II

Adaptive Controller II performs friction compensation according to the technique of [Craig, 1988] described in Section 3.3. The control signal input is based on the computed torque method with an adaptive rule for updating the unknown parameters. Adaptive Controller II assumes knowledge of the motor inertia and applies the adaptation feature to the unknown friction parameters. Four different versions of the controller are developed, each with a different model of

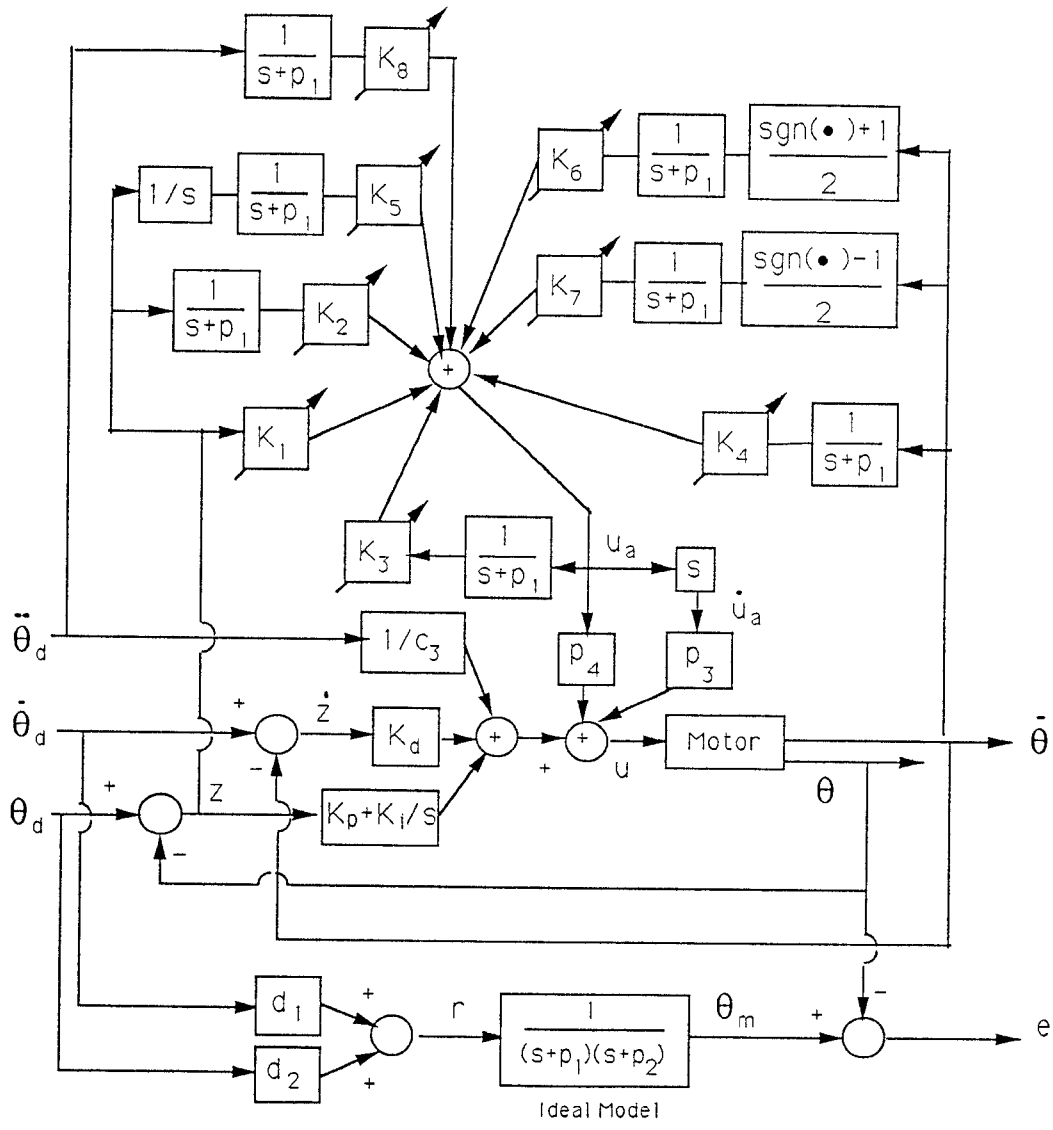

Figure 3.5: Adaptive Controller I

friction. The simplest model includes kinetic plus viscous friction as in Craig's design. The other three include additional terms to provide a more complete model of friction. The control system stability analysis detailed below follows [Craig, 1988].

To begin the controller development, the experimental system dynamics (3.2) need to be written in the form of (3.15). Solving for input u from (3.2) gives

$$u = (1/c_3)\ddot{\theta}_p + (c_1/c_3)\dot{\theta}_p + (c_2/c_3)T_f \ . \tag{3.51}$$

Then by defining M and Q by

$$M = 1/c_3 \ , \tag{3.52}$$

$$Q = (c_1/c_3)\dot{\theta}_p + (c_2/c_3)T_f \ , \tag{3.53}$$

u can be expressed as in (3.15). M represents the inertia of the motor and is known. Q incorporates all of the friction since the first term on the right hand side of (3.53) represents viscous friction (and back emf) and the second term includes other friction terms like kinetic friction. Therefore, Q can be redefined to supply different friction models.

Friction model (a) is the simple kinetic plus viscous friction model used by Craig in his design such that

$$Q^{(a)} = p_1\dot{\theta}_p + p_2 sgn(\dot{\theta}_p) \tag{3.54}$$

where p_1 and p_2 are the unknown parameters. Thus, $r = 2$, where r is the number of unknown parameters. Model (b) assumes the asymmetric kinetic

plus viscous friction model represented by:

$$\begin{aligned} Q^{(b)} &= p_1\dot{\theta}_p\tfrac{1+sgn(\dot{\theta}_p)}{2} + p_2\dot{\theta}_p\tfrac{1-sgn(\dot{\theta}_p)}{2} \\ &\quad + p_3\tfrac{sgn(\dot{\theta}_p)+1}{2} + p_4\tfrac{sgn(\dot{\theta}_p)-1}{2} \end{aligned} \tag{3.55}$$

where p_1 and p_2 are the unknown viscous friction parameters in the positive and negative directions, respectively and p_3 and p_4 are the unknown kinetic friction parameters in the positive and negative directions, respectively. In this case $r = 4$.

Model (c) includes a linear model of Stribeck friction in addition to kinetic plus viscous friction. From (2.38) and (2.40) with $a = 2$, Stribeck friction can be modelled as

$$F_{str} = (F_s - F_k)e^{-(\dot{\theta}_p/\dot{\theta}_{str})^2}sgn(\dot{\theta}_p)\ . \tag{3.56}$$

However, Adaptive Controller II requires dynamics that are linear in the unknown parameters. To derive a linear model, the exponential in (3.56) is replaced with its Taylor series approximation as follows:

$$\begin{aligned} F_{str} &= (F_s - F_k)[1 - (\tfrac{\dot{\theta}_p}{\dot{\theta}_{str}})^2]sgn(\dot{\theta}_p) \\ &= (F_s - F_k)sgn(\dot{\theta}_p) - (\tfrac{F_s-F_k}{\dot{\theta}^2_{str}})(\dot{\theta}_p)^2sgn(\dot{\theta}_p)\ . \end{aligned} \tag{3.57}$$

Adding this term to the kinetic plus viscous friction model of (3.54) gives

$$Q^{(c)} = p_1\dot{\theta}_p + p_2sgn(\dot{\theta}_p) + p_3\dot{\theta}_p{}^2sgn(\dot{\theta}_p) \tag{3.58}$$

and $r = 3$.

For comparative purposes, Model (d) includes kinetic plus viscous plus Stribeck friction terms according to the linear model (2.44) by

[Canudas de Wit, 1989] such that $r = 3$ and

$$Q^{(d)} = p_1\dot{\theta}_p + p_2 sgn(\dot{\theta}_p) + p_3|\dot{\theta}_p|^{1/2} sgn(\dot{\theta}_p) \ . \tag{3.59}$$

$\hat{Q}$ is the estimate of Q and is written identically to Q except that the unknown parameters are replaced with estimates

$$\hat{Q}^{(a)} = \hat{p}_1\dot{\theta}_p + \hat{p}_2 sgn(\dot{\theta}_p) \tag{3.60}$$

Therefore, $\tilde{Q} = Q - \hat{Q}$ can then be written as

$$\tilde{Q}^{(a)} = (p_1 - \hat{p}_1)\dot{\theta}_p + (p_2 - \hat{p}_2)sgn(\dot{\theta}_p) \ , \tag{3.61}$$

which can also be expressed as

$$\tilde{Q}^{(a)} = W(\dot{\theta}_p)\Phi \ , \tag{3.62}$$

$$W(\dot{\theta}_p) \ = \ [\dot{\theta}_p \quad sgn(\dot{\theta}_p)] \ , \tag{3.63}$$

$$\Phi = P - \hat{P} = \begin{bmatrix} p_1 - \hat{p}_1 \\ \\ p_2 - \hat{p}_2 \end{bmatrix} \ , \tag{3.64}$$

where $P = [p_1 \quad p_2]^T$ and $\hat{P} = [\hat{p}_1 \quad \hat{p}_2]^T$. The above expression can be used for any of the other friction models by adding the appropriate terms to W and Φ.

The input control torque applied to the motor is given by (3.16) which leads to the error equation (3.17). Since $\tilde{M} = M - \hat{M} = 1/c_3 - 1/c_3 = 0$, the error equation for Adaptive Controller II with any of the four friction models becomes

$$\ddot{e} + K_v\dot{e} + K_p e = c_3 W\Phi \ . \tag{3.65}$$

From [Craig, 1988] let e_1 represent a filtered error signal such that

$$e_1(s) = (s + \psi)e(s) \,. \tag{3.66}$$

Then

$$\begin{aligned} e_1(s) &= \tfrac{s+\psi}{s^2+K_v s+K_p}(c_3 W\Phi)(s) \\ &= G(s)(c_3 W\Phi)(s) \,. \end{aligned} \tag{3.67}$$

ψ should be chosen such that $G(s)$ is a strictly positive real (SPR) transfer function. Then, given the minimal state-space realization of (3.67)

$$\begin{aligned} \dot{x} &= Ax + B(c_3 W\Phi) \\ e_1 &= Cx \end{aligned} \tag{3.68}$$

where $x = [e \quad \dot{e}]^T$, we have by the Kalman-Yakubovich Lemma that there exist positive definite matrices R and Q such that

$$\begin{aligned} A^T R + RA &= -Q \\ RB &= C^T \,. \end{aligned} \tag{3.69}$$

A state-space realization for (3.67) is given by (3.69) with

$$A \cdot = \begin{bmatrix} 0 & 1 \\ -K_p & -K_d \end{bmatrix} \,, \quad B = \begin{bmatrix} 0 \\ 1 \end{bmatrix} \,, \quad C = [\psi \quad 1] \tag{3.70}$$

which is controllable and is observable if

$$rank[C^T \quad (CA)^T] = rank \begin{bmatrix} \psi & -K_p \\ 1 & \psi - K_d \end{bmatrix} = 2 \,. \tag{3.71}$$

To show stability of the equilibrium point $(e, \dot{e}) = (0, 0)$, a Lyapunov function candidate is selected to be

$$V(e, \dot{e}, \Phi) = V(x, \Phi) = x^T R x + \Phi^T \Gamma^{-1} \Phi \ , \tag{3.72}$$

where

$$\Gamma = diag[\gamma_1, \gamma_2, ..., \gamma_r] \qquad \gamma_i > 0 \tag{3.73}$$

such that V is a positive definite function. Differentiating V with respect to time yields

$$\dot{V} = x^T Q x + 2\Phi^T [W^T c_3 e_1 + \Gamma^{-1} \dot{\Phi}] \ . \tag{3.74}$$

Let

$$\dot{\Phi} = -\Gamma W^T c_3 e_1 \ . \tag{3.75}$$

Then

$$\dot{V} = -x^T Q x \ , \tag{3.76}$$

and hence by Lyapunov's theorem [Vidyasagar, 1978], because Q is positive definite, $x^T = (e, \dot{e}) = (0, 0)$ is an asymptotically stable equilibrium point.

The parameter adaptation law can be derived from (3.75). Specifically, since $\Phi = P - \hat{P}$ and P is assumed to be constant or slowly-varying, the parameter adaptation law is

$$\dot{\hat{P}} = -\dot{\Phi} = \Gamma W^T c_3 e_1 = \Gamma W^T c_3 (e + \dot{e}) \ . \tag{3.77}$$

Figure 3.6 shows the block diagram for Adaptive Controller II. Note that K_d and K_p in Figure 3.6 have absorbed the constant $1/c_3$.

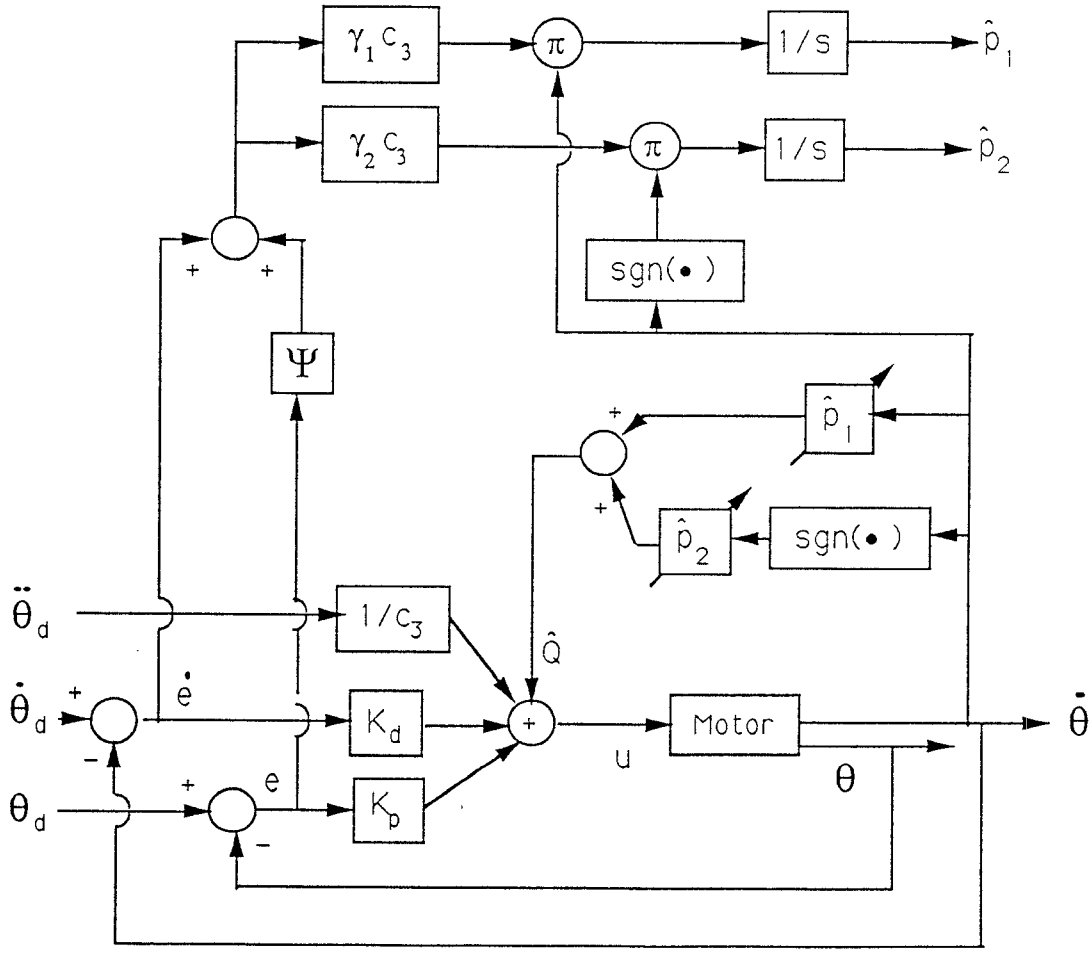

Figure 3.6: Adaptive Controller II

3.4.3 Adaptive Controller III

Adaptive Controller III provides friction-compensating control according to the strategy of [Walrath, 1984] described in Section 3.3. This strategy uses the Dahl model of friction to dynamically predict and compensate for friction. Specifically, friction is computed according to a first-order equation (3.20) characterized by a time constant τ. Walrath empirically derived a relationship for τ as a function of operating conditions and found that $1/\tau$ was a linear function of $\ddot{\theta}_p$ (3.24). As previously noted, this relationship is inconsistent with Dahl's model which predicts $1/\tau$ as a linear function of $\dot{\theta}_p$ (3.23).

On the other hand, a *consistent* relationship for τ was found for the electric motor of this study. Indeed, experiments similar to Walrath's were performed on the motor to determine τ as a function of operating conditions. The empirically derived relationship took the form

$$1/\tau = \omega = a + b\,|\dot{\theta}_p| \tag{3.78}$$

where a and b are constants. Thus, $1/\tau$ is a linear function of $\dot{\theta}_p$ as predicted by Dahl. Details of the experiments are provided in Section 4.5.4. Relationship (3.78) is incorporated in Adaptive Controller III in place of Walrath's calculation of τ (3.24).

Additionally, while Walrath's controller only used proportional feedback control in conjunction with the friction compensation, Adaptive Controller III uses

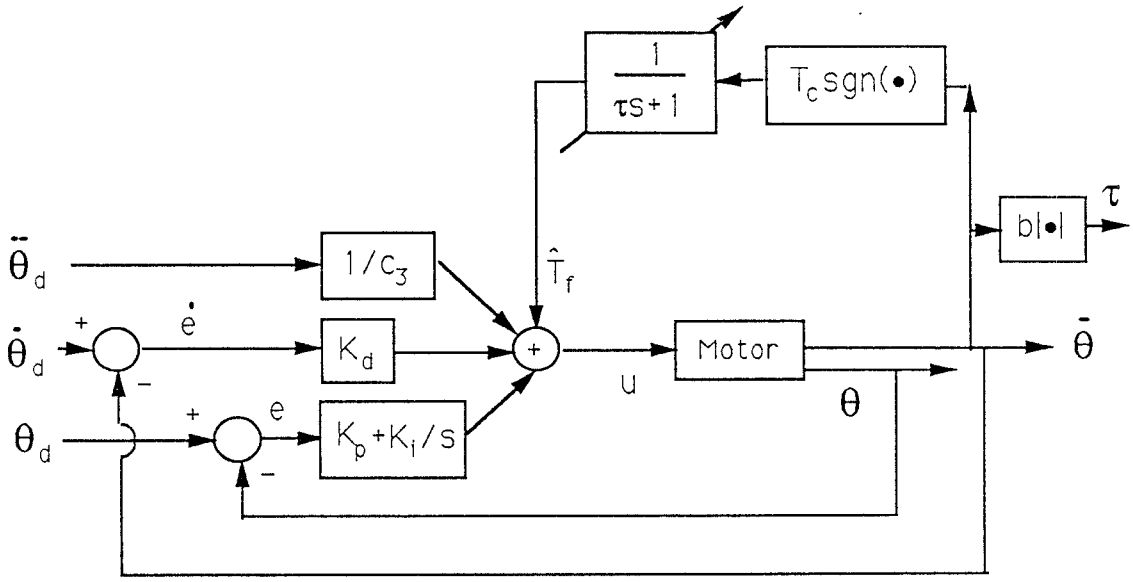

Figure 3.7: Adaptive Controller III

feedback control based on the computed torque method with integration. The control input u is defined by

$$u = (1/c_3)\ddot{\theta}_p + K_v\dot{e} + K_p e + K_i\int e + \hat{T}_f \tag{3.79}$$

where $\hat{T}_f$ is the friction torque estimate. Figure 3.7 shows a block diagram of Adaptive Controller III.

Since Walrath did not provide a stability analysis for his controller, an original stability analysis has been developed based on the passivity formalism. The definitions and theorems of the passivity formalism used below are taken from [Hill and Moylan, 1976,Hill and Moylan, 1977,Hill and Moylan, 1980].

Definition: A system of the form

$$\dot{x} = f(x) + G(x)u$$

$$y = h(x) + J(x)u \tag{3.80}$$

with supply rate (an abstraction of input power associated with the concept of stored energy in a physical system)

$$w(u,y) = y^T Q y + 2y^T S u + u^T R u \tag{3.81}$$

is dissipative if

$$\int_{t_0}^{t_1} w(t)dt \geq 0 \tag{3.82}$$

along trajectories of the system (3.80), for all locally square integrable $u(\cdot)$, all $t_1 \geq t_0$, and $x(t_0) = 0$. If

$$w(u,y) = u^T y - \epsilon y^T y \tag{3.83}$$

for $\epsilon > 0$ then the system is Y-strongly passive (YSP).

Consider Adaptive Controller III with friction prediction and derivative feedback only as shown in Figure 3.8. Then according to [Hill and Moylan, 1977], if both H_1 and H_2 are YSP, then the feedback system is asymptotically stable. The fact that $H_2 = 1$ from Figure 3.8 is SPR implies that H_2 is YSP [Åström and Wittenmark, 1989]. It remains to prove that H_1 is YSP.

System H_1 can be described by the following equations:

$$\ddot{\theta}_p + c_1\dot{\theta}_p = -c_2 T_f + c_2\hat{T}_f + c_3 K_d \dot{e}\ , \tag{3.84}$$

$$\dot{T}_f = -\omega T_f + \omega T_c sgn(\dot{\theta}_p)\ , \tag{3.85}$$

$$\dot{\hat{T}}_f = -\hat{\omega}\hat{T}_f + \hat{\omega} T_c sgn(\dot{\theta}_p)\ . \tag{3.86}$$

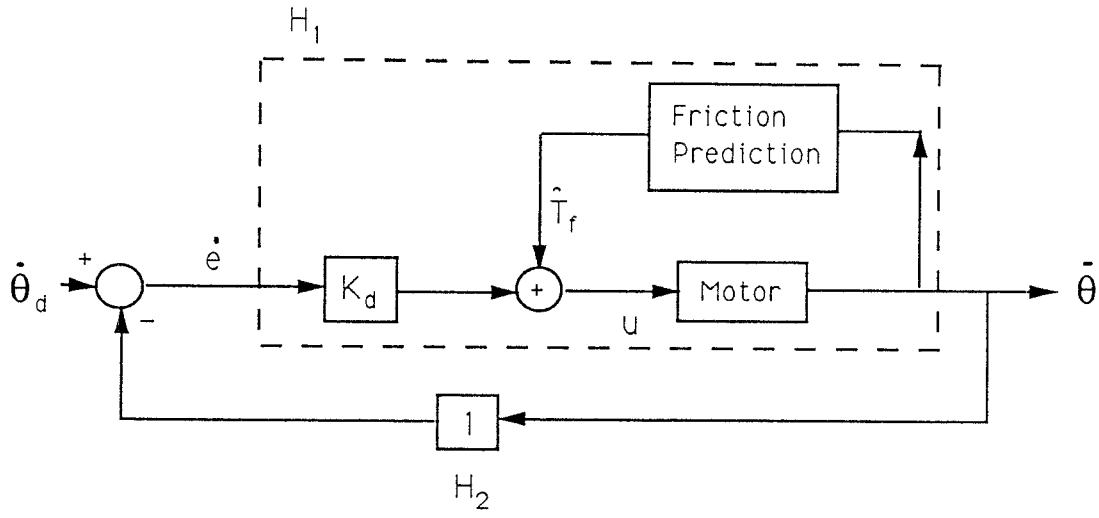

Figure 3.8: Adaptive Controller III Model for Stability Proof Using Passivity Formalism

Assuming $a \approx 0$ from (3.78) then $\omega = b|\dot{\theta}_p|$ and $\hat{\omega} = \hat{b}|\dot{\theta}_p|$ and so (3.85) and (3.86), respectively, become

$$\dot{T}_f = -b|\dot{\theta}_p|T_f + bT_c\dot{\theta}_p \ , \tag{3.87}$$

$$\dot{\hat{T}}_f = -\hat{b}|\dot{\theta}_p|\hat{T}_f + \hat{b}T_c\dot{\theta}_p \ . \tag{3.88}$$

Defining the four states $(x_1, x_2, x_3, x_4) = (\theta_p, \dot{\theta}_p, T_f, \hat{T}_f)$, H_1 can be presented in the form of (3.80) as

$$\begin{bmatrix} \dot{x_1} \\ \dot{x_2} \\ \dot{x_3} \\ \dot{x_4} \end{bmatrix} = \begin{bmatrix} x_2 \\ -c_1x_2 - c_2x_3 + c_2x_4 \\ -b|x_2|x_3 + bT_cx_2 \\ \hat{b}|x_2|x_4 + \hat{b}T_cx_2 \end{bmatrix} + \begin{bmatrix} 0 \\ c_3K_d \\ 0 \\ 0 \end{bmatrix} u \ , \tag{3.89}$$

$$y = x_2 \tag{3.90}$$

where $u = \dot{e}$. Now define $\phi : \mathcal{R}^4 \mapsto \mathcal{R}$ as

$$\begin{aligned}\phi(x) &= \frac{c_2}{c_3 K K_d}[\frac{K}{2c_2}{x_2}^2 + x_3(x_1 - \gamma_1/b) - \tfrac{1}{2}T_c b(x_1 - \gamma_1/b)^2 + \int b x_1 x_3 |x_2| \\ &\quad + x_4(x_1 - \gamma_2/\hat{b}) - \tfrac{1}{2}T_c \hat{b}(x_1 - \gamma_2/\hat{b})^2 + \int \hat{b} x_1 x_4 |x_2|]\end{aligned} \tag{3.91}$$

where K, γ_1, and γ_2 are constants to be defined later. Differentiating (3.91) with respect to time yields the supply rate

$$\dot{\phi}(x) = uy - \epsilon y^2 + \frac{c_2}{c_3 K K_d}[x_2 x_3 - K x_2 x_3 + \gamma_1 |x_2| x_3 + x_2 x_4 + K x_2 x_4 + \gamma_2 |x_2| x_4] \tag{3.92}$$

where $\epsilon = c_1/c_3 K_d > 0$. First consider the case when $x_2 = \dot{\theta}_p \geq 0$. Then (3.92) becomes

$$\dot{\phi}(x) = uy - \epsilon y^2 + \frac{c_2}{c_3 K K_d}[(1 - K + \gamma_1)|x_2| x_3 + (1 + K + \gamma_2)|x_2| x_4] \,. \tag{3.93}$$

So choose $\gamma_1 > -1$ and $\gamma_2 < -1$ such that $\gamma_1 + \gamma_2 = -2$, then $K = 1 + \gamma_1 = -1 - \gamma_2 > 0$ and

$$\dot{\phi}(x) = uy - \epsilon y^2 \,. \tag{3.94}$$

If on the other hand $x_2 = \dot{\theta}_p \leq 0$, then (3.92) becomes

$$\dot{\phi}(x) = uy - \epsilon y^2 + \frac{c_2}{c_3 K K_d}[(-1 + K + \gamma_1)|x_2| x_3 + (-1 - K + \gamma_2)|x_2| x_4] \,. \tag{3.95}$$

Choose $\gamma_1 < 1$ and $\gamma_2 > 1$ such that $\gamma_1 + \gamma_2 = 2$ then $K = 1 - \gamma_1 = -1 + \gamma_2 > 0$ and (3.94) holds.

According to [Hill and Moylan, 1976] to show that H_1 is dissipative with respect to the supply rate given by (3.94), $\phi(0) = 0$ and $\phi(x) \geq 0 \; \forall x$ must hold.

These do not hold for the function $\phi(\cdot)$ as defined by (3.91). However, for $x_2 = \dot{\theta}_p \geq 0$ (or $x_2 = \dot{\theta}_p \leq 0$) $x_1 x_3 = T_f \theta_p \geq 0$ and $x_2 x_4 = \hat{T}_f \theta_p \geq 0$. Additionally, x_1 and x_3 are both bounded since $0 \leq x_1 = \theta_p \leq 2\pi$ and $-T_c \leq x_3 = T_f \leq T_c$. Therefore $\phi(\cdot)$ from (3.91) is bounded below. Define C as the greatest lower bound of $\phi(x)$. Then there exists some $x_0 \in \mathcal{R}^4$ such that $\phi(x_0) = C$. Next define the map $\Psi : X \mapsto Y$ such that $\Psi(x_0) = 0$, i.e.,

$$\Psi(x) = x - x_0 = y \ . \tag{3.96}$$

Then define $\bar{\phi}(\cdot)$ by

$$\bar{\phi}(y) = \phi(\Psi^{-1}(y)) = \phi(y + x_0) \ . \tag{3.97}$$

So $\bar{\phi}(0) = C$ and $\bar{\phi}(y) \geq C \ \forall y$. Finally, let $\tilde{\phi}(\cdot)$ be defined by

$$\tilde{\phi}(y) = \bar{\phi}(y) - C \ . \tag{3.98}$$

Then $\tilde{\phi}(0) = 0$ and $\tilde{\phi}(y) \geq 0 \ \forall y$. Note that $\dot{\tilde{\phi}}(y) = \dot{\bar{\phi}}(y) = \dot{\phi}(y)$ which is given by (3.94). Thus H_1 is YSP and the feedback system of Figure 3.8 is input-output asymptotically stable. This implies that $\dot{\theta}_p$ will follow $\dot{\theta}_d$.

Chapter 4

Experimental Program

4.1 Hardware Description

The experimental system (shown in Figure 4.1 [Wang, 1987]) consisted of a direct-drive, brush-type dc motor, angular position and velocity sensors, a power amplifier, an IBM AT personal computer (PC), and supporting hardware and software for communication and control. A DDA06 board manufactured by Metrabyte provided digital-to-analog (D/A) conversion and digital I/O, and a Metrabyte DASH16 board provided analog-to-digital (A/D) conversion. The motor, manufactured by Inland Motors, used samarium-cobalt permanent magnets and produced a peak output torque of 40 lbf-in and a maximum no-load speed of 14 rad/s [Frank, 1986]. The motor parameters measured by

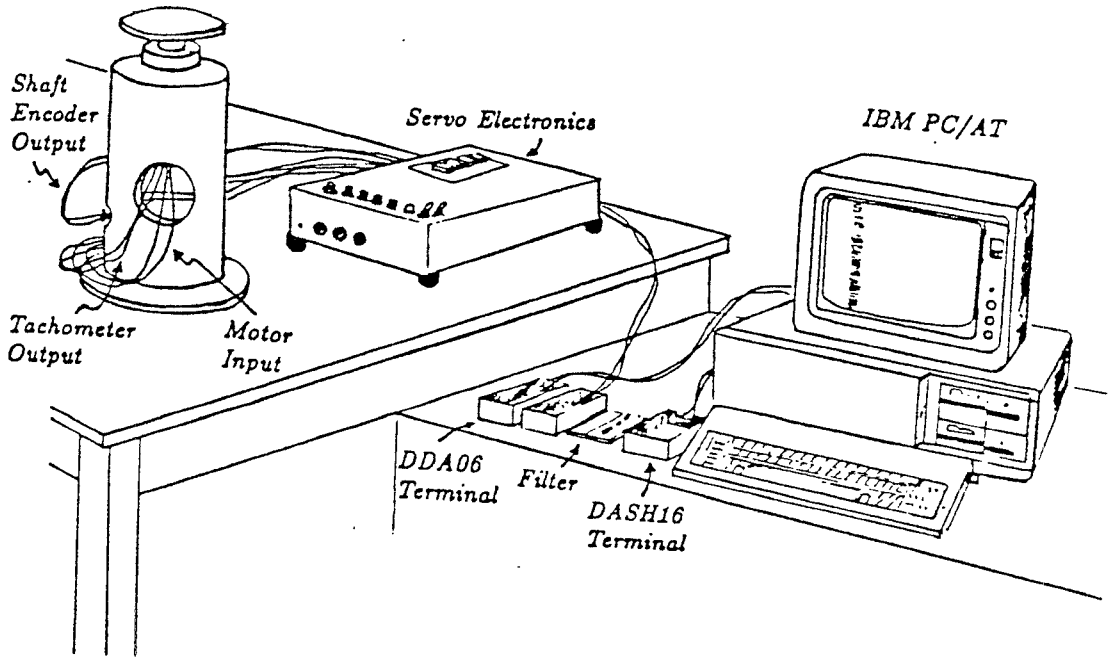

Figure 4.1: Experimental System (reproduced with permission from L.-S. Wang MS thesis)

[Frank, 1986,Wang, 1987] were as follow:

K_t	$\triangleq$	motor torque constant	=	21.62	lbf-in/amp
K_v	$\triangleq$	motor voltage constant	=	2.443	volt-s/rad
R	$\triangleq$	equivalent motor resistance	=	33.6	ohms
J	$\triangleq$	inertia of motor, shaft, and table	=	0.1	lbf-in-s^2/rad

The IBM PC was used to control the operation of the motor. By means of controller software, the PC generated a digital control signal. Before being input to the motor this digital control signal passed through the DDA06 D/A converter where it was converted into an analog voltage signal. The original

digital signal ranged from 0 to 4095 (12 bit signals) where ideally 0 converted to -10 volts and 4095 converted to +10 volts. In reality a digital signal equal to 2005 corresponded to 0 volts. Additionally, the digital signal was limited in the software to the range 5 to 4005 to avoid saturation in the D/A converter and power amplifier. From the D/A converter the voltage signal passed through the power amplifier. The amplifier multiplied the voltage signal by a factor of 6.02 [Wang, 1987]. The output of the power amplifier was input to the motor.

Angular position of the motor was measured by an optical shaft encoder. Two digital I/O channels of the DDA06 board were used to input the 12 bit encoder data to the PC. This yielded a position measurement resolution of 0.00154 radians (0.088 degrees).

A tachometer measured angular velocity of the motor. The tachometer measurement, an analog voltage signal, was passed through a low-pass filter to remove high-frequency noise before being converted to a digital signal through one channel of the DASH16 board. In the A/D converter the analog voltage signal which ranged from -10 volts to +10 volts was converted to an integer from -2048 to +2047. The tachometer was scaled such that it developed 0.408 volts per rad/s [Frank, 1986], i.e., 2.45 rad/s per volt, which yielded a velocity measurement resolution of 0.012 rad/s.

The digital sampling rate was set using the timer on the DASH16 board. A 50 Hz sampling rate was used throughout the experimental program.

4.2 System Model and Verification

Neglecting the equivalent inductance of the motor, the following equations provide a second order model of the motor:

$$\tau = K_t i = J\ddot{\theta}_p + \mu\dot{\theta}_p + T_f \tag{4.1}$$

$$V = Ri + V_b \tag{4.2}$$

$$V_b = K_v\dot{\theta}_p \tag{4.3}$$

where:

τ is torque to the motor (lbf-in)

i is current through the motor (amps)

V is voltage across motor (volts)

Substituting (4.3) into (4.2) and solving for i yields:

$$i = V/R - K_v\dot{\theta}_p/R \tag{4.4}$$

Then substituting (4.4) into (4.1) for i gives the system dynamics as:

$$\ddot{\theta}_p + (K_tK_v/RJ + \mu/J)\dot{\theta}_p = -(1/J)T_f + (K_t/RJ)V \tag{4.5}$$

which is identical to (3.2) for $c_1 = K_tK_v/RJ + \mu/J$, $c_2 = 1/J$, $c_3 = K_t/RJ$, and $u = V$.

The system can also be modelled in state-space form where the state vector is $[\theta_p \quad \dot{\theta}_p]$, and the input to the system is the motor voltage, i.e., $u = V$. The

state-space description of the system is then:

$$\dot{x} = Ax + Bu + NL \tag{4.6}$$

where:

$$A = \begin{bmatrix} 0 & 1 \\ 0 & -c_1 \end{bmatrix}, \quad B = \begin{bmatrix} 0 \\ c_3 \end{bmatrix}, \quad NL = \begin{bmatrix} 0 \\ -c_2 T_f \end{bmatrix} \tag{4.7}$$

For system simulations, friction was modelled as kinetic plus viscous friction. The friction parameters, assumed to be constant, were measured in previous work by [Wang, 1987] as follows:

$$\begin{aligned} F_s &= \begin{cases} 0.73 \text{ lbf-in}, & \dot{\theta}_p > 0 \\ -1.12 \text{ lbf-in}, & \dot{\theta}_p < 0 \end{cases} \\ F_k &= \begin{cases} 0.63 \text{ lbf-in}, & \dot{\theta}_p > 0 \\ -0.81 \text{ lbf-in}, & \dot{\theta}_p < 0 \end{cases} \\ \mu &= 0.048 \text{ lbf-in-s/rad} \end{aligned} \tag{4.8}$$

For the simulations, the magnitude of F_k and F_s were defined as the average of the measured magnitudes in the positive and negative velocity directions, i.e., $F_k \stackrel{\Delta}{=} 0.72 \text{ sgn}(\dot{\theta}_p)$ and $F_s \stackrel{\Delta}{=} 0.92 \text{ sgn}(\dot{\theta}_p)$. Integration of the two-dimensional state-space system was performed in simulations using a midpoint technique with a 1 millisecond time step. The nonlinear friction term was assumed to be constant throughout each time step.

In order to verify the motor model, results of experiments performed on the motor were compared to simulator results. The experiments consisted of

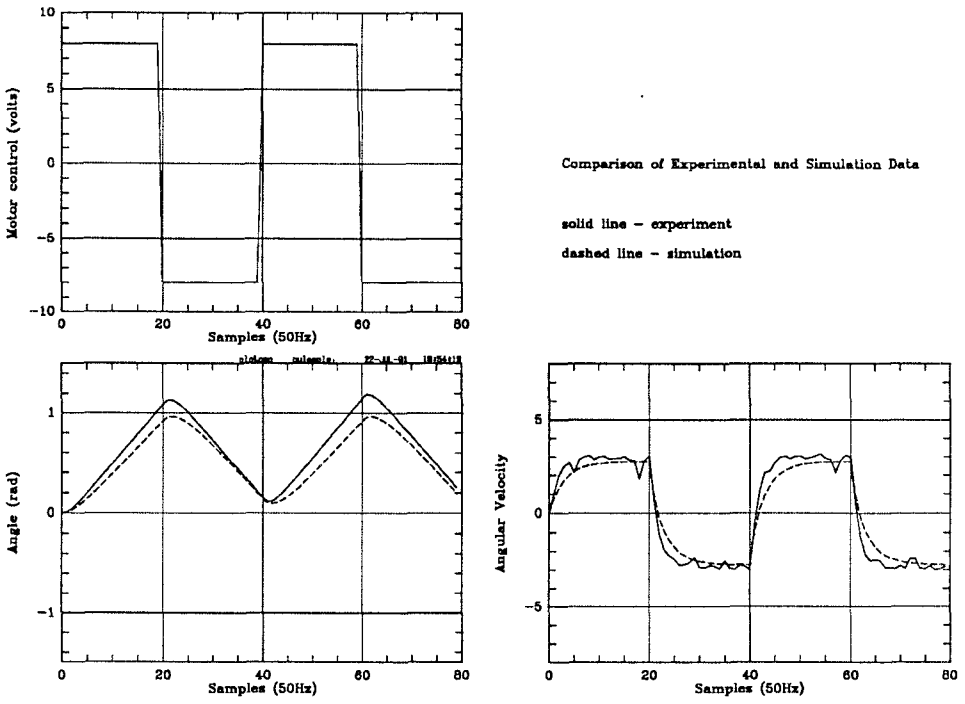

Figure 4.2: Comparison of Measured and Calculated Responses to the Same Input

sending voltage pulses to the motor and measuring the angular position and velocity responses. The same pulse signal was input to the simulated motor and the resulting position and velocity responses were calculated.

A comparison of the measured and calculated responses to the same input is shown in Figure 4.2. In this experiment a constant -8 volts was input to the motor for 20 samples (0.4 seconds) followed by a constant +8 volts for 20 samples, etc. As can be seen in the figure, the simulator responded somewhat more slowly than the actual motor. Figure 4.3 shows the same comparison except that in the simulator calculation motor inertia J was reduced to 0.04 lbf-in-s^2/rad. The comparison reveals better correspondence between the experimental and

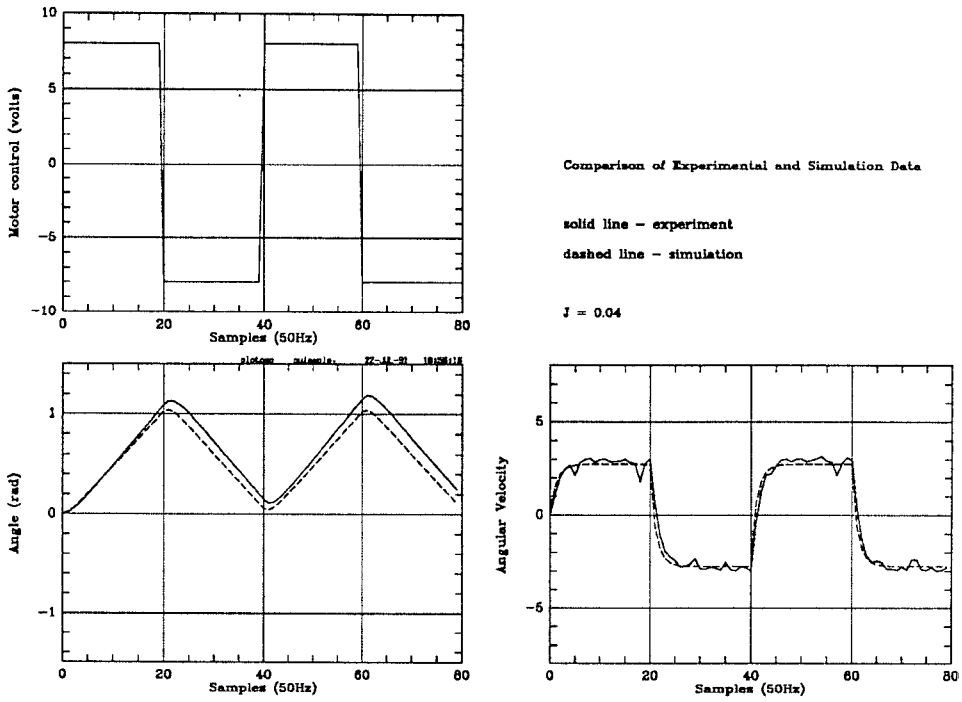

Figure 4.3: Comparison of Measured and Calculated Responses to the Same Input, $J = 0.04$

simulator responses which may indicate that motor inertia has been overestimated. Nonetheless, when using the motor model to determine PID controller gains, as will be described in the next section, the value of the inertia J was not changed to 0.04 lbf-in-s^2/rad since it had an insignificant effect on the controller gain selection.

In both Figures 4.2 and 4.3, it can be seen that the measured motor velocity response is not smooth as predicted by the simulator. This is because the simulator does not include a model of torque ripple. Torque ripple can be observed in Figure 4.4 which shows the angular velocity response of the motor to a constant low voltage input. In effect, torque ripple generates a position-

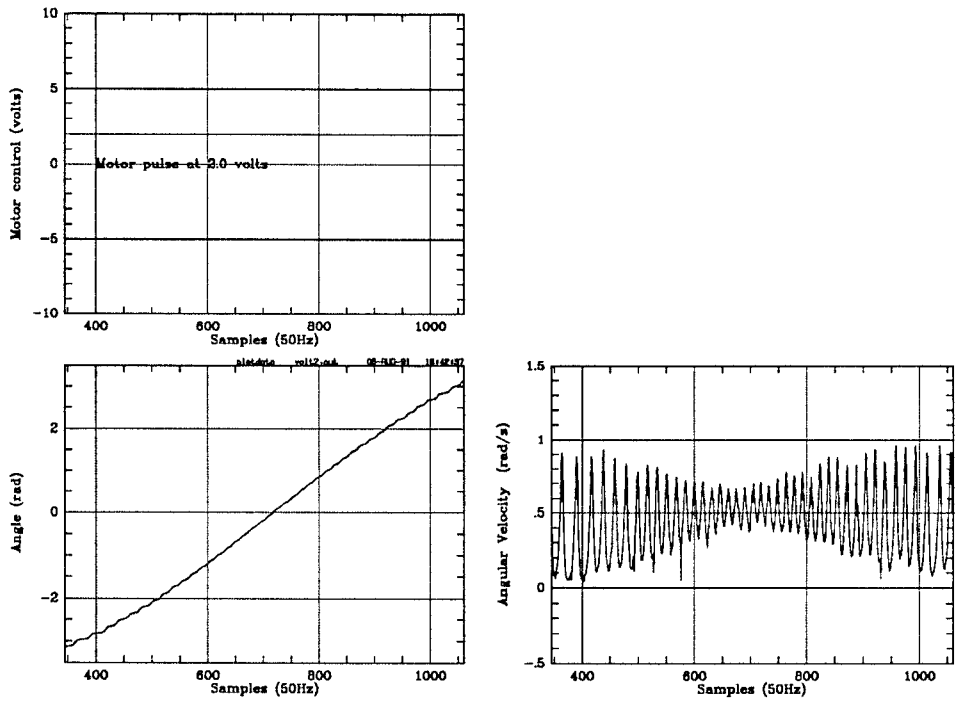

Figure 4.4: Experimental Evidence of Torque Ripple in Motor

dependent deviation. An investigation of the effect of torque ripple on the results of the experimental program is described in Section 4.6.

Based on the techniques described in Chapter 2, the experimental system can be analyzed for the possibility of stick-slip oscillations. According to Section 2.3, phase plane analysis can be used to determine a minimum velocity below which a stick-slip limit cycle might occur. Substituting the model parameters into the equation for slipping conditions (2.31) yields:

$$J\ddot{x} + \mu(x - V) + Kx = F_k \tag{4.9}$$

where V and x are as described in Section 2.3. System stiffness K has been added for completeness and is estimated to be $K = 1.5 \times 10^6$ lbf-in/rad [Frank, 1986].

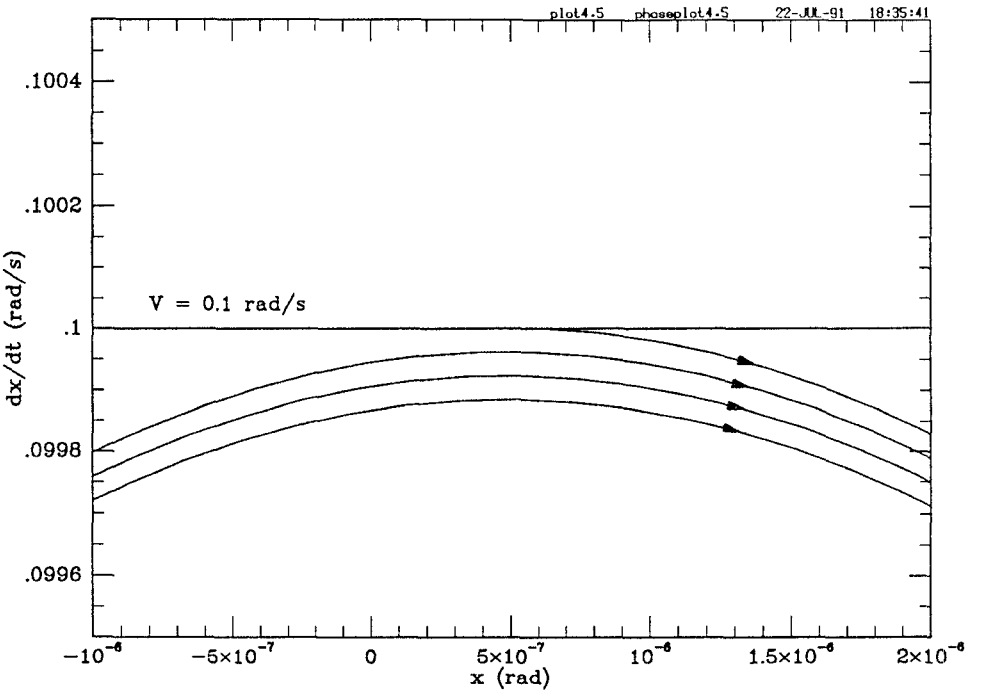

Figure 4.5: Phase-Plane Plot Close-up for System with Static, Kinetic and Viscous Friction, $V = 0.1$ rad/s

The solution to (4.9) is:

$$\begin{aligned} x &= (F_k + \mu V)/K + a_1 e^{-\beta t} cos\lambda t + a_2 e^{-\beta t} sin\lambda t \\ \dot{x} &= e^{-\beta t}[(-a_1\beta + a_2\lambda)cos\lambda t + (-a_2\beta - a_1\lambda)sin\lambda t] \end{aligned} \tag{4.10}$$

where $\beta = \mu/2J$, $\lambda = \sqrt{K/J - \beta^2}$, $a_1 = (F_s - F_k - \mu V)/K$, $a_2 = (V + \beta a_1)/\lambda$.

Using (4.11) the phase plane plot of the system with kinetic and static friction can be made for a given V. Figure 4.5 shows the phase plane plot for $V = 0.1$ rad/s. Under these conditions no stick-slip is predicted. However, for $V = 0.01$ rad/s, phase plane analysis predicts the possibility of a limit cycle as shown in Figure 4.6. Using this graphical technique, the critical velocity is calculated as approximately 0.019 rad/s which is of the same order as the resolution of the

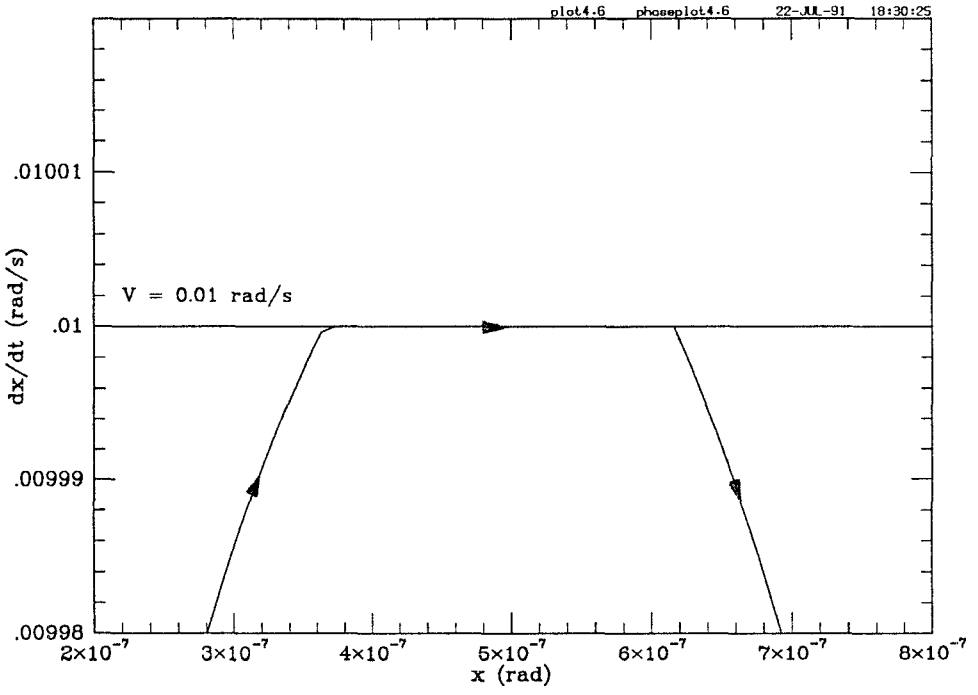

Figure 4.6: Phase-Plane Plot Close-up for System with Static, Kinetic and Viscous Friction, $V = 0.01$ rad/s

tachometer measurement.

4.3 Experiment Design

The experimental program on the electric motor consisted of comparative position trajectory tracking tests using five different controllers. The purpose of the program was to explore the relative effectiveness of these controllers. In each experiment the motor was required to track a sinusoidal position trajectory such that:

$$\theta_d = Asin(2\pi ft)$$

$$\dot{\theta}_d = 2\pi f A cos(2\pi f t) \tag{4.11}$$

$$\ddot{\theta}_d = -(2\pi f)^2 A sin(2\pi f t)$$

where A is the amplitude and f the frequency of the demanded trajectory. This required sinusoidal motion provided a useful means for investigating friction compensation since the motor was forced to repeatedly pass through zero velocity where friction behavior is most difficult to control. The sinusoidal motion also provided a reasonably realistic scenario since manipulators are often required to perform repetitive tasks that demand sinusoidal joint motions. Additionally, robotic manipulators that are airborne or operate in environments such as factories are susceptible to disturbances. The manipulator may be required to stabilize a given position despite these disturbances. Sinusoidal trajectory tracking can be viewed as roughly equivalent to position regulation under sinusoidal disturbances.

The sinusoidal trajectories tracked in the experimental program ranged in frequency f from 0.1 Hz to 1.0 Hz. The lower limit of this range was selected to minimize motor velocity and to not introduce large errors due to velocity measurement resolution. The upper limit of this range was selected to maximize motor velocity without generating gross errors due to the limitations of the 50 Hz sampling rate. A 0.25 radian amplitude A was used for all sinusoidal trajectory tracking experiments.

The first of the five controllers tested was a PID controller that used optimized gains determined as described in Section 4.4. This PID controller was designed to provide excellent linear control and be used as a benchmark for comparison with the other four nonlinear controllers. A PID controller was chosen as the benchmark since it is not only a very typical design but also effective for controlling dc motors. The second controller employed dither to illustrate the relative effectiveness of a smoothing technique for friction compensation. The final three controllers, Adaptive Controllers I, II, and III, were tested to illustrate the improved accuracy provided by adaptive friction compensation. Additionally, these controllers were used to investigate a variety of friction models.

The direct-drive feature of the electric motor was advantageous for investigating friction-compensating control strategies. In particular, friction was generated only in the motor bearings. Gears would have introduced more friction making the nature of the system's friction more complex. The absence of gears in the direct-drive system provided an isolated friction source and thus a more straightforward test bed for experimental research.

4.4 Optimal PID Controller Design

The PID controller gains were selected to optimize the motor response to a 0.25 radian step demand in angular position. CONSOLE, a numerical optimization

tool described in [Fan et al., 1987], was used to perform the optimization. The gains, K_p, K_i, and K_d, were used as the three design parameters in the optimization problem. Two functional objectives were specified, one to minimize the overshoot of the step response and one to maximize the rise of the step response. In performing the optimization, CONSOLE called a simulation of the controller and the motor. The motor was modelled as described in Section 4.2. The controller was modelled according to the following equation:

$$u = \ddot{\theta}_d/c_3 + K_p e + K_i \int e + K_d \dot{e} \tag{4.12}$$

Figure 4.7 shows the resulting response of the simulated motor to the 0.25 radian position step demand when using the PID controller with optimized gains determined by CONSOLE. The optimized controller gains are as follows:

$$\begin{aligned} K_p &= 126 \quad \text{volt/rad} \\ K_i &= 22.0 \quad \text{volt/rad-s} \\ K_d &= 4.32 \quad \text{volt-s/rad} \end{aligned}$$

Figure 4.8 shows the actual motor response to a 0.25 radian position step demand using the PID controller with the above optimized controller gains. The smooth, fast, and accurate response observed in this figure verifies the effectiveness of the selected optimal controller.

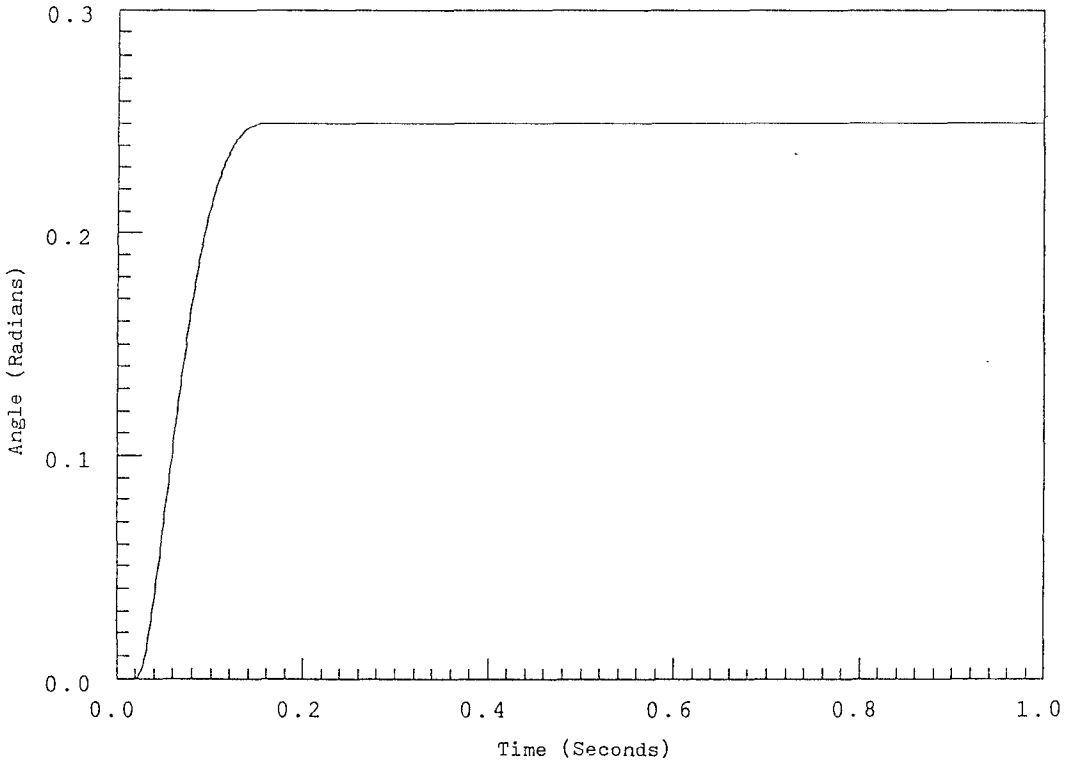

Figure 4.7: Simulated Data for PID Controlled Motor Response to 0.25 Radian Position Step

4.5 Implementation of Control Strategies

All of the five controllers tested were implemented digitally on the IBM PC. The sampling rate of 50 Hz was assumed to provide a small enough sample size such that the digital implementations were fairly good approximations of the continuous controllers. Tustin's rule was used for transformations from differential equations to difference equations [Franklin et al., 1990]:

$$\frac{d}{dt} \mapsto \frac{2}{T}\left(\frac{1-z^{-1}}{1+z^{-1}}\right) \tag{4.13}$$

The implementation of the PID controller was described fully in the previous

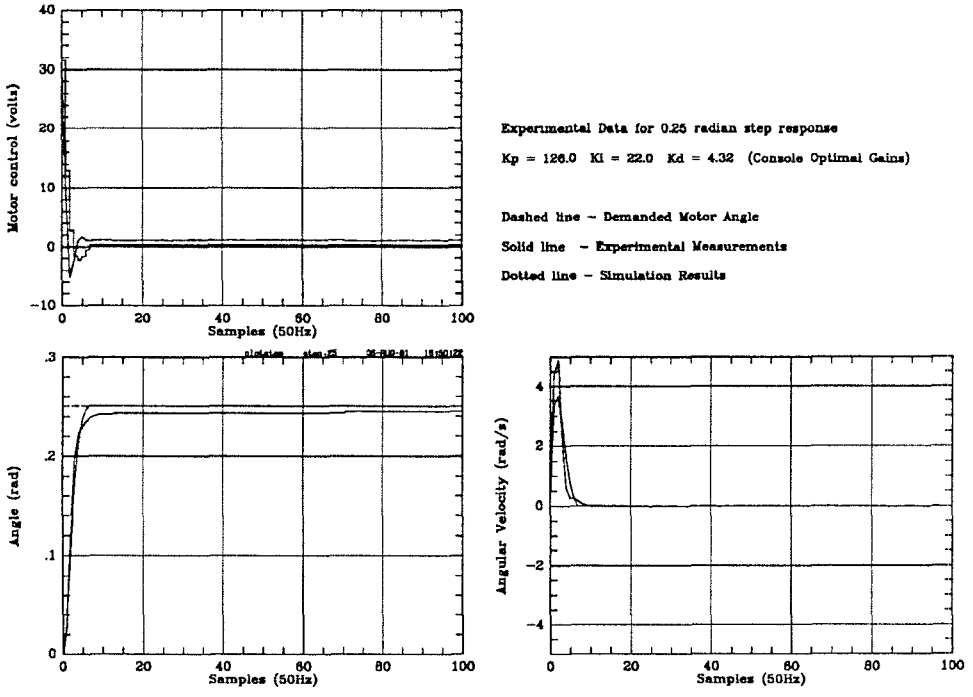

Figure 4.8: Experimental Data for PID Controlled Motor Response to 0.25 Radian Position Step

section. Details of the implementation of the four nonlinear controllers are provided below.

4.5.1 Controller with Dither

The controller with dither was implemented identically to the PID controller except that a dither signal was added to the control input. The frequency of the dither signal was 25 Hz which is the maximum possible given the 50 Hz sampling rate. The amplitude of the dither signal was 4 volts. This corresponds to 2.6 lbf-in which is more than twice the magnitude of the static friction.

4.5.2 Adaptive Controller I

Adaptive Controller I was implemented according to the equations of Section 3.4.1. The ideal model of (3.29) was defined by the following parameters:

$$\begin{aligned} d_1 &= 23.33 \quad s^{-1} \\ d_2 &= 210 \quad s^{-2} \\ p_1 &= 14 \quad s^{-1} \\ p_2 &= 15 \quad s^{-1} \end{aligned}$$

The gains of the adaptive component were $p_3 = 1$ and $p_4 = 9$.

The gains in the adaptation law (3.50) were selected such that $B_j = B$, $\forall j$ and $C_j = C$, $\forall j$ where B and C are constants. A variety of B and C values were used since it was found that while higher values of B and C improved controller performance, they also magnified system noise. Additionally, both tracking accuracy and noise magnification were increased when the controller was used to track a high frequency sinusoidal trajectory as opposed to a low frequency sinusoidal trajectory. For example, $B = 250$, $C = 150$ provided good performance for the 0.5 Hz sinusoidal trajectory tracking experiment. However, these gains led to instability in the 1.0 Hz experiment. For the 1.0 Hz experiment $B = 20$, $C = 10$ provided the best performance.

Adaptive Controller I was designed to make the servomechanism follow the output of the ideal model. Therefore, to make the results of the experiments consistent with the other controllers it was necessary for the *output* of the ideal

model θ_m, $\dot{\theta}_m$, and $\ddot{\theta}_m$ to be defined by the sinusoidal trajectory equations of (4.12). Let $H(s)$ be the transfer function of the ideal model (3.29) and $H^{-1}(s)$ be $1/H(s)$. Then the demand trajectory used for Adaptive Controller I was $\theta_d{}^{(I)} = H^{-1}(s)\theta_d$ so that $\theta_m = H(s)\theta_d{}^{(I)} = \theta_d$. Since the demand signals in all of the experiments were sinusoidal, the new demand trajectory $\theta_d{}^{(I)}$ was easily computed using the gain and phase of $H^{-1}(j\omega)$, i.e.,

$$\theta_d{}^{(I)} = MAsin(2\pi ft + \phi) \tag{4.14}$$

where M and ϕ are the magnitude and phase of $H^{-1}(j\omega)$, respectively, evaluated at $\omega = 2\pi f$. $\dot{\theta}_d{}^{(I)}$ and $\ddot{\theta}_d{}^{(I)}$ were found similarly.

4.5.3 Adaptive Controller II

Adaptive Controller II was implemented according to the equations of Section 3.4.2. Since integral control was not used in the nonadaptive feedback loop, K_p and K_d were recalculated using CONSOLE. $K_p = 129$ volt/rad and $K_d = 4.24$ volt-s/rad were the resulting optimized PD controller gains. For the filtered error calculation of (3.66), $\psi = 2$ was chosen such that $G(s)$ of (3.67) was SPR and the observability requirement of (3.71) was satisfied.

The adaptive gains γ_i were chosen to balance the effects of adaptation speed and noise. High gains yielded noisier but faster adaptation while low gains yielded less noisy but slower adaptation. The best values were found to be

$\gamma_i = 1, \forall i$.

According to the stability analysis of Section 3.4.2 [Craig, 1988], the angular position error e is expected to go to zero. However, the adaptive parameter errors $p_i - \hat{p}_i$ will go to zero only if the input to the system is persistently exciting (PE). The criteria for persistent excitation is [Craig, 1988]:

$$0 < aI_r \leq \int_{t_0}^{t_0+N} W_d{}^T W_d \; dt \leq bI_r \tag{4.15}$$

for all t_0 where a, b, and N are all positive, and W_d is W evaluated on the desired trajectory instead of the measured trajectory. In the presence of bounded disturbances, however, the PE condition is difficult to state [Craig, 1988]. This difficulty is relevant since noise, torque ripple, and possibly unmodelled friction dynamics provided bounded disturbances in the motor experiments. Nonetheless, limited identification of friction parameters was performed using Adaptive Controller II. For these experiments $\psi = 27$ and $\gamma_i = 1, \forall i$ were used.

4.5.4 Adaptive Controller III

Adaptive Controller III was implemented according to the equations of Section 3.4.3. The equation for friction time constant τ as a function of operating conditions was derived experimentally following the technique described in Section 3.3 [Walrath, 1984]. Five different sinusoidal tracking experiments were performed using Adaptive Controller III with constant τ. Each experiment was repeated

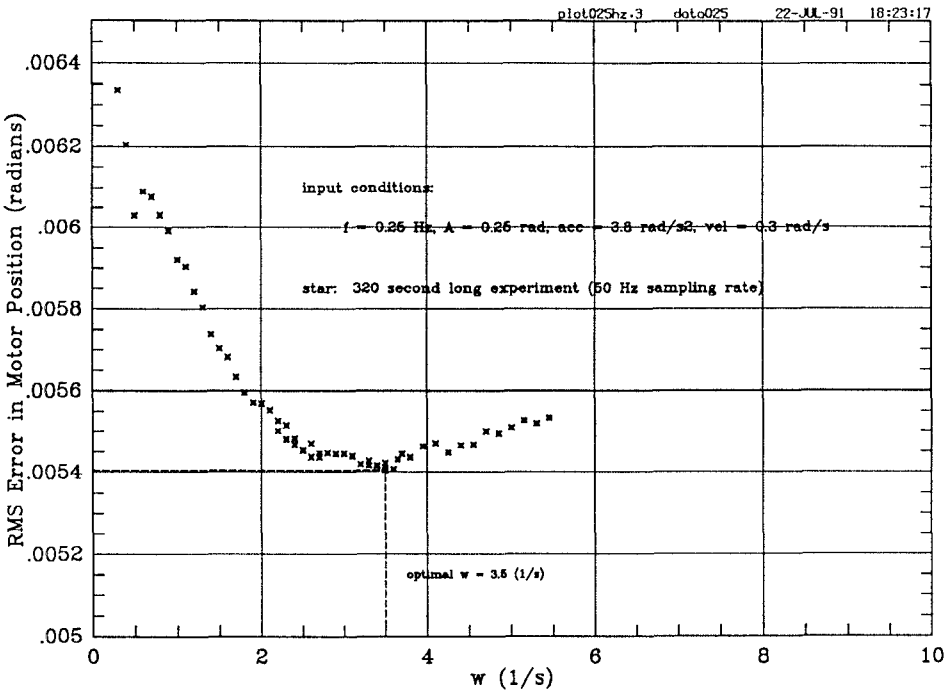

Figure 4.9: Experimental Results Used to Determine Optimal ω ($f = 0.25$ Hz)

many times, each time varying only τ, until the optimum τ was found.

Figure 4.9 shows the results of one of the five experiments. Root-mean-square (RMS) angular position error is plotted against $\omega = 1/\tau$ for sinusoidal trajectory tracking with $f = 0.25$ Hz and $A = 0.25$ rad. These experimental operating conditions resulted in an RMS acceleration of 3.8 rad/s^2, and an RMS velocity of 0.3 rad/s. Each point on the plot represents a single repetition of the experiment. The repetitions of this experiment were each run for 320 seconds. The optimal ω was found to be 3.5 s^{-1} which yielded an RMS position error of 0.0054 rad. Figure 4.10 plots the optimal values of ω for all five experiments as a function of RMS acceleration and velocity. From the velocity plot, ω_{opt} is observed to be a linear function of RMS velocity. The relationship was derived

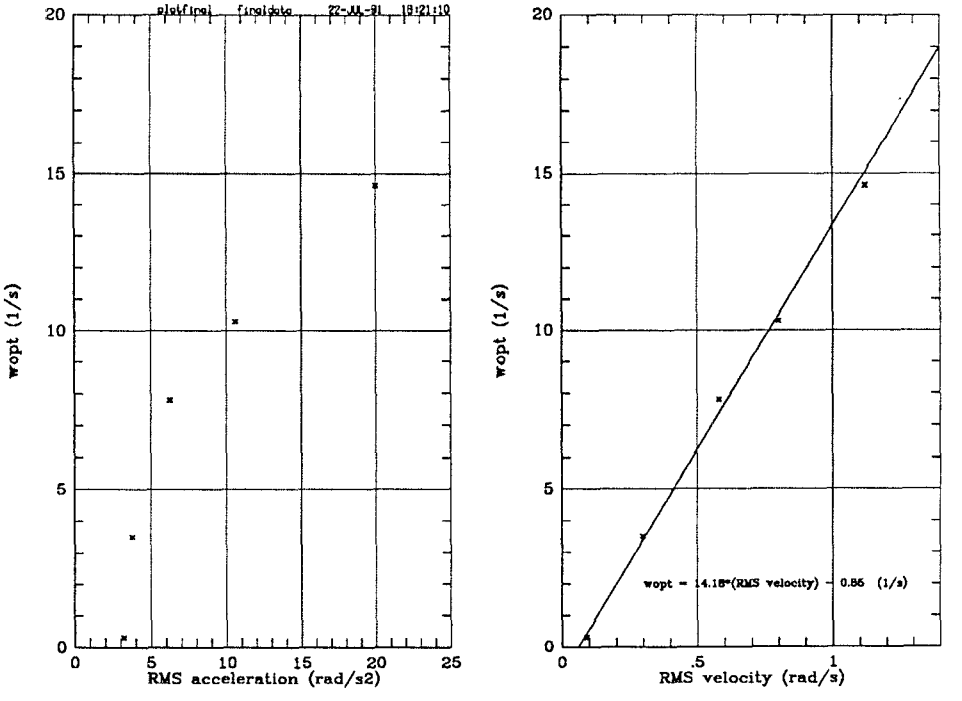

Figure 4.10: Optimal Values of ω as a Function of Operating Conditions

from this plot as follows:

$$\omega_{opt} = 1/\tau_{opt} = 14.18 \ \dot{\theta}_{rms} - 0.85 \ \ s^{-1} \tag{4.16}$$

(4.16) was implemented in Adaptive Controller III as a predictive means of determining τ. The absolute value of $\dot{\theta}_p$ was passed through a 1.0 rad/s digital low-pass filter to yield an approximation for $\dot{\theta}_{rms}$.

4.6 Results

The results of four seconds (200 samples) of the sinusoidal trajectory tracking experiment with the benchmark PID controller for $f = 0.5$ Hz are shown in Figure 4.11. The plot in the upper left corner shows the control input to the

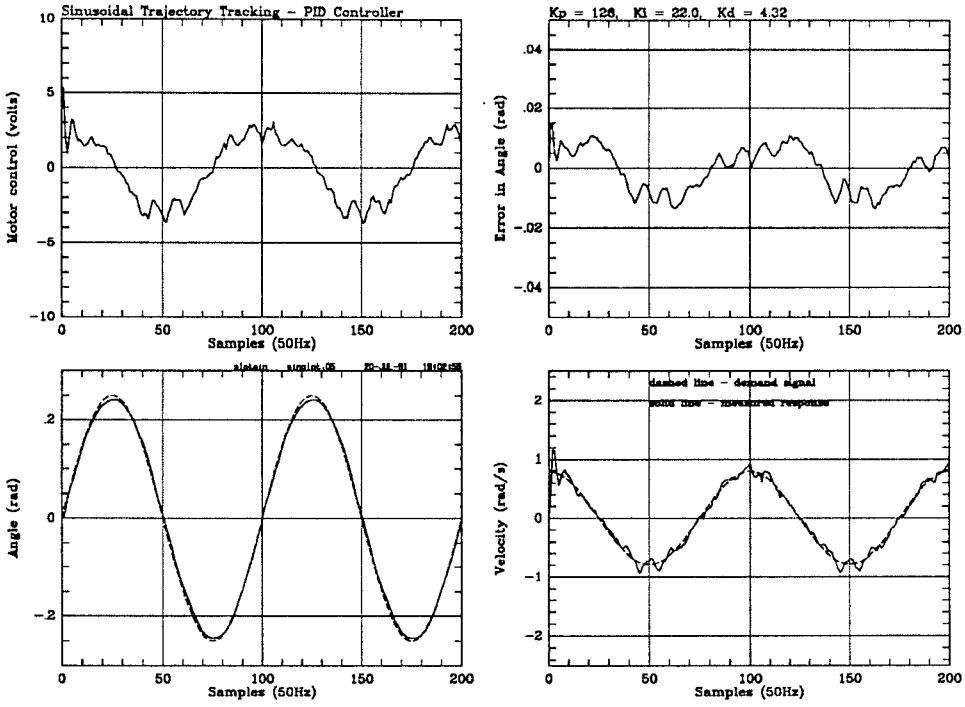

Figure 4.11: Results of Sinusoidal Trajectory Tracking Experiment with PID Controller

motor as a function of time. The plot in the lower left corner shows the motor angle as a function of time. The dashed line is the demanded position θ_d, and the solid line is the measured position θ_p. The position error, $\theta_d - \theta_p$ is shown in the upper right corner, and the demanded and measured velocities $\dot{\theta}_d$ and $\dot{\theta}_p$ are shown in the bottom right plot. The RMS position error for 16 seconds of this experiment was 0.0069 radians. The initial position of the motor was at 0.0 radians.

Figures 4.12, 4.13, 4.14, and 4.15 show the same plot as Figure 4.11 for the same experiment performed with the controller with dither, and Adaptive Controller I, II, and III, respectively. Note that for Adaptive Controller

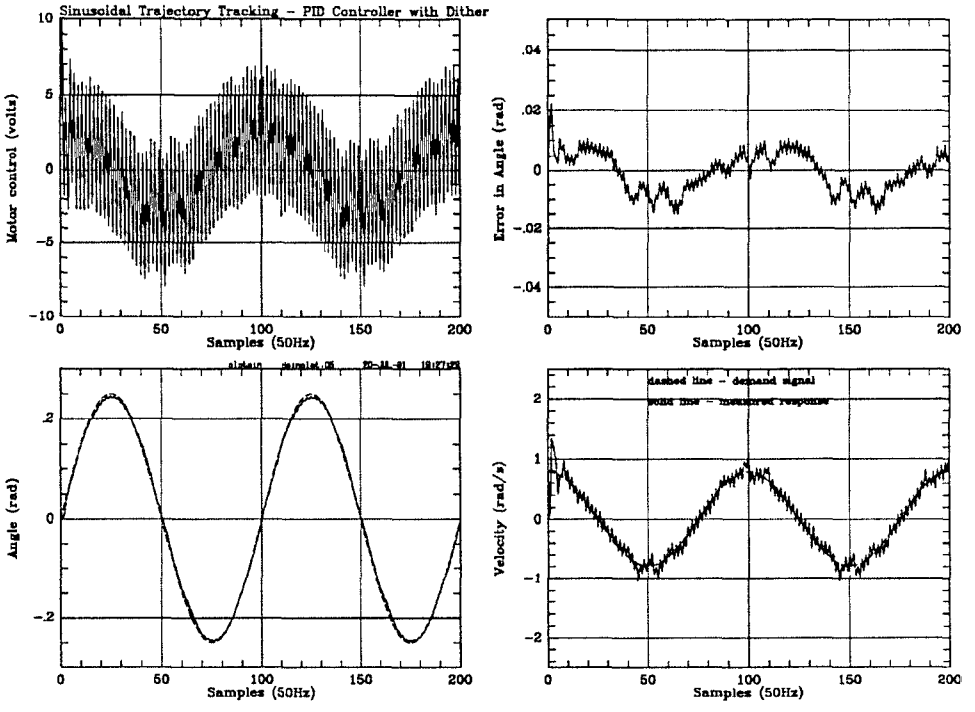

Figure 4.12: Results of Sinusoidal Trajectory Tracking Experiment with PID Controller with Dither

I in Figure 4.13, the measured signal follows the ideal model output (dotted line), not the actual demand signal (dashed line). As described in Section 4.5.2 the ideal model output is the same as the demand signal used for the other four controllers. Consequently, error in angle of Figure 4.13 is calculated as the difference between the ideal model output and the measured signal. For Adaptive Controllers II and III, in Figures 4.14 and 4.15, the component of input torque used for friction compensation is plotted. As can be seen in Figure 4.15, the shape of the friction-compensating torque generated by Adaptive Controller III is as predicted by Dahl's friction model. For all three adaptive controllers, the four seconds of the experiment shown are *not* the first four seconds of the experiments. A later four second period is shown since each controller takes

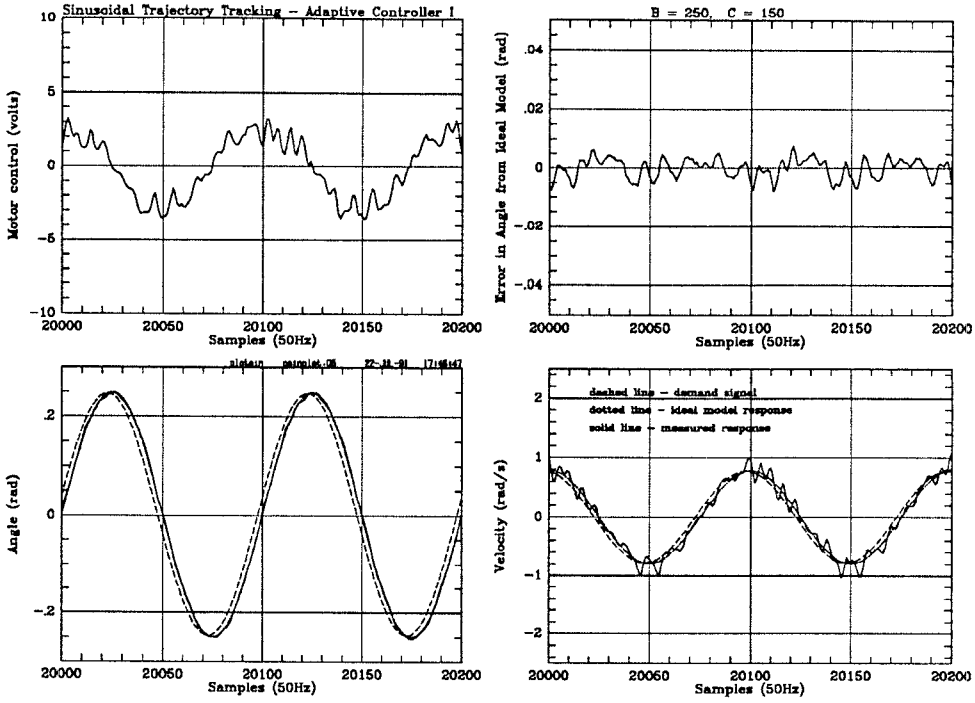

Figure 4.13: Results of Sinusoidal Trajectory Tracking Experiment with Adaptive Controller I

a little while to adapt. The exception is Adaptive Controller I which took a long while to adapt. Figure 4.14 shows the Adaptive Controller II experiment beginning 400 seconds (20,000 samples) into the experiment. The other two controllers are shown beginning 12 seconds (600 samples) into the experiment.

The RMS position error for each of the controllers is listed in Table 4.1. Each RMS position error is calculated based on 16 seconds (800 samples) of data. To further appreciate the differences in performance achieved by the different controllers, the position error from each controller is plotted as a function of time on the same graph as the position error from the benchmark PID controller. Figures 4.16, 4.17, 4.18, and 4.19 show the absolute value of PID controller

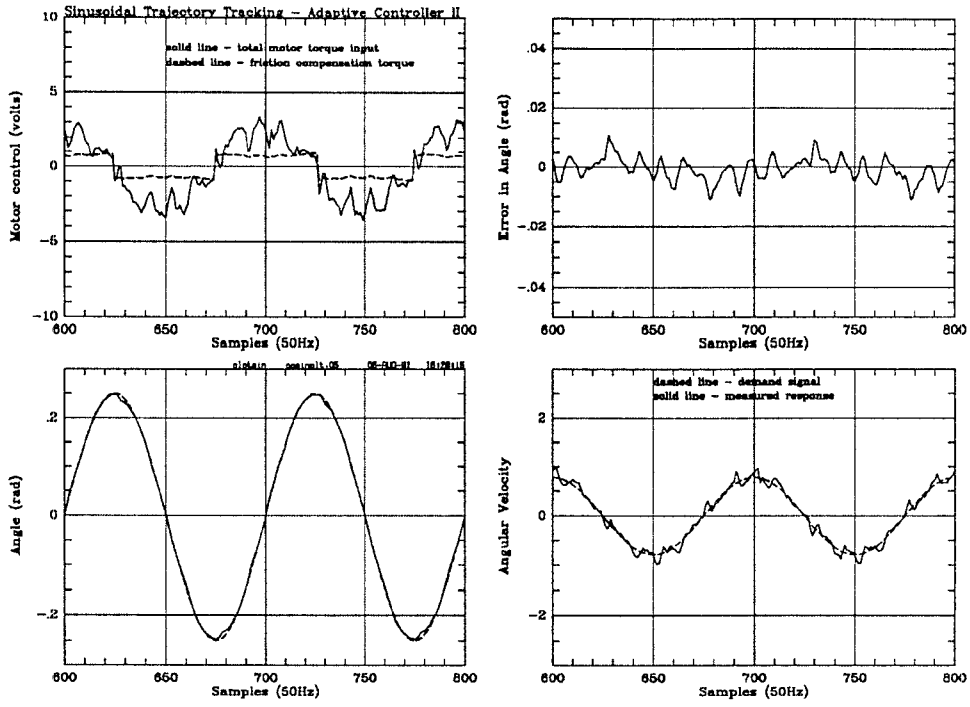

Figure 4.14: Results of Sinusoidal Trajectory Tracking Experiment with Adaptive Controller II

position error compared to the position error from the controller with dither, Adaptive Controllers I, II, and III, respectively. In each case the PID controller result is shown in a solid line and the nonlinear controller result is shown in a dashed line. Note that the two seconds (100 samples) shown correspond to the first two seconds of the experimental results shown in Figures 4.11 - 4.15.

As can be seen in Figure 4.16, the controller with dither does not significantly improve the tracking performance. This is most likely due to the fact that the dither frequency is limited to 25 Hz. In fact, tests were done at a 100 Hz digital sampling rate that showed that the controller with a 50 Hz dither signal provided almost twice as much percent reduction in RMS error than the 25 Hz dither

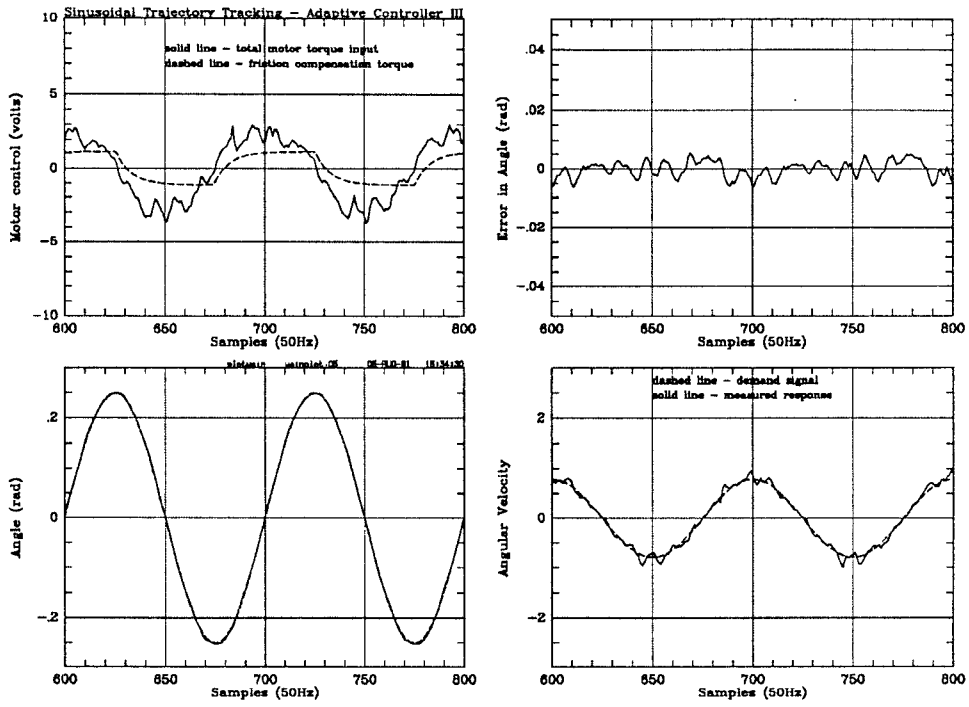

Figure 4.15: Results of Sinusoidal Trajectory Tracking Experiment with Adaptive Controller III

signal. Additionally, while the controller with the 25 Hz dither signal generated significant vibrations in the motor, the controller with the 50 Hz dither signal showed no evidence of vibrations.

Figure 4.17 illustrates that Adaptive Controller I made significant improvements on the PID controller performance. According to Table 4.1, the RMS error was reduced by 52 percent for this experiment. The adaptive controller gains used were $B = 250$, $C = 150$. The same experiment run with $B = 20$, $C = 10$ only yielded a 20 percent reduction in RMS error over the PID controller.

Figure 4.18 shows results of the improved performance provided by Adaptive Controller II. From Table 4.1, the RMS position error was reduced by 41 percent.

Type of Controller	Trajectory Frequency f (Hz)	RMS Position Error (rad)	Time Elapsed Before Error Calculated	% Error Reduction from PID
PID	1.0	0.0106	0	-
Dither	1.0	-	-	-
AC I	1.0	0.0048	400	55
AC II	1.0	0.0079	12	25
AC III	1.0	0.0054	12	49
PID	0.5	0.0069	0	-
Dither	0.5	0.0066	0	4
AC I	0.5	0.0033	400	52
AC II	0.5	0.0041	12	41
AC III	0.5	0.0028	12	59
PID	0.25	0.0063	0	-
Dither	0.25	0.0055	0	13
AC I	0.25	0.0043	400	32
AC II	0.25	0.0037	12	41
AC III	0.25	0.0036	12	43
PID	0.1	0.0060	0	-
Dither	0.1	0.0045	0	25
AC I	0.1	-	-	-
AC II	0.1	0.0044	12	27
AC III	0.1	0.0040	12	33

Table 4.1: Results of Sinusoidal Tracking Experiments

Similarly, Figure 4.19 illustrates the effectiveness of Adaptive Controller III. According to Table 4.1, Adaptive Controller III reduced RMS error by 59 percent. A comparison of these plots and performance results suggests that Adaptive Controller II is not as effective at friction compensation as Adaptive Controller III. This can be explained by noting that there are a couple of relatively large error peaks in Figure 4.18 for Adaptive Controller II. Referring back to Figure 4.14, one can observe from the plot in the upper left corner that Adaptive Controller II overcompensates when friction changes instantaneously. That is,

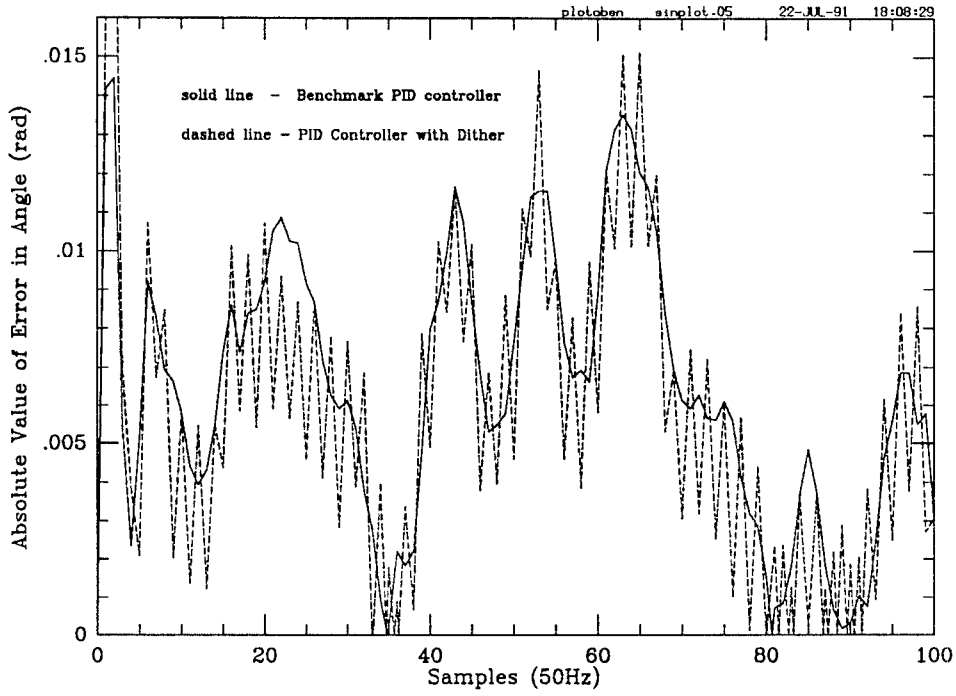

Figure 4.16: Position Error for PID Controller with Dither Compared to Benchmark PID Controller

after the instantaneous change in friction compensation, the magnitude of the input torque drops to zero in response to the overcompensation. The large error peaks seen from the plot in the upper right corner (as well as in Figure 4.18) correspond in time to the instantaneous friction changes. This overcompensation and corresponding large error indicates that the classical friction model does not describe friction during transient velocity reversals as well as the Dahl model.

Table 4.1 provides a comprehensive account of the results of the experimental program. As indicated by the significant percent reductions in RMS position error, each of the three adaptive controllers effectively improved tracking performance for the range of sinusoidal trajectory frequencies tested. The lower

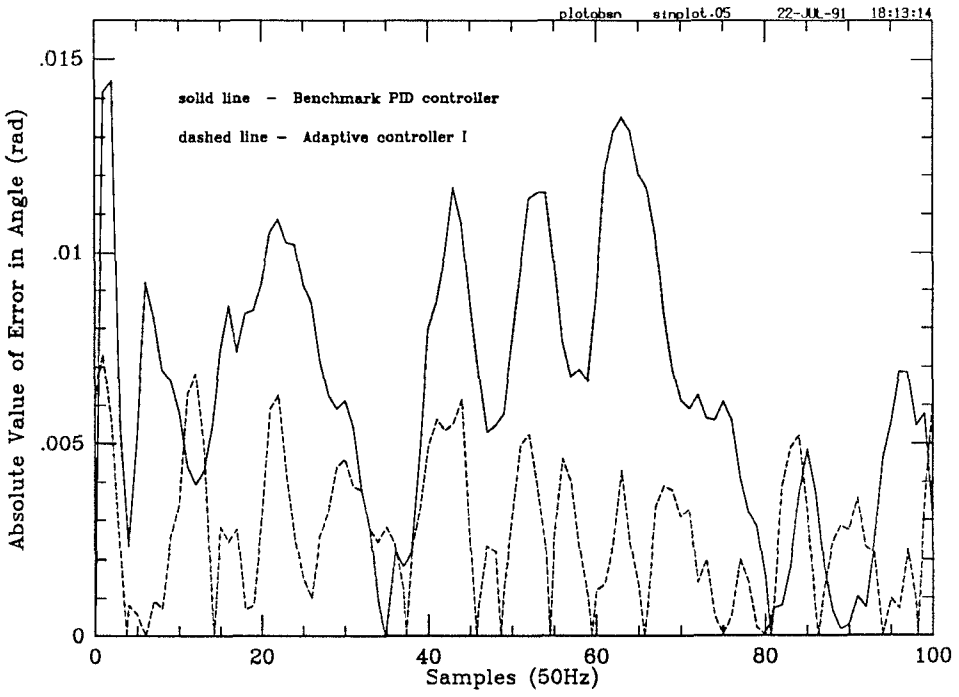

Figure 4.17: Position Error for Adaptive Controller I Compared to Benchmark PID Controller

values of percent reduction in RMS error for the 0.1 Hz experiment are most likely due to the resolution of the position measurements.

The numbers listed in Table 4.1 are averages of results from experiments made over a period of a few days. However, over the course of about six months during which these experiments were performed, there was a great deal of repeatability in the percent reduction in RMS position error achieved by the three adaptive controllers. The experiments were run during different seasons and during different stages of motor "warm-up" such that friction parameters may have varied from experiment to experiment due to temperature differences. Additionally, over the six month period the friction parameters may have changed

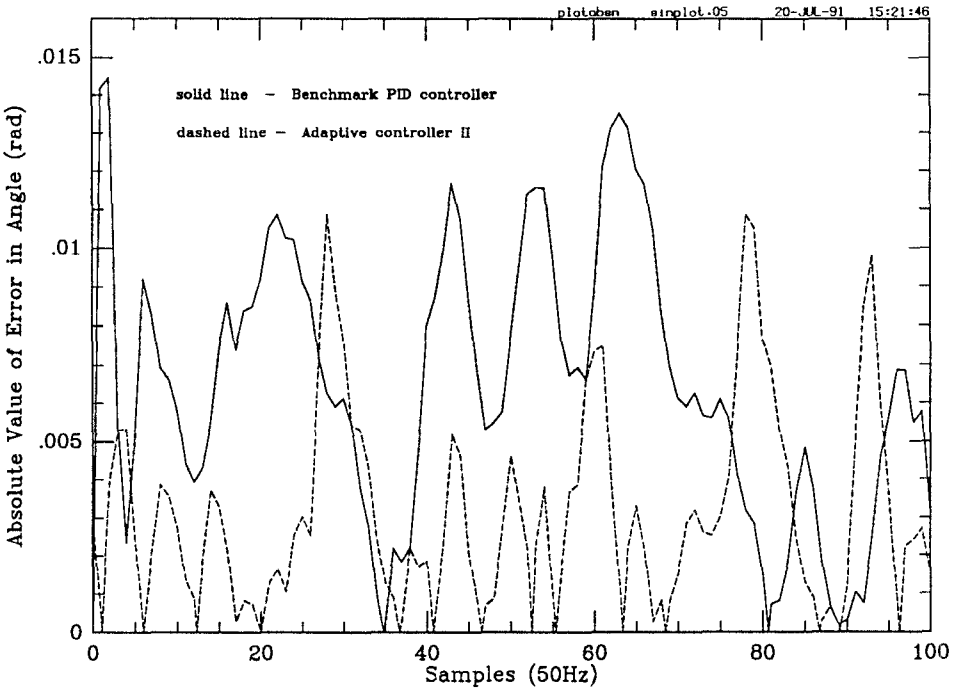

Figure 4.18: Position Error for Adaptive Controller II Compared to Benchmark PID Controller

due to system aging. The fact that the adaptive controllers were consistently effective under these varying conditions provides evidence for the effectiveness of the adaptability of these controllers.

The controller with dither was increasingly effective with decreasing trajectory frequency. Since a higher dither frequency is more desirable for effective nonlinearity smoothing, the result can be attributed to the fact that at lower trajectory frequencies the dither frequency was higher *relative* to the trajectory frequency.

The results for Adaptive Controller II provided in Table 4.1 correspond to experiments performed using Model (a) friction. Experiments using Model (b)

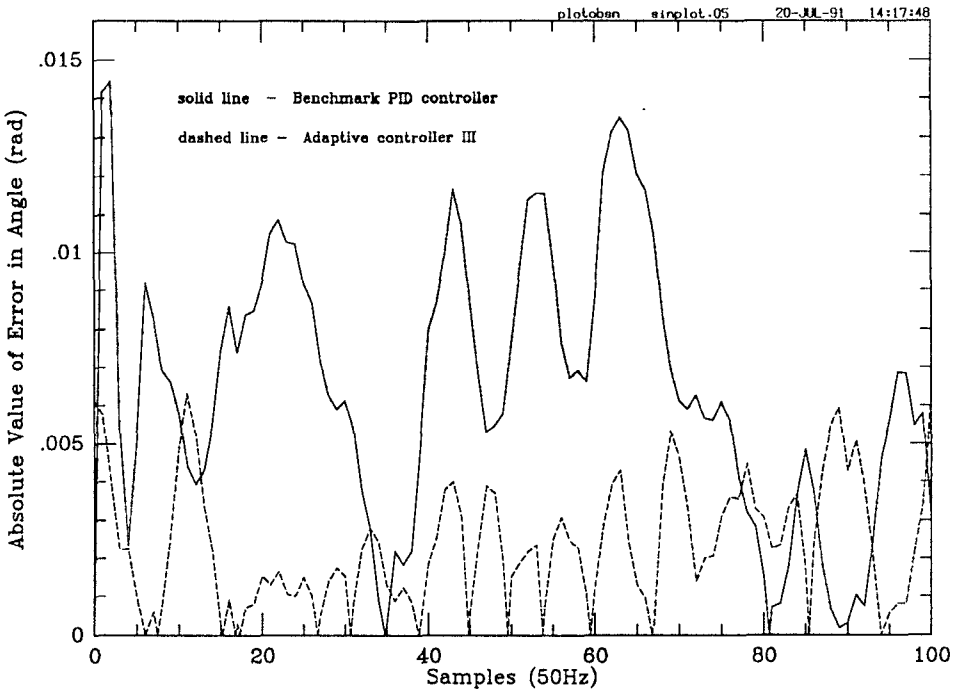

Figure 4.19: Position Error for Adaptive Controller III Compared to Benchmark PID Controller

friction showed an insignificant change in performance. This result indicates that for this set of experimental conditions, additional adaptive terms to account for friction asymmetries are not necessary. Experiments using Models (c) and (d) for friction showed only a slight improvement in performance as compared to the Model (a) experiments. Specifically, the percent reduction in RMS position was increased by < 1 percent for Model (c) and < 2 percent for Model (d). Since the additional friction terms in Model (c) and Model (d) were intended to account for Stribeck friction, this result is to be expected. Specifically, it can be attributed to the fact that Stribeck friction is probably not completely measured by the experimental system since the critical Stribeck velocity may be approximately of the same order as the velocity measurement resolution.

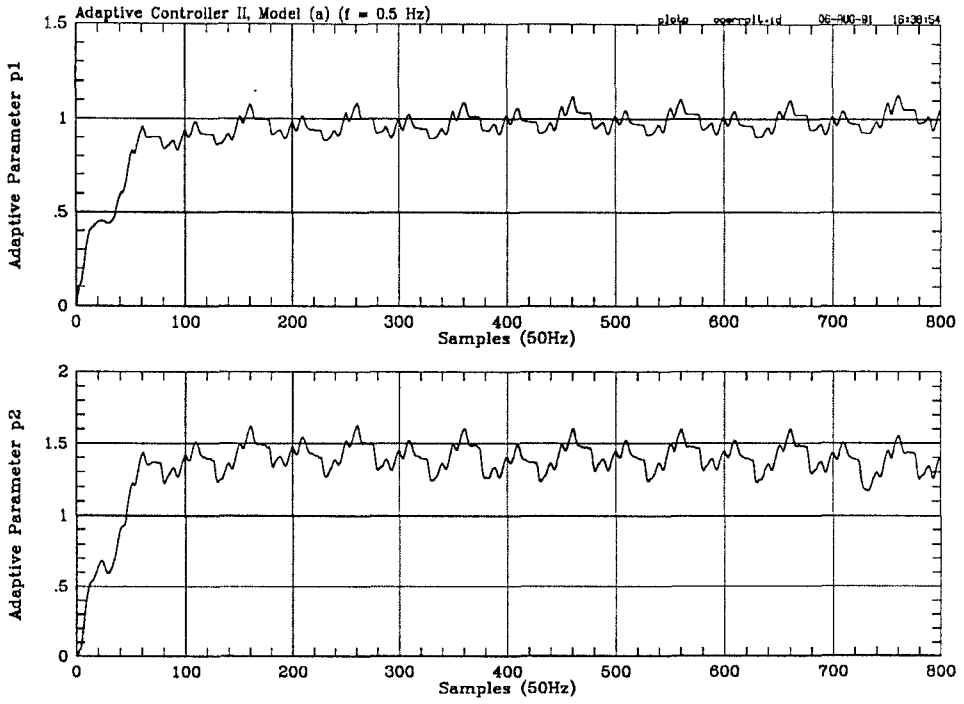

Figure 4.20: Parameter Adaptation for Adaptive Controller II, Model (a)

Adaptive Controller II was successful at identifying the friction parameters of Model (a) only. Figure 4.20 shows $\hat{p}_1$ and $\hat{p}_2$ of Model (a) for the first 16 seconds of the experiment. $\hat{p}_1$ which according to (3.53) and (3.54) corresponds to c_1/c_3 converged to 1.1 volt-s/rad. This compares to an expected value of $c_1/c_3 = 2.5$ volt-s/rad from Section 4.1 and (4.5). It is possible that the difference between the estimated and expected values is due to an inaccurate value of the motor voltage constant K_v. $\hat{p}_2$ which according to (3.53) and (3.54) corresponds to $(c_2/c_3)|F_k|$ converged to 1.3 volts. This compares well to the expected value of $(c_2/c_3)|F_k| = 1.1$ volts from Section 4.1, (4.5) and assuming $|F_k| = 0.72$ lbf-in. In fact, assuming the expected value of c_2/c_3 is correct, the converged value of $\hat{p}_2$ predicts that $|F_k| = 0.83$ lbf-in. It seems reasonable that this value is slightly

higher than the expected 0.72 lbf-in since $\hat{p}_2$ may be accounting for static friction as well as kinetic friction.

As described above the disadvantages of the controller with dither were predominately a result of the limitations associated with the 50 Hz sampling rate used in the experimental program. Since the dither frequency was limited to 25 Hz, the controller was less effective in compensating for friction than the adaptive controllers. Additionally, undesirable system vibrations resulted.

The main disadvantage associated with Adaptive Controller I was its excessively slow rate of adaptation. Although tracking performance began to improve immediately, it was not until 400 seconds into the experiment that the best results were achieved. Another disadvantage was that the adaptive gains had to be adjusted for the different experiments. This implies that gain scheduling would need to be applied for general use of Adaptive Controller I. Additionally, Adaptive Controller I forces the output to follow the output of the ideal model instead of the demand signal. Accommodating this effect was straightforward for the sinusoidal demand signals of this experimental program. However, it could be more complicated to do so for a more general demand signal.

Adaptive Controller II had the disadvantage that for the implementation that yielded the best results, the adaptive parameters tended to drift and performance deteriorated after a while. This could be avoided by resetting the parameters when they went out of a predefined range as suggested by [Craig, 1988].

Adaptive Controller III, on the other hand, was very reliable and performed best of all the controllers. However, this controller is disadvantaged in that it requires a lengthy experiment up front to determine the constants in the relationship between the friction time constant τ and the RMS velocity. Additionally, since kinetic friction T_c is held constant, Adaptive Controller III is not best suited for adapting to changes in friction due to temperature or aging. This could be fixed, however, by adding an adaptive component to update T_c.

Finally, as described in Section 4.2 torque ripple adds a position-dependent component to the motor dynamics and could have affected how each of the controllers performed. All of the data in Table 4.1 applies to experiments run such that the initial position was 0.0 radians. However, it was observed that the performance of the controllers varied when different initial positions were used. To investigate this torque ripple effect, the experiment with $f = 0.5$ Hz was run again on the PID controller and Adaptive Controllers II and III at 15 different initial positions chosen randomly. The results of these experiments are shown in Table 4.2. According to these results, neither Adaptive Controller II nor III performed on average as well as at an initial position of 0.0 radians. However, the greater effectiveness of Adaptive Controller III relative to Adaptive Controller II was observed at every initial position. Therefore, it can be concluded that while torque ripple does affect somewhat the performance of these two adaptive controllers, it does not affect their relative effectiveness.

Initial Position (rad)	RMS Position Error with PID Controller (rad)	% RMS Position Error Reduction from PID	
		AC II	AC III
-2.698	0.0086	16	23
-2.484	0.0082	26	33
-2.075	0.0091	21	23
-1.546	0.0081	30	35
-1.080	0.0079	30	39
-0.709	0.0079	28	29
-0.261	0.0072	33	36
-0.069	0.0071	32	41
0.000	0.0067	34	52
0.086	0.0068	34	46
0.689	0.0060	28	42
1.172	0.0061	15	56
1.758	0.0066	18	39
2.484	0.0076	32	37
2.720	0.0074	22	39
Average	0.0074	27	38
Std. Dev.	0.00087	6.4	8.9

Table 4.2: Experimental Results at Different Initial Positions ($f = 0.5$ Hz)

The effect of digital sampling rate on the performance of Adaptive Controller II and III was also investigated by repeating the experiments of the experimental program with a 100 Hz sampling rate. Table 4.3 lists the results of these experiments. According to Table 4.3, the increased sampling rate did not have a dramatic effect on the performance of Adaptive Controller III. However, Adaptive Controller II performed significantly better with the 100 Hz sampling rate than with the 50 Hz sampling rate, particularly for experiments with $f = 0.5$ Hz and $f = 1.0$ Hz. This improved performance may be explained by the fact that overcompensation provided by Adaptive Controller II for instantaneous changes

Trajectory frequency f (Hz)	% RMS Position Error Reduction from PID			
	AC II		AC III	
	50 Hz	100 Hz	50 Hz	100 Hz
1.0	25	64	49	42
0.5	41	60	59	56
0.25	41	45	43	56
0.1	27	35	33	29

Table 4.3: Comparison of Tracking Experiment Results with 50 Hz and 100 Hz Sampling Rates

in friction is not as prolonged with a 100 Hz sampling rate as it is with a 50 Hz sampling rate. Based on the results of Table 4.3, one can conclude that the relative effectiveness of Adaptive Controllers II and III is greatly affected by the digital sampling rate.

Chapter 5

Conclusions

In this thesis a comprehensive investigation was presented of control strategies for friction compensation in servomechanisms. Both the theoretical and experimental results of the investigation provide insights into improving precision control of a servomechanism in the presence of non-negligible friction. The major conclusions of the investigation are as follows:

- For friction-compensating control, friction model components must be selected carefully since different components predict varied dynamic responses and are relevant under different operating conditions. For example, if the servomechanism is to be controlled for high velocity, unidirectional applications, a simple viscous friction model that provides damping is most likely sufficient. If velocity reversals are desired, the classical friction model and the Dahl friction model are more appropriate options. If measurement resolution is such that Stribeck friction cannot be measured,

then modelling Stribeck friction terms will not be useful. However, these terms may become important if measurement resolution is very good and low velocity applications are desired.

- Adaptive Controllers I, II, and III all provide improved servomechanism position control compared to an optimized PID controller. Theoretical analyses predict that in the absence of noise and friction modelling errors, Adaptive Controllers I and II will drive position error to zero and Adaptive Controller III will drive velocity error to zero. Experimental results support this prediction for low-frequency sinusoidal position trajectory tracking experiments on a direct-drive dc motor. Additionally, the experimental results of this thesis coupled with the results of [Gilbart and Winston, 1974,Craig, 1988,Walrath, 1984] provide evidence for the general applicability of these adaptive controllers.

- An adaptive controller can be more effective than a traditional controller with dither for friction compensation in servomechanisms. In particular if the controller is implemented digitally and the sampling rate is limited, dither may be relatively less effective and may generate undesirable vibrations in the servomechanism.

- The Dahl model provides a realistic and reliable model of friction, particularly during sinusoidal motion of the mechanism. Evidence for this can be found (1) in the fact that the empirically derived model of the friction time

constant τ as a linear function of velocity is consistent with Dahl's original model and (2) by the relatively high effectiveness of Adaptive Controller III which is based on the Dahl model. This conclusion is noteworthy since friction is typically considered to behave according to the classical friction model.

- The "adaptability" of the adaptive controllers tested in this thesis performs effectively since performance results were repeatable over the course of six months. Additionally, Adaptive Controller II can be used for friction parameter identification.

- Mechanical considerations play an important role in the performance of the adaptive controllers. For example, the effectiveness of both Adaptive Controllers II and III deteriorates with increasing torque ripple magnitude. On the other hand, the effectiveness of Adaptive Controller II improves with increased digital sampling rate while the effectiveness of Adaptive Controller III does not.

To further explore friction compensation in servomechanisms, future work should involve continued testing of the friction-compensating adaptive controllers. Experimental programs that consider different servomechanisms and supporting hardware and/or experiments other than sinusoidal position trajectory tracking would help determine the general effectiveness of the controllers. If an experimental setup were to be used with sufficiently high measurement

resolution, the effectiveness of friction compensation in the Stribeck velocity regime could be investigated. Additionally, the consequences of frictional time lag on friction-compensating control strategies for servomechanisms need to be explored experimentally. This time lag was not considered in the experiments of this thesis. However, theory predicts that the time lag affects friction dynamics in such a manner that the potential for stick-slip oscillations is less than otherwise expected.

Finally, research should be pursued to understand the relationship between the classical friction model and the Dahl friction model. Based on the results of this thesis, the Dahl model provides a reasonable representation of friction behavior about the zero-velocity point and thus cannot be ignored. A determination of how to link the Dahl model of pre-sliding displacements with the classical model of sticking and sliding would provide a more complete and cohesive understanding of friction that could potentially be used to improve friction-compensating control strategies.

Bibliography

[Åström and Wittenmark, 1989] Åström, K. and B. Wittenmark, *Adaptive Control,* Addison-Wesley, Reading, MA, 1989.

[Armstrong, 1988] Armstrong, B., *Dynamics for Robot Control: Friction Modeling and Ensuring Excitation During Parameter Identification,* PhD thesis, Stanford University, Department of Electrical Engineering, May 1988.

[Armstrong, 1989] Armstrong, B., Control of machines with non-linear, low-velocity friction: a dimensional analysis, in *Lecture Notes in Control and Information Sciences, 139,* edited by V. Hayward and O. Khatib, pp. 180–195, Springer-Verlag, 1989.

[Armstrong-Hélouvry, 1990] Armstrong-Hélouvry, B., Stick-slip arising from Stribeck friction, in *Proceedings of the 1990 International Conference on Robotics and Automation,* pp. 1377–1382, IEEE, Cincinnati, OH, May 1990.

[Armstrong-Hélouvry, 1991] Armstrong-Hélouvry, B., *Control of Machines with Friction,* Kluwer Academic Publishers, Boston, 1991.

[Avollone and Baumeister III, 1987] Avollone, E. A. and T. Baumeister III (eds.), *Marks' Standard Handbook for Mechanical Engineers,* McGraw-Hill, New York, ninth edition, 1987.

[Bartusek, 1989] Bartusek, J., *Design and Digital Signal Processor Implementation of a Controller for Flexible Structures,* Master's Thesis 90-3, Systems Research Center, U. of Maryland, College Park, MD, 1989.

[Bass, 1960] Bass, R., Mathematical legitimacy of equivalent linearization by describing functions, in *1st IFAC Congress Proceedings, Moscow,* pp. 895–905, Butterworks, London, 1960.

[Bowden and Tabor, 1982] Bowden, F. and D. Tabor, *Friction: An Introduction to Tribology,* Krieger Publishing Company, Malabar, Florida, 1982.

[Boyce and DiPrima, 1977] Boyce, W. E. and R. C. DiPrima, *Elementary Differential Equations and Boundary Value Problems,* John Wiley and Sons, New York, 1977.

[Brace and Byerlee, 1966] Brace, W. and J. Byerlee, Stick-slip as a mechanism for earthquakes, *Science, 153,* 990–992, 1966.

[Brock, 1988] Brock, D., Enhancing the dexterity of a robot hand using controlled slip, in *Proceedings of the 1988 International Conference on Robotics and Automation,* pp. 249–251, IEEE, Philadelphia, PA, April 1988.

[Brockett and Cebuhar, 1988] Brockett, R. and W. Cebuhar, Smoothing and linearization of discontinuous control systems, in *Dynamical Systems Approaches to Nonlinear Problems in Systems and Circuits,* edited by Salam and Levi, pp. 199–208, SIAM, 1988.

[Burdekin et al., 1978] Burdekin, M., N. Back, and A. Cowley, Experimental study of normal and shear characteristics of machined surfaces in contact, *Journal of Mechanical Engineering Science, 20,* 129–132, 1978.

[Canudas de Wit, 1989] Canudas de Wit, C., Experimental results on adaptive friction compensation in robotic manipulators: low velocities, in *Lecture Notes in Control and Information Sciences, 139,* edited by V. Hayward and O. Khatib, pp. 196–214, Springer-Verlag, 1989.

[Canudas et al., 1986] Canudas, C., K. Astrom, and K. Braun, Adaptive friction compensation in dc motor drives, in *Proceedings of the 1986 International Conference on Robotics and Automation,* pp. 1556–1561, IEEE, San Francisco, CA, April 1986.

[Cebuhar, 1988] Cebuhar, W. A., *Smoothing and Approximate Linearization of Discontinuous Control Systems,* PhD thesis, Harvard University, Department of Applied Mathematics, Cambridge, MA, July 1988.

[Cheng and Kikuchi, 1985] Cheng, J. and N. Kikuchi, An incremental constitutive relation of unilateral contact friction for large deformation analysis, *Journal of Applied Mechanics, 52,* 639–648, September 1985.

[Courtney-Pratt and Eisner, 1957] Courtney-Pratt, J. and E. Eisner, The effect of a tangential force on the contact of metallic bodies, *Proceedings of the Royal Society, A238,* 529–550, 1957.

[Craig, 1988] Craig, J., *Adaptive Control of Mechanical Manipulators,* Addison-Wesley, Reading, MA, 1988.

[Dahl, 1976] Dahl, P., Solid friction damping of mechanical vibrations, *AIAA Journal, 14,* 1675–1682, December 1976.

[Dahl, 1977] Dahl, P., Measurement of solid friction parameters of ball bearings, in *Proceedings of the 6th Annual Symposium on Incremental Motion, Control Systems and Devices,* pp. 49–60, University of Illinois, 1977.

[Derjaguin et al., 1957] Derjaguin, B., V. Push, and D. Tolstoi, A theory of stick-slip sliding of solids, in *Procedings of the Conference on Lubrication and Wear,* pp. 257–268, Institution of Mechanical Engineers, London, October 1957.

[Donald and Pai, 1990] Donald, B. and D. Pai, On the motion of compliantly-connected rigid bodies in contact, part ii: a system for analyzing designs for assembly, in *Proceedings of the 1990 International Conference on Robotics and Automation,* pp. 1756–1762, IEEE, Cincinnati, OH, May 1990.

[Dorf, 1983] Dorf, R. C., *Modern Control Systems,* Addison-Wesley, Reading, MA, 1983.

[Dudley and Swift, 1949] Dudley, B. and H. Swift, Frictional relaxation oscillations, *Philosophical Magazine, 40,* 849–861, 1949.

[Dupont, 1991] Dupont, P. E., Avoiding stick-slip in position and force control through feedback, in *Proceedings of the 1991 International Conference on Robotics and Automation,* pp. 1470–1475, IEEE, Sacramento, CA, April 1991.

[Electro-Craft Corp, 1980] Electro-Craft Corp (ed.), *DC Motors, Speed Controls, Servo Systems,* Electro-Craft Corporation, Hopkins, MN, fifth edition, 1980.

[Fan et al., 1987] Fan, M., L. Wang, J. Koninckx, and A. Tits, *CONSOLE Users Manual,* Technical Report 87-212, Systems Research Center, 1987.

[Frank, 1986] Frank, G., *Design and Real-Time Control of a Flexible Arm,* Master's Thesis 86-69, Systems Research Center, U. of Maryland, College Park, MD, 1986.

[Franklin et al., 1990] Franklin, G. F., J. D. Powell, and M. L. Workman, *Digital Control of Dynamic Systems,* Addison-Wesley, Reading, MA, second edition, 1990.

[Gassenfeit and Soom, 1988] Gassenfeit, E. H. and A. Soom, Friction coefficients measured at lubricated planar contacts during start-up, *Journal of Tribology, 110,* 533–538, January 1988.

[Ghanadan, 1990] Ghanadan, R., *Adaptive PID Control of Nonlinear Systems,* Master's Thesis 90-10, Systems Research Center, U. of Maryland, College Park, MD, 1990.

[Gilbart and Winston, 1974] Gilbart, J. W. and G. C. Winston, Adaptive compensation for an optical tracking telescope, *Automatica, 10,* 125–131, 1974.

[Gilbart et al., 1970] Gilbart, J. W., R. V. Monopoli, and C. F. Price, Improved convergence and increased flexibility in the design of model reference adaptive control systems, in *Proceedings of the Ninth Symposium on Adaptive Processes,* pp. IV.3.1–IV.3.10, 1970.

[Gogoussis and Donath, 1987] Gogoussis, A. and M. Donath, Coulomb friction joint and drive effects in robot mechanisms, in *Proceedings of the 1987 International Conference on Robotics and Automation,* pp. 828–836, IEEE, Raleigh, NC, March-April 1987.

[Haessig and Friedland, 1990] Haessig, Jr., D. A. and B. Friedland, On the modelling and simulation of friction, in *Proceedings of the 1990 American Control Conference,* pp. 1256–1261, San Diego, CA, May 1990.

[Hess and Soom, 1990] Hess, D. P. and A. Soom, Friction at a lubricated line contact operating at oscillating sliding velocities, *Journal of Tribology, 112,* 147–152, January 1990.

[Hill and Moylan, 1976] Hill, D. and P. Moylan, The stability of nonlinear dissipative systems, *IEEE Transactions on Automatic Control, 21,* 708–711, October 1976.

[Hill and Moylan, 1977] Hill, D. and P. Moylan, Stability results for nonlinear feedback systems, *Automatica, 13,* 377–382, 1977.

[Hill and Moylan, 1980] Hill, D. and P. Moylan, Dissipative dynamical systems: basic input-output and state properties, *Journal of the Franklin Institute, 309,* 327–357, May 1980.

[Horowitz, 1988] Horowitz, F., Mixed state variable friction laws: some implications for experiments and a stability analysis, *Geophysical Research Letters, 15,* 1243–1246, October 1988.

[Karnopp, 1985] Karnopp, D., Computer simulation of stick-slip friction in mechanical dynamic systems, *Journal of Dynamic Systems, Measurement, and Control, 107,* 100–103, March 1985.

[Kato et al., 1972] Kato, S., N. Sato, and T. Matsubayashi, Some considerations on characteristics of static friction of machine tool slideway, *Journal of Lubrication Technology, 94,* 234–247, 1972.

[Kubo et al., 1986] Kubo, T., G. Anwar, and M. Tomizuka, Application of nonlinear friction compensation to robot arm control, in *Proceedings of the 1986*

International Conference on Robotics and Automation, pp. 722–727, IEEE, San Francisco, CA, April 1986.

[Mason, 1982] Mason, M. M., *Manipulator Grasping and Pushing Operations,* PhD thesis, MIT, Department of Electrical Engineering and Computer Science, 1982, AI Lab Tech. Report AI-TR-690.

[Mason and Wang, 1988] Mason, M. and Y. Wang, On the inconsistency of rigid-body frictional planar mechanics, in *Proceedings of the 1988 International Conference on Robotics and Automation,* pp. 524–528, IEEE, Philadelphia, PA, April 1988.

[Mees, 1981] Mees, A., *Dynamics of Feedback Systems,* John Wiley and Sons, New York, 1981.

[Nussbaum and Ruina, 1987] Nussbaum, J. and A. Ruina, A two degree-of-freedom earthquake model with static/dynamic friction, *Pure and Applied Geophysics, 125,* 629–656, 1987.

[Rabinowicz, 1951] Rabinowicz, E., The nature of the static and kinetic coefficients of friction, *Journal of Applied Physics, 22,* 1373–1379, November 1951.

[Rabinowicz, 1956] Rabinowicz, E., Stick and slip, *Scientific American, 194(5),* 109–118, May 1956.

[Rabinowicz, 1958] Rabinowicz, E., The intrinsic variables affecting the stick-slip process, in *Proceedings of the Physical Society of London,* pp. 668–675, 1958, Volume 71.

[Rabinowicz, 1965] Rabinowicz, E., *Friction and Wear of Materials,* John Wiley and Sons, 1965.

[Radcliffe and Southward, 1990] Radcliffe, C. and S. Southward, A property of stick-slip friction models which promotes limit cycle generation, in *Proceedings of the 1990 American Control Conference,* pp. 1198–1203, San Diego, CA, May 1990.

[Rice and Ruina, 1983] Rice, J. and A. Ruina, Stability of steady frictional slipping, *Journal of Applied Mechanics, 50,* 343–349, June 1983.

[Rice and Tse, 1986] Rice, J. and S. Tse, Dynamic motion of a single degree of freedom system following a rate and state dependent friction law, *Journal of Geophysical Research, 91,* 521–530, January 1986.

[Ruina, 1983] Ruina, A., Slip instability and state variable friction laws, *Journal of Geophysical Research, 88,* 10359–10370, December 1983.

[Sampson et al., 1943] Sampson, J., F. Morgan, D. Reed, and M. Muskat, Friction behavior during the slip portion of the stick-slip process, *Journal of Applied Physics, 14,* 689–700, December 1943.

[Shen and Wang, 1964] Shen, C. and H. Wang, Nonlinear compensation of a second- and third-order system with dry friction, *IEEE Transactions on Applications and Industry, 83,* 128–136, March 1964.

[Skoog and Blankenship, 1970] Skoog, R. and G. Blankenship, Generalized pulse-modulated feedback systems: norms, gains, Lipschitz constants and stability, *IEEE Transactions on Automatic Control, AC-15,* 300–315, 1970.

[Slotine and Li, 1991] Slotine, J. E. and W. Li, *Applied Nonlinear Control,* Prentice-Hall, Englewood Cliffs, NJ, 1991.

[Tou and Schultheiss, 1953] Tou, J. and P. Schultheiss, Static and sliding friction in feedback systems, *Journal of Applied Physics, 24,* 1210–1217, September 1953.

[Townsend and Salisbury, 1987] Townsend, W. and J. Salisbury, Jr., The effect of coulomb friction and stiction on force control, in *Proceedings of the 1987 International Conference on Robotics and Automation,* pp. 883–889, IEEE, Raleigh, NC, March-April 1987.

[Tsypkin, 1984] Tsypkin, I. Z., *Relay Control Systems,* Cambridge University Press, New York, 1984.

[Vidyasagar, 1978] Vidyasagar, M., *Nonlinear Systems Analysis,* Prentice-Hall, Englewood Cliffs, NJ, 1978.

[Villanueva-Leal and Hinduja, 1984] Villanueva-Leal, A. and S. Hinduja, Modelling the characteristics of interface surfaces by the finite element method, *Proceedings of the Institution of Mechanical Engineers, 198C,* 9–23, 1984.

[Walrath, 1984] Walrath, C., Adaptive bearing friction compensation based on recent knowledge of dynamic friction, *Automatica, 20,* 717–727, 1984.

[Wang, 1987] Wang, L., *Control System Design for a Flexible Arm,* Master's Thesis 87-164, Systems Research Center, U. of Maryland, College Park, MD, 1987.

[White, 1979] White, F. M., *Fluid Mechanics,* McGraw-Hill, New York, 1979.

[Willems, 1971] Willems, J. C., Dissipative dynamical systems part i: general theory, in *Archive for Rational Mechanics and Analysis,* pp. 322–351, Springer-Verlag, 1971.